Fall 2013

Advanced Control Strategies for Mobile Hydraulic Applications

Davide Cristofori
Purdue University

Graduate School ETD Form 9
(Revised 12/07)

PURDUE UNIVERSITY
GRADUATE SCHOOL
Thesis/Dissertation Acceptance

This is to certify that the thesis/dissertation prepared

By Davide Cristofori

Entitled
Advanced Control Strategies for Mobile Hydraulic Applications

For the degree of Doctor of Philosophy

Is approved by the final examining committee:

Andrea Vacca
Chair

Monika Ivantysynova

John H. Lumkes Jr.

Kartik B. Ariyur

To the best of my knowledge and as understood by the student in the *Research Integrity and Copyright Disclaimer (Graduate School Form 20)*, this thesis/dissertation adheres to the provisions of Purdue University's "Policy on Integrity in Research" and the use of copyrighted material.

Approved by Major Professor(s): Andrea Vacca

Approved by: Bernard Engel 11/22/2013
Head of the Graduate Program Date

ADVANCED CONTROL STRATEGIES FOR MOBILE HYDRAULIC APPLICATIONS

A Dissertation

Submitted to the Faculty

of

Purdue University

by

Davide Cristofori

In Partial Fulfillment of the

Requirements for the Degree

of

Doctor of Philosophy

December 2013

Purdue University

West Lafayette, Indiana

ACKNOWLEDGEMENTS

I would like to express my gratitude to my adviser Dr. Andrea Vacca for his guidance over these years. Also, I would like to thank the rest of the committee members: Prof. Monika Ivantysynova, Prof. John H. Lumkes Jr., and Dr. Kartik B. Ariyur.

I would like to extend my gratitude to faculties, staff, and researchers who contributed to make Maha Lab (Purdue University) a very stimulating and successful research environment.

Furthermore, I would like to thank CNH Industrial (Burr Ridge, IL) and CCEFP (a NSF Engineering Research Center) for the research funds as well as Parker Hannifin Mobile Systems (Elk Grove Village, IL) for the test equipment.

TABLE OF CONTENTS

Page

Page

LIST OF TABLES

LIST OF FIGURES

Figure Page

Figure Page

Figure Page

Figure Page

Figure Page

Figure Page

LIST OF SYMBOLS

Plant

Symbol	Description	Units
A_{PT}, A_{PR}, A_{PL}, A_{RT}, A_{RT}	Metering areas of the proportional directional valve control spool: from the pressure source port to the tank port (A_{PT}); from the pressure source port to the workport which produces the mechanical arm raise (A_{PR}); from the pressure source port to the workport which produces the mechanical arm lowering (A_{PL}); from the workport which produces the mechanical arm raise to the tank port (A_{RT}); from the workport which produces the mechanical arm lowering to the tank port (A_{LT}).	$[m^2]$
A_{PWe}, A_{PWr}, A_{WeT}, A_{WrT}	Metering areas of the proportional directional valve control spool: from the pressure source port to the workport which produces the actuator extension (A_{PWe}); from the pressure source port to the workport which produces the actuator retraction (A_{PWr}); from the workport which produces the actuator extension to the tank port (A_{WeT}); rom the workport which produces the actuator retraction to the tank port (A_{WrT}).	$[m^2]$
A_R, A_L	Areas of the piston of a generic actuator: R, raise chamber; L, lowering chamber.	$[m^2]$
A_e, A_r	Areas of the piston of a generic actuator: e, extension chamber; r, retraction chamber.	$[m^2]$
B	Bulk modulus of the fluid.	$[Pa]$
c_d	Discharge coefficient of the orifice.	$[-]$
c_{PC}; c_M	Viscous friction: P, piston and cylinder of the hydraulic linear actuator; M, main spool of the proportional directional valve.	$[Ns/m]$
c_{To}	Linearized tire viscous damping.	$[Ns/m]$
C_{HR},C_{HL}	Hydraulic capacitance of the transmission line: R, raise chamber; L, lowering chamber.	$[m^3/Pa]$

Symbol	Description	Units
C_{HRo}; C_{HLo}	Linearized hydraulic capacitance of the transmission line: R, raise chamber; L, lowering chamber.	$[m^3/Pa]$
C_n	Normalized user input command.	$[\pm 1]$
F_i	Force acting on the generic i^{th} mass.	$[N]$
F_{QR}; F_{QL}	Force of the hydraulic linear actuator due to flow entering its chambers: R, raise chamber; L, lowering camber.	$[N]$
F_{QRo}; F_{QLo}	Force of the hydraulic linear actuator due to flow entering its chambers in the linearized model: R, raise chamber; L, lowering camber.	$[N]$
$F_{r,i}$	Force exerted by the i^{th} actuator rod on the mechanical arm.	$[N]$
g	Acceleration of gravity = 9.81 m/s^2	$[m/s^2]$
i_n	Electric current on the proportional solenoid of the proportional directional valve.	$[\pm 1]$
i_R; i_L	Electric current on the solenoid which produces the raise (R) or lowering (L) of the mechanical arms.	$[A]$
I_L	Moment of inertia of the load with respect to the center of rotation.	$[m^2 kg]$
J_ψ	Cost function of the crane vibrations.	$[deg \cdot s]$
J_{cab}	Cost function of the cab vibrations in the wheel loader (time domain).	$[m/s]$
J_{bkt}	Cost function of the boom vibrations in the wheel loader (time domain).	$[m/s]$
J_{cabFFT}	Cost function of the cab vibrations in the wheel loader (frequency domain).	$[m/s]$
J_{bktFFT}	Cost function of the boom vibrations in the wheel loader (frequency domain).	$[m/s]$
K_{HR}; K_{HL}	Hydraulic stiffness of the hydraulic actuator chambers: R, raise chamber; L, lowering chamber.	$[N/m]$
K_{HRo}; K_{HLo}	Linearized hydraulic stiffness of the hydraulic actuator chambers: R, raise chamber; L, lowering chamber.	$[N/m]$
K_{To}	Linearized tire stiffness.	$[N/m]$
M_L; M_{PR}; M_A; M_I; M_T	Mass: L, load; PR, piston and rod of the hydraulic actuator; A, mechanical arm of the machine; I, implement; T, tractor.	$[kg]$
p_{WR}; p_{WL}	Pressure at the workport of the directional valve: R, raise workport; L, lowering workport.	$[Pa]$
p_{We}; p_{Wr}	Pressure at the workport of the directional valve which controls the extension (e) or retraction (r) of the actuator.	$[Pa]$

Symbol	Description	Units
p_R; p_L	Pressure in the hydraulic actuator chambers: R, raise chamber; L, lowering chamber.	$[Pa]$
p_{Ce}; p_{Cr}	Pressure in the cylinder chambers which controls the extension (e) or retraction (r) of the actuator.	$[Pa]$
p_{R0}; p_{L0}	Initial value of the pressure in the hydraulic actuator chambers: R, raise chamber; L, lowering chamber.	$[Pa]$
p_{LS}	Load-sensing pressure.	$[Pa]$
p_P	Pump delivery pressure.	$[Pa]$
p_C	Flow-sharing compensator inlet pressure.	$[Pa]$
Q_R; Q_L	Flow rate entering the hydraulic actuator chambers: R, raise chamber; L, lowering chamber.	$[m^3/s]$
Q_e; Q_r	Flow rate entering the hydraulic actuator chambers producing the extension (e) or retraction (r) of the actuator.	$[m^3/s]$
Q_{PR}	Flow rate from the hydraulic power supply port to the raise workport.	$[m^3/s]$
Q_{PL}	Flow rate from the hydraulic power supply port to the lowering workport.	$[m^3/s]$
Q_{PT}	Flow rate from the hydraulic power supply port to the tank port	$[m^3/s]$
Q_{RT}	Flow rate from the raise workport to the tank port.	$[m^3/s]$
Q_{LT}	Flow rate from the lowering workport to the tank port.	$[m^3/s]$
$Q_{R,net}$, $Q_{L,net}$	Net flow rate for the transmission lines: R, raise side; L, lowering side.	$[m^3/s]$
r_L	Distance between the load center of mass and the center of rotation.	$[m]$
R_{HR},R_{HL}	Hydraulic resistance of the transmission line: R, raise side; L, lowering side.	$[sPa/m^3]$
R_{He},R_{Hr}	Hydraulic resistance of the transmission line: e, extension side; r, retraction side.	$[sPa/m^3]$
s	Laplace transform argument.	$[rad/s]$
t	Time.	$[s]$
T_i	Torque acting on the generic i^{th} mass.	$[Nm]$
V_R, V_L	Volumes of the chambers of a generic hydraulic actuator: R, raise chamber; L, lowering chamber.	$[m^3]$
V_e, V_r	Volumes of the chambers of a generic hydraulic actuator: e, extension side; r, retraction side.	$[m^3]$
W	Disturbance force.	$[N]$

Symbol	Description	Units
x_i	Linear position of the i^{th} mass with respect to the x-axis.	$[m]$
$x_{r,i}$	Stroke of the i^{th} hydraulic actuator rod.	$[m]$
x_{R0}, x_{L0}	Initial length of the chamber of a generic hydraulic actuator: R = raising side of the chamber; L = lowering chamber.	$[m]$
(x_L, z_L); (x_{PR}, z_{PR}); (x_A, z_A); (x_P, z_P); (x_M, z_M); (x_p, z_p)	Position of a rigid body along x-axis and z-axis: L, load; PR, piston and rod of the linear hydraulic actuator; A, mechanical arm of the machine; P, pilot stage of the proportional directional valve; M, main stage of the proportional directional valve; p, pivot.	$[m]$
$(\dot{x}_L, \dot{z}_L)$; $(\dot{x}_{PR}, \dot{z}_{PR})$; $(\dot{x}_A, \dot{z}_A)$; $(\dot{x}_P, \dot{z}_P)$; $(\dot{x}_M, \dot{z}_M)$; $(\dot{x}_p, \dot{z}_p)$	Velocity of a rigid body along x-axis and z-axis: L, load; PR, piston and rod of the linear hydraulic actuator; A, mechanical arm of the machine; P, pilot stage of the proportional directional valve; M, main stage of the proportional directional valve; p, pivot.	$[m/s]$
$(\ddot{x}_L, \ddot{z}_L)$; $(\ddot{x}_{PR}, \ddot{z}_{PR})$; $(\ddot{x}_A, \ddot{z}_A)$; $(\ddot{x}_P, \ddot{z}_P)$; $(\ddot{x}_M, \ddot{z}_M)$; $(\ddot{x}_p, \ddot{z}_p)$	Acceleration of a rigid body along x-axis and z-axis: L, load; PR, piston and rod of the linear hydraulic actuator; A, mechanical arm of the machine; P, pilot stage of the proportional directional valve; M, main stage of the proportional directional valve; p, pivot.	$[m/s^2]$
$\ddot{z}_{cab}$; $\ddot{z}_{bkt}$	Vertical acceleration of the cab and bucket in case study 2 (wheel loader).	$[m/s^2]$
z_{road}	Road profile (expressed as height relative to a horizontal line).	$[m]$
α_i	Angle of rotation of the i^{th} mechanical arm with respect to a pivot of the implement.	$[rad]$
β_{rel}	Angle between wheel loader boom and vertical axis.	$[deg]$
Δp_i	Pressure differential across the i^{th} metering area.	$[Pa]$
ζ	Damping ratio of a second order linear system.	$[-]$
ψ	Rotation of the outer boom in case study 1 (hydraulic crane).	$[rad]$
ρ	Fluid density.	$[kg/m^3]$
ω_n	Natural frequency of a second order linear system.	$[rad/s]$
ω_{HP}	High-pass filter cut-off pulsation.	$[rad/s]$

Controller

Symbol	Description
D	Set of derivative terms.
D^*	Sum of controller and plant derivative terms.
I	Set of integral terms.
I^*	Sum of controller and plant integral terms.
P	Set of proportional terms.
P^*	Sum of controller and plant proportional terms.
V	Noise in the measurement.
W	Disturbance.
δD	Derivative term to compensate un-modeled dynamics.
δI	Integral term to compensate un-modeled dynamics.
δP	Proportional term to compensate un-modeled dynamics.

Extremum-Seeking Optimization Algorithm

Symbol	Description
J	Cost function evaluated on the basis of the system output for a given set of control parameters.
k	k^{th}-iteration.
$\boldsymbol{\alpha}$	Vector of the amplitudes of the additive perturbations.
$\boldsymbol{\beta}$	Vector of the amplitudes of the multiplicative perturbations.
$\boldsymbol{\gamma}$	Vector of integrator gains.
$\boldsymbol{\vartheta}$	Vector representing the set of control parameters.
$\boldsymbol{\varphi}$	Vector of high pass filter pole.
$\boldsymbol{\phi}$	Vector of the phase lags between additive and multiplicative amplitudes.
$\boldsymbol{\omega}$	Vector of the pulsations of the perturbations.

Subscript	Description
0	Initial condition.
D	Desired component of the dynamics (dynamics in absence of vibrations).
FB	Feed-Back.
i	Identifier of the i^{th} mechanical arm.
L	Load.
n	Normalized.

Subscript	Description
N	Number of mechanical arms.
r	Rod of the actuator.
SP	Set-Point.
o	Linearization point.
P	Hydraulic power supply port.
T	Return to tank port.
U	Undesired component of the dynamics (oscillatory of the dynamics).

LIST OF ABBREVIATIONS

MHM	Mobile Hydraulic Machines
HM	Hydro-Mechanical: HMR, based on hydraulic Resistance; HMRP, based on hydraulic resistance on a Pilot line; HMRM, based on hydraulic resistance on a Main transmission line; HMC, based on hydraulic Capacitance; HMRC, based on hydraulic Resistance and Capacitance;
EH	Electro-Hydraulic
PFC	Pressure Feedback Control
WP	Workport of a proportional directional valve
SP	Set-Point (reference value)
FB	Feed-Back
OC	Operator comfort mode
LT	Load transport mode
PRC	Passive ride control
ARC	Active ride control
LS	Load-Sensing

ABSTRACT

Cristofori, Davide. Ph.D., Purdue University, December 2013. Advanced Control Strategies for Mobile Hydraulic Applications. Major Professor: Andrea Vacca.

Mobile hydraulic machines are affected by numerous undesired dynamics, mainly discontinuous motion and vibrations. Over the years, many methods have been developed to limit the extent of those undesired dynamics and improve controllability and safety of operation of the machine. However, in most of the cases, today's methods do not significantly differ from those developed in a time when electronic controllers were slower and less reliable than they are today.

This dissertation addresses this aspect and presents a unique control method designed to be applicable to all mobile hydraulic machines controlled by proportional directional valves. In particular, the proposed control method is targeted to hydraulic machines such as those used in the field including construction (wheel loaders, excavators, and backhoes, etc.), load handling (cranes, reach-stackers, and aerial lift, etc.), agriculture (harvesters, etc.), forestry, and aerospace. For these applications the proposed control method is designed to achieve the following goals:

A. Improvement of the machine dynamics by reducing mechanical vibrations of mechanical arms, load, as well as operator seat;
B. Reduction of the energy dissipation introduced by current vibration damping methods;
C. Reduction of system slowdowns introduced by current vibration damping methods.

Goal A is generally intended for all machines; goal B refers to those applications in which the damping is introduced by means of energy losses on the main hydraulic transmission line; goal C is related to those applications in which the vibration attenuation is introduced by slowing down the main transmission line dynamics.

Two case studies are discussed in this work:

1. Hydraulic crane: the focus is on the vibrations of the mechanical arms and load (goals A and B).
2. Wheel loader: the focus is on the vibrations of the driver's seat and bucket (goals A and C).

The controller structure is basically unvaried for different machines. However, what differs in each application are the controller parameters, whose adaptation and tuning method represent the main innovations of this work.

The proposed controller structure is organized so that the *control parameters are adapted* with respect to the instantaneous operating point which is identified by means of feedback sensors. The Gain Scheduling technique is used to implement the controller whose set of parameters are function of the specific identified operating point.

The optimal set of control parameters for each operating point is determined through the *non-model-based controller tuning.* The technique determines the optimal set of controller parameters through the optimization of the experimental machine dynamics. The optimization is based on an innovative application of the Extremum Seeking algorithm. The optimal controller parameters are then indexed into the Gain Scheduler.

The proposed method does not require the modification of the standard valve controlled machine layout since it only needs for the addition of feedback sensors. The feedback signals are used by the control unit to modify the electric currents to the proportional directional valves and cancel the undesired dynamics of the machine by controlling the actuator motion. In order for the proposed method to be effective, the proportional valve bandwidth must be significantly higher than the frequency of the undesired dynamics. This condition, which is typically true for heavy machineries, is further investigated in the research.

The research mostly focuses on the use of pressure feedback. In fact, although the use of position, velocity, or acceleration sensors on the vibrating bodies of the machine would provide a more straightforward measurement of the vibration, they are extremely rare on mobile hydraulic machines where mechanical and environmental stress harm their integrity. A comparison between pressure feedback and acceleration feedback alternatives of the proposed method is investigated with the aim to outline the conditions making one alternative preferable over the other one (for those applications were both alternatives are technically viable in terms of sensors and wiring reliability).

A mid-sized hydraulic crane (case study 1) was instrumented at Maha Fluid Power Research Center to study the effectiveness of the proposed control method, its stability and its experimental validation. Up to 30% vibration damping and 40% energy savings were observed for a specific cycle over the standard vibration damping method for this application. The proposed control method was also applied to a wheel loader (case study 2), and up to 70% vibrations attenuation on the bucket and 30% on the driver's cab were found in simulations. These results also served to demonstrate the applicability of the control method to different hydraulic machines.

Improved system response and a straightforward controller parameters tuning methodology are the features which give to the proposed method the potential to become a widespread technology for fluid power machines. The proposed method also has potential for improving several current vibration damping methods in terms of energy efficiency as well as simplification of both the hydraulic system layout and tuning process.

CHAPTER 1. INTRODUCTION

This introductory chapter will first describe the motivations for the research by providing a brief overview of the problem addressed by the proposed control strategy. Afterwards, the goals of the research will be formalized. The completion of all the goals is articulated in two case studies, which will be briefly presented in the last section of this chapter. In particular, the first case study is focused on reducing the vibration of the mechanical arms of a hydraulic crane. The second case study is focused on reducing the vibration of the implement and of the tractor of a wheel loader traveling on uneven ground.

1.1 Background and Motivation

Vibrations of hydraulic machines are a problem which affects almost all applications. Examples are represented by the vibrations of the mechanical arms and loads (cranes, telehandlers, and excavators, etc.) as well as the vibrations of the tractor cab (wheel loaders, harvesters, etc.). In fact, mechanical oscillations occur whenever a mechanical system contains storage elements for potential and kinetic energies (Sinha, A. K., 2010): even the simplest hydraulic machine can store potential energy in the fluid pressure and it can store kinetic energy in its mass (mainly load and mechanical arms). Additionally, vibrations are promoted by: discontinuities in the hydro-mechanical system (e.g. operation of on/off valves, static friction, actuator end stops, etc.); discontinuous inputs (e.g. sudden variation of the operator command); disturbances (e.g. vehicle driving on uneven ground).

Hydraulic machines used to handle large loads give rise to significant vibrations which may harm the safety of the operator as well as the productivity and durability of the machine. In addition, increasingly stringent regulations on admissible vibrations on machine's seat (International Organization for Standardization, 2004) are contributing to the need for proper vibration damping methods in mobile hydraulic machines.

The design of a vibration damping method for hydraulic machines is challenging not only because of the above mentioned aspects, but also because hydromechanical systems are inherently characterized by strong nonlinearities (e.g. quadratic terms of the orifice equation, metering notches on control valves spools, etc.) and unpredictable variability of system parameters (e.g. mass of the load handled by a crane, digging resistance for an excavator, etc.).

Through decades, several methods have been proposed and today almost each application uses a specific damping method, as it will be shown in Chap. 2. Among the proposed methods, those who were proven to reduce vibrations to an acceptable level have become widespread into commercial vehicles even if in many cases they complicate the hydraulic circuit and penalize other aspects, such as energy efficiency, and machine responsiveness. The limitations of those drawbacks, together with improved vibration damping effectiveness, cost reduction, and reliability are the goals of the method proposed in this dissertation.

Although mechanical vibrations in all mobile hydraulic machines are originated by similar physical mechanisms and they are typically characterized by frequencies below 20Hz, a general vibration damping method has not been formulated yet. Then, unlike current vibration damping method which are usually applicable to specific machines, the proposed control method formulation make it suitable to be applied to all valve controlled hydraulic machines. In order for the proposed method to be effective, the proportional valve bandwidth must be significantly higher than the frequency of the undesired dynamics. This condition, which is typically true for heavy machineries, is further investigated in the research.

1.2 Goals of the Research

The goal of the present work is to formulate and test an innovative vibration damping method applicable to all mobile hydraulic machines whose actuators are controlled by proportional directional valves. Detailed objectives for the proposed control method are:

A. Improvement of the machine dynamics by reducing mechanical vibrations of mechanical arms, load, as well as operator seat;
B. Reduction of the energy dissipations introduced by current vibration damping methods;
C. Reduction of system slowdowns introduced by current vibration damping methods.

The goal A is generally intended for all hydraulic machines; the goal B is related to those hydraulic machines in which the damping is introduced by means of energy losses on the main hydraulic transmission line; the goal C refers to those hydraulic machines in which the vibration attenuation is introduced by reducing the dynamics of the main transmission line.

The present work discusses all mentioned objectives by presenting two different case studies:

1. Case study 1 - Hydraulic Crane: the goal A and B are pursued.
2. Case study 2 - Wheel Loader: the goal A and C are pursued.

By analyzing to different machines, this work aims to illustrate the capability of the proposed control method to be applied to all valve controlled hydraulic machines.

1.3 Case Studies

Two case studies are considered in this work: the hydraulic crane and the wheel loader. Those two hydraulic machines are in most of the cases, as many other hydraulic machines, controlled via proportional directional valves, and therefore the proposed control method can be applied. The proposed control method is suitable not just for standard valve controlled systems (e.g. open center systems, load-sensing systems, etc.), it can also be applied to more recent independent metering techniques (the interested reader will find more details in the publication by Lumkes J., and Andruch J., 2011). Additionally, a similar formulation of the control algorithm can be adapted to machines based on displacement controlled actuation (the interested reader will find more details in the publication by Rahmfeld R., and Ivantysynova M., 2001). For all these different hydraulic circuit configurations, the bandwidth of the control valve must be sufficiently faster than the vibrations (as it often occurs in case of machines handling large loads).

The proposed method does not require the modification of the standard valve controlled hydraulic circuit, except for the addition of feedback sensors. The main focus of the research is on the use of pressure sensors on the workports of the proportional directional valve, and the alternative represented by the use of accelerometers on the vibrating part of the machine is studied to provide a comparison. In fact, although pressure sensors present

The following sections (Sect. 1.3.1 and 1.3.2) will provide a brief introduction of the two case studies with the main purpose to refer their features to the goals described in Sect. 1.2. The complete description of case study 1 (crane) is articulated in Chap. 5, 6, and 7, while case study 2 (wheel loader) is described in Chap. 8, 9, and 10.

1.3.1 Case Study 1: Hydraulic Crane

The hydraulic crane subject of this study is represented in Fig. 1 (Atlas®, model 125.1 A5, Atlas Maschinen Gmnh®, 1996). The crane is constituted by several mechanical arms, including: main boom, outer boom, telescopic boom and five telescopic stages. In Fig. 1, L represents the length in case all telescopic stages are retracted and W is the admissible load; L_1 represents the length in case only one stage is extended and W_1 is the admissible load; L_5 represents the length in case all stages are extended and W_5 is the admissible load.

The crane is designed for a truck installation; however, a special stand was designed to install it at Maha Fluid Power Research Center (Purdue University) in order to use it as experimental set-up as part of this research. More details about the experimental set-up will be provided in Chap. 5.

In general, hydraulic cranes are characterized by vibrations of the mechanical arms whose traditional damping method is based on:

- Introduction of dynamic orifices on pilot lines;
- Introduction of specific valves (e.g. pressurizing valve) on main transmission line;

- Use of counterbalance valves settings which are more energy dissipative than the settings which would guarantee their primary functions;
- Use of proportional directional valve designed to introduce meter-in and meter-out energy dissipations during the actuation of aiding loads.

Detailed description of the above mentioned techniques will be presented in Chap. 2 (state of the art).

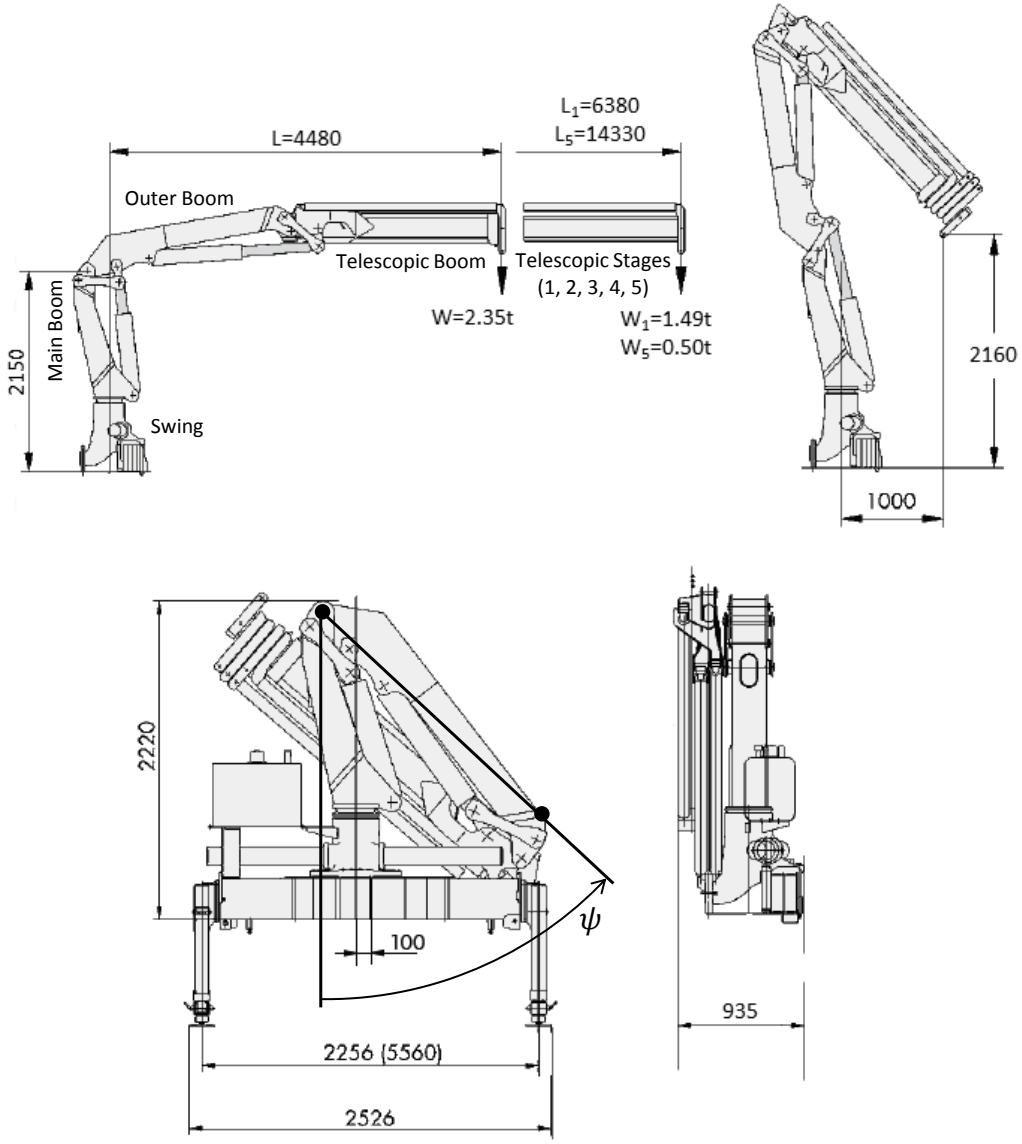

Fig. 1: Technical drawings of the reference hydraulic crane: dimensions, admissible loads, and nomenclature. All dimensions are in [mm]; maximum loads are indicated by W and are expressed in [t].

In this case study (with reference to the goals defined in Sect. 1.2) the goal A will be demonstrated by reducing of the oscillation of the outer boom. In particular, beside the addition of the pressure

sensors on the directional valve workport, no change will be made to the original hydraulic system. The increased stability obtained from goal A will allow to estimate the potential energy savings (goal B) which could be obtained by removing the above listed traditional vibration damping method. Moreover, those changes imply a simplification of the hydraulic system layout.

In the sections relative to the case study 1, the quantity which will be used to quantify the undesired vibration of the outer boom is the rotation angle ψ, as represented in Fig. 1. Therefore, from the control perspective, the problem can be represented by the simplified block diagram in Fig. 2a: C_n represents the normalized operator command (action of the operator on the outer boom control lever); i_n represents the normalized current to the section of the directional valve which controls the outer boom; p_{WR} and p_{WL} are the pressure at the raise and lowering workports of the section of the directional valve which control the outer boom; ψ is the outer boom rotation angle.

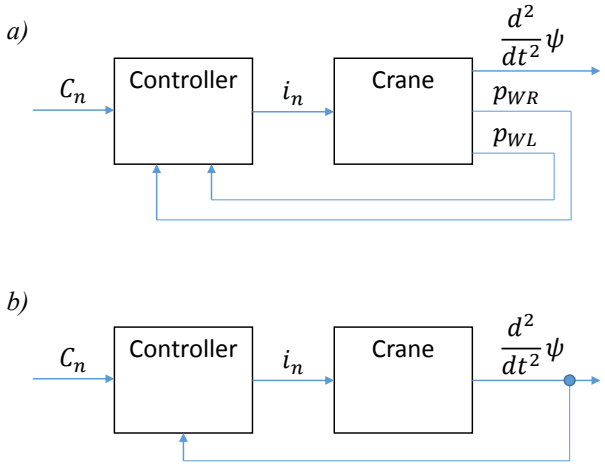

Fig. 2: Block diagrams representative of the control method applied to case study 1 - hydraulic crane: a) pressure feedback; b) acceleration feedback.

In addition, a model to estimate the acceleration of the mechanical arms from the pressure measurements will be presented in Sect. 6.4. The purpose of this analysis is to compare the performance of a pressure feedback based active vibration damping controller (with reference to Fig. 2a) with an alternative based on the direct measurement of the acceleration (with reference to Fig. 2b).

1.3.2 Case Study 2: Wheel Loader

In this study two wheel loaders were considered: CNH Case Construction 621F and 1021F (CNH America LLC ©, 2012).

The initial part of the research consisted in testing the proposed vibration damping method through a series of simulations performed with a numerical model of the machine 1021F. The numerical model was developed and validated by the research sponsor and additional features were added within this research as described in Sect. 9.2. The simulation results convinced the research

sponsor to proceed with the second part of the project, namely the experimental validation of the proposed control method. The research sponsor provided an electrohydraulic prototype of the machine 621F and additional sensors and control/acquisition hardware were added within this research as described in Sect. 8.2.

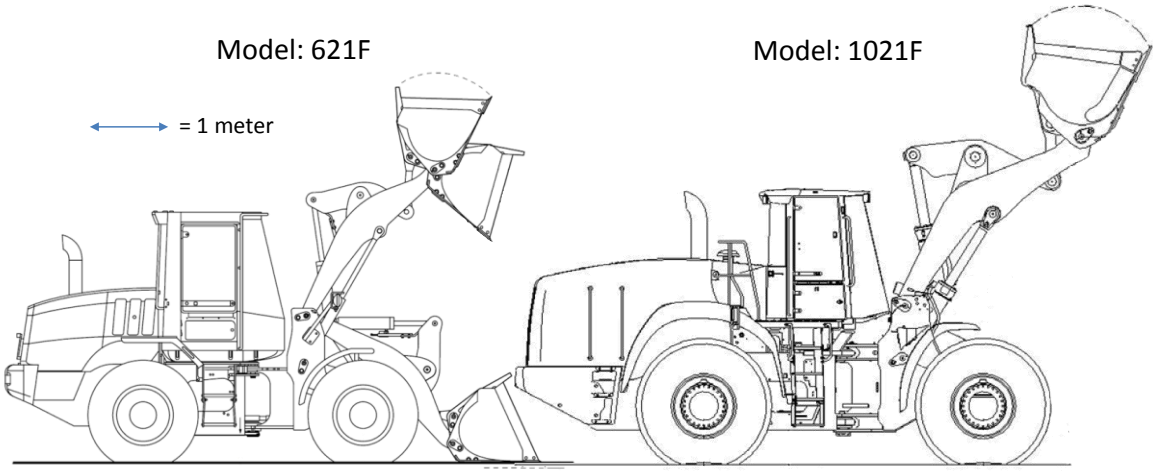

Fig. 3: Comparison between the wheel loaders Case Construction 621F and 1021F (CNH America LLC ©, 2012).

Table 1: Specifications of CNH Case Construction 621F and 1021F (CNH America LLC ©, 2012).

Specification	Model	
	621F	1021F
Maximum net power	128 kW	239 kW
Operating weight	12 tons	30 tons
Operating load	4.5 tons	8 tons

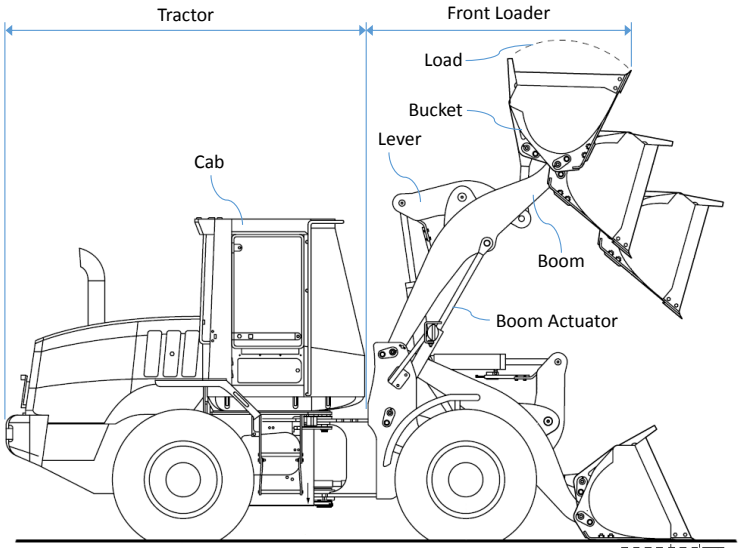

Fig. 4: Nomenclature used in this dissertation to refer to the different parts of the wheel loader.

A comparison between the dimensions of the two wheel loaders subject of this study is shown in Fig. 3. A summary of the specifications of the two machines is presented in Table 1. Both wheel loaders have a standard construction, and the terminology used in this work to refer to its different parts is illustrated in Fig. 4: the term *implement* will be used to refer to the assembly constituted by the hydraulic actuators, the mechanical arms, and the load.

Typical wheel loaders are not provided with shock absorbers and users report issues related to the vibrations originated by the travel on uneven ground. In particular, two problems arise:

- Vibrations of the cab during the vehicle travel reduce the operator comfort and they can represent a health hazard (International Organization for Standardization, 2004). This condition will be indicated as *operator comfort mode* (OC mode) in this document.
- Vibrations on the bucket during the travel of the machine may cause the loss of transported material. This condition will be indicated as *load transport mode* (LT mode) in this document.

The goal for this case study is the development of a control method to achieve the following goals:

1) Operator comfort mode improvement.
2) Load transport mode improvement.
3) Reduction of the implement slow-down and discontinuous motion caused by the state of the art vibration damping techniques (as it will be described in Chap. 2).

With reference to the goals of the research defined in Sect. 1.2, the first two goals of this case study are represented by the goal A, while the third goal is represented by the goal C. Additionally, the removal of the current vibration damping methods imply a simplification of the hydraulic system in terms of layout and tuning.

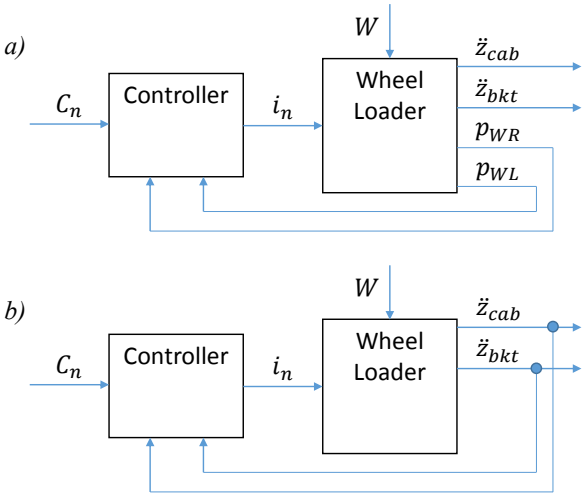

Fig. 5: Block diagrams representative of the proposed control method applied to case study 2 - wheel loader: a) pressure feedback; a) acceleration feedback.

In the sections relative to the case study 2 (Chap. 8, 9, and 10), the quantity which will be used to quantify the operator comfort mode is the cab vertical acceleration $\ddot{z}_{cab}$, and the quantity which will be used to quantify the load transport mode is the bucket vertical acceleration $\ddot{z}_{bkt}$. Therefore, from the control perspective, the problem can be represented by the simplified block diagram in Fig. 5: C_n is the normalized operator command (action of the operator on the outer boom control lever); i_n is the normalized current to the section of the directional valve which controls the outer boom; W is the disturbance produced by the uneven road profile z_{road}.

Fig. 5a shows the case in which the feedback signals are provided by pressure sensors (p_{WR} and p_{WL} are the pressures at the workports producing the raise and lowering of the boom respectively). Fig. 5b shows an alternative implementation in which the feedback signals are provided by accelerometers ($\ddot{z}_{cab}$ and $\ddot{z}_{bkt}$ are the cab and bucket vertical accelerations). Results obtained with the block diagram in Fig. 5a will be presented in Sect. 10.3, whereas a comparison between the results obtained with the block diagram in Fig. 5a and Fig. 5b are presented in Sect. 10.4.

CHAPTER 2. STATE OF THE ART

This chapter presents an overview of the vibrations damping methods for mobile machines. Several classifications can be made. A general classification which can be applied regardless of the type of hydraulic machine is based on the used technology and it distinguishes: hydromechanical (HM) and electrohydraulic (EH) methods. Strengths and weaknesses of the different methods will be pointed out. A final discussion will reference to some key features of the described methods to introduce the basic idea of the proposed vibration damping method.

2.1 Hydro-Mechanical Methods

HM methods are based on phenomena involving exclusively hydraulic and mechanical domains. Feedback loops are based exclusively on mechanical signals and hydraulic signals: the feedback signal choice is often limited to fluid pressure only. This aspect, together with the complexity of handling such signals (compared to electronic signals), represent one of the greatest limitations of HM methods.

The functioning of HM methods can be explored by recalling the analogy which relates the electrical voltage and current to the hydraulic pressure and flow respectively (Akers A. et al., 2006). Typically HM methods introduce into the system additional hydraulic resistance (HMR), additional hydraulic capacitance (HMC), or the combination of previous (HMRC).

Hydraulic resistance can be added to hydraulic pilot lines (HMRP), to modify the dynamics of pressure signals used as feedback of control valves. An example is provided by the common design of piloted directional valves which is represented in Fig. 6: adjustable orifices (O1 and O2) can be manually tuned to determine the response of the main stage (Cundiff J. S., 2002).

Another example is provided by the orifice on the pilot line of load sensing systems (Krus P., and Palmberg J. O., 1988) or on the pilot lines of counterbalance valves (in Fig. 7 it is presented the simplified schematic of the reference crane). In HMRP methods, due to the small flow rates involved, energy losses are also limited; however, being the size of the resistive element fixed, vibration damping effectiveness worsens moving away from the design operating condition.

Hydraulic resistance can also be added on main flow lines (HMRM) to modify the dynamics of the actuator. In case of load lifting machines, hydraulic resistance is typically introduced to damp the machine in case of aiding loads (Nervegna N., 2003).

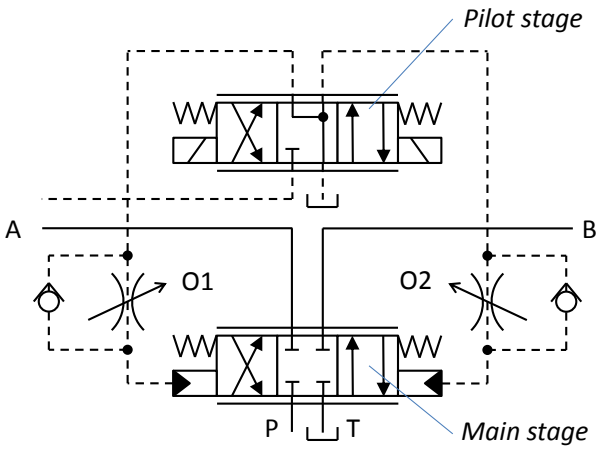

Fig. 6: Schematic of a traditional pilot operated proportional directional valve: O1 and O2 highlight the dynamics orifices on the pilot lines.

A first example is represented by particular settings of counterbalance valves. Basically, the primary functions of the counterbalance valves are: prevent over pressurization of the transmission line; hold the load in position when no flow is directed to the actuator; permit control of the actuator in the case of aiding loads. In many cases, counterbalance valves are also used to perform the function of reducing machine vibrations by means of special settings which are more dissipative respect to those required for the primary functions. Additional details about counterbalance valves functioning can be found in (Anderson, B. R. 2009). An example of counterbalance valve installation is presented in Fig. 7 for the reference crane.

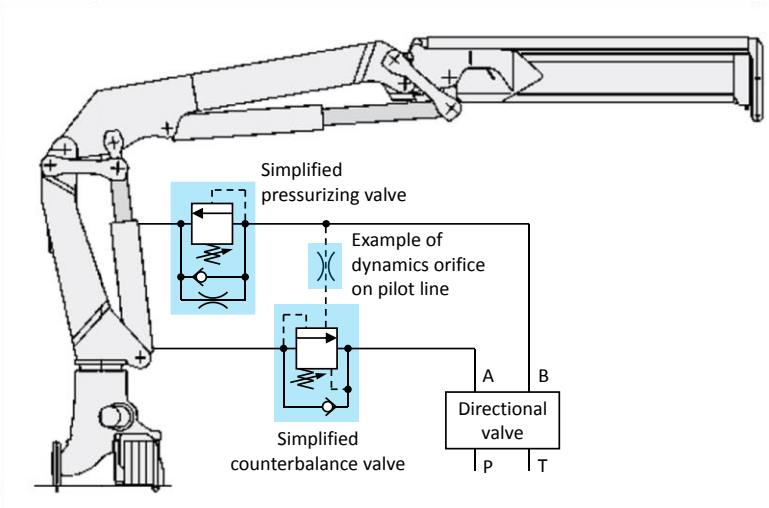

Fig. 7: Examples of traditional vibration damping methods used in hydraulic cranes.

Another example of HMRM, not as common as the previous, is represented by the so called “pressurizing valve” which is shown in the simplified schematic of the reference crane in Fig. 7. The pressurizing valve contributes to the reduction of vibrations in the lowering phase, but it also negatively affects the energy efficiency of the machine.

Another technique is represented by the specific design of proportional valves to meter both the input and output port of the actuator. With reference to Fig. 6, it would mean the main stage spool is designed in such a way to generate pressure drops from the P port to the actuator (meter-in) and from the actuator to T (meter-out) which are aimed to reduce vibrations in the machine. Unless rare cases where a feedback system is applied to automatically adjust the metering losses according to the entity of the vibrations (Sun Hydraulics Co., 2012), even HMRM methods are affected by vibration damping effectiveness worsening when moving away from the design operating condition.

Capacitance is typically added to the system (HMC) through the introduction of accumulators. In this case, the system damping is not increased since at first approximation the accumulator is not a dissipative component, nevertheless, it slows down the system dynamics and this in some cases is sufficient to achieve the desired system stability.

The combination of resistive and capacitive effects (HMRC) allows combining the benefits of both HMR and HMC methods: the resistance dissipates the vibration energy and the capacitance modifies the system responsiveness. A typical example is provided by the passive ride control (PRC) used to reduce vibrations perceived by the operators of wheel loaders during the travel on uneven ground. In the PRC, the so called stabilizing valve is interfaced between the boom actuator raise chamber and the accumulator, as it is shown in the simplified schematic in Fig. 8.

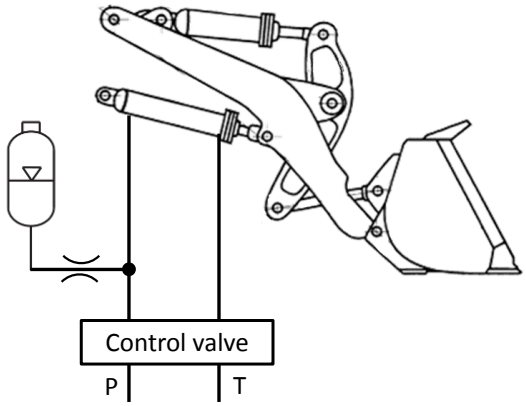

Fig. 8: Simplified schematic of the wheel loader passive ride control.

The cylinder chamber oscillation produces a flow which goes back and forth respect to the accumulator: the capacitance of the accumulator slows down this dynamics and the resistance of the stabilizing valve dissipates the oscillatory energy of the fluid. Further developments of this method are the use of feedback signals (mainly the accumulator pressure) to control the spool of the stabilizing valve as a sort of adaptation to the mass of the load. To improve the range of

operating conditions in which the vibration damping is effective, the hydromechanical feedback has to be implemented and the hydraulic circuit becomes more complicated: cost, volume and sizing effort increase as well. Additionally, boom controllability is reduced during those transient conditions in which accumulator pressure equalizes the actuator pressure.

2.2 Electro-Hydraulic Methods

EH methods use electrically actuated valves operated by an electronic controller. EH presents several advantages respect to EM. Firstly, it offers the opportunity to choose any signal to close the feedback loop. For example, direct measurement of the vibrations through accelerometers feedback sensors becomes possible. Additionally, EH makes possible to switch different control logics and control parameters to ensure optimal control performance even in case of different operating conditions. An example is represented by the possibility to switch the control target from load transport mode to operator comfort mode in case study 2 (wheel loader).

Consequently, EH methods present potential for system simplification (respect to closed loop HM methods), more efficient energy management (respect to HMR methods), and vibration damping effectiveness on extended range of operating conditions (respect to all HM methods).

Among the EH methods, it is possible to distinguish two categories:

- Electro-Hydraulic methods based on Direct feedback (EHD): methods in which the dynamics of the vibrating body is directly measured (by means of accelerometers, inertial platforms, linear position sensors, etc.);
- Electro-Hydraulic methods based on Indirect feedback (EHI): methods in which the dynamics of the vibrating body is indirectly measured. In this case, feedback sensors are used by the control algorithm to estimate the vibrating body dynamics.

EH methods have been successfully applied to a large variety of fields, including: active suspensions (Hong K. S. et al., 2002; Guglielmino E., and Edge K. A., 2001); vehicles braking systems (Milanes V. et al., 2002); hydraulic robots (Conrad F., 1993); earthquake simulators (Plummer A. R., 2007); and other applications (Edge K. A., 2003).

However, in mobile hydraulic machines, mechanical vibrations are in most of the cases still today addressed through HM methods, specifically designed for each application. A first general reason is that for these applications, malfunctioning can seriously harm the safety of people and therefore well-established technologies (HM) are typically preferred to newer ones (EH). Beside this, another fact is that the most convenient choice of the feedback signal from the control theory point of view might be in practice unusable. In other words, although the controller design is easier in case of EHD respect to EHI method, the first option is often unreliable in fluid power applications because the sensors are subject to harsh operating conditions and consequently excessive mechanical and environmental stresses.

One of the rare exceptions to this statement is represented by the active seat used in construction and agricultural machines (Nevala K., and Jarviluoma M., 1997), which is represented in the simplified schematics is Fig. 9. This method feeds-back the acceleration of the seat and the controller manages the motion of a linear actuator installed underneath the seat to reduce the vibrations perceived by the operator. The active seat is an example of EHD which fulfills reliability requirement and it is today widespread. However, further diffusion is limited by the additional system complexity and costs. Moreover, active seat lacks of generality because it does not reduce the entire machine vibrations, it just does it locally.

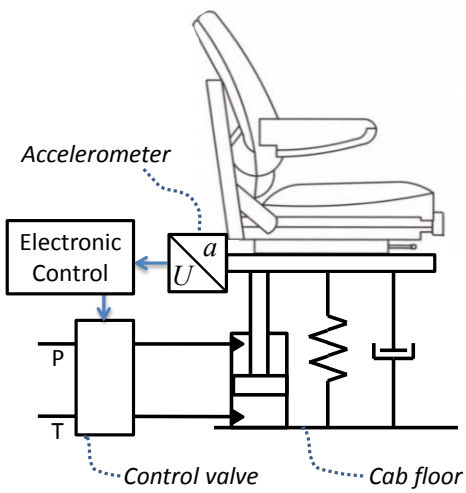

Fig. 9: Simplified schematics of the "active seat".

Unlike EHD methods, EHI methods can be designed in order to use other types of sensors which can be installed in a more reliable assembly. In particular, pressure feedback control uses pressure as feedback signal since pressure sensors can be located in an area of the machine which is protected from mechanical and environmental stress. Pressure feedback control has been applied both to valve controlled systems (to control the directional valve spool, e.g. Krus P., and Palmberg J. O., 1988) and displacement controlled systems (to control the swash plate angle, e.g. Rahmfeld, R., and Ivantysynova, M., 2004). In both cases, pressure feedback control basically measures the pressure oscillation in the actuator cylinder and uses that information to estimate the mechanical vibration. Finally, in order to cancel the vibration, the controller properly manages the flow to the actuator.

In the case of displacement controlled machines, the control methods in literature typically are not based on the exclusive use of pressure sensors (Williamson C. A., et al., 2009), which are often used in combinations with other sensors.

In the case of valve controlled machines, some of the control methods in literature require the implementation of large part of the machine model into the electronic controller (Krus P., and

Gunnarsson S., 1993; Bu F., and Yao B., 2001; DeBoer C. C., and Yao B., 2001; Garimella P., and Yao B., 2002; Cao J., et al., 2007). Consequently, large part of the controller design has to be repeated for every application: this lack of generality in the controller formulation and tuning is one of the causes which prevented the diffusion into commercial machines of those methods.

2.3 Discussion of the Method Proposed in this Research

To summarize the previous sections, Table 2 reports the main features of the presented methods. Considering the potential of pressure feedback control, this work aims to propose a further development in this direction, whose main innovations are:

- Adaptive implementation: The proposed controller exploits the potential of the EH methods of switching control logic according to the operation of the machine. Additionally, controller gains are managed by a gain scheduler (Åström K. J., and Wittenmark B., 2008) in order to adapt to the variation of the operating condition.
- Non-model-based control parameters tuning. In order to tune the parameters of the controller, no analytical model of the machine is required. In fact, the tuning process can be performed directly through experimentation of the actual machine. Basically, for a specific input of the machine and set of control parameters, vibrations are measured. A new formulation of the extremum seeking algorithm (Ariyur K. B., and Krstić M., 2003) is used as offline iterative optimizer to determine the set of control parameters suitable to minimize the vibrations.

Table 2: Summary of the vibration damping method and their distinctive features.

Technology			Example	Feedback signal type	Adaptation to varying operating condition	Physical principle exploited to attenuate the vibration	Pros	Cons
HM	HMR	HMRP	Dynamic orifices on pilot lines of counterbalance valves.	Almost exclusively pressure signal.	If any, few parameters are adapted because of the complexity of dealing with pressure signals (compared to electrical signal).	Low pass filtering of pilot signals: although the system damping does not increase, the system dynamics is slowed down.	Energy efficient; Simple.	Low performance; Slow system response.
		HMRM	Spring setting and area ratios of counterbalance valves above the load holding settings.			Increased damping of the transmission line.	High performance.	Energy dissipation.
	HMC		Accumulators on main transmission line.			Although the system damping does not increase, the system dynamics is slowed down.	Energy efficient.	Low performance; Slow system response.
	HMRC		Passive ride control in wheel loaders.			Energy content of oscillatory term of actuator pressure is dissipated across resistance.	High performance; Energy efficient.	System complexity.
EH	EHD		Trajectory tracking; Active seat.	Electrical signals coming from sensors which directly measure acceleration, velocity or position of the vibrating body.	All the electrical signals can be easily handled by the electronic controller.	Operation of one or more actuators to produce a control action which is out-of-phase respect to the vibrations.	High performance; Energy efficient.	Reliability issues; System complexity; Costs.
	EHI		Pressure feedback control method.	Electrical signal coming from any sensor except those listed in EHD.			High performance; Energy efficient; System simplicity.	Control algorithm formulation.

CHAPTER 3. VIBRATIONS IN MOBILE HYDRAULIC MACHINES

This chapter presents a general explanation of the phenomenon of vibrations in mobile hydraulic machines.

First, the oscillatory nature of hydraulic systems will be illustrated by focusing on an elementary system composed by a hydraulic actuator and an inertial load. To make the analysis of its dynamics clearer, this system will be transformed into an equivalent lumped parameter mechanical system.

Next, the features of the hydraulic circuit will be discussed in order to show it can be responsible for the attenuation or damping of the systems oscillations.

Then, the inputs for the case of hydraulic machines will be discussed. In fact, even in inherently oscillatory systems, actual oscillations occur only if it is excited by specific inputs. The distinction between desired inputs (operator command) and undesired inputs (disturbance) will be pointed out.

3.1 Oscillatory Nature of Hydraulic Systems

This section describes the basics of the vibration mechanism taking place in hydraulic machines. The simplest load kinematic is sufficient for this purpose; therefore, the case in Fig. 10a will be taken as reference. In this case, the complex kinematics of the implement is simplified to a pure inertial case.

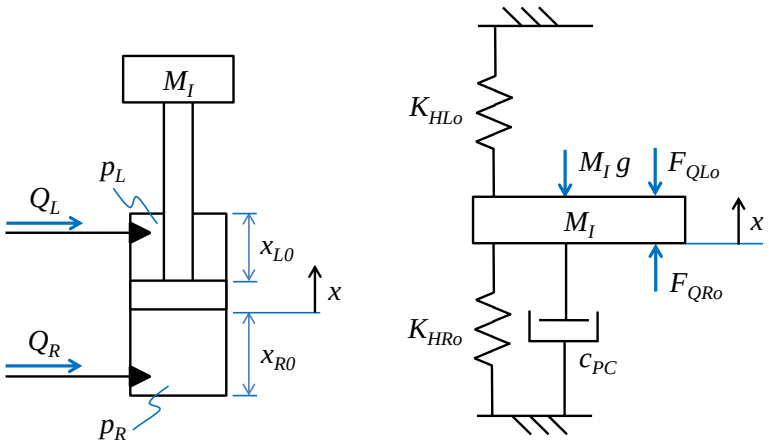

a) *b)*

Fig. 10: a) Elementary hydraulic actuator system; b) Analogous lumped parameter mechanical system.

The implement mass is evaluated as the sum of the masses of rod, piston, mechanical arms and load: $M_I = M_{RP} + M_A + M_L$. The flows entering the raise and lowering chambers are indicated by Q_R and Q_L respectively. The pressure in the raise and lowering chambers are indicated by p_R and p_L respectively. The motion of the actuator is along the x-axis. The position of the actuator will be identified by x and in this simplified case it coincides with the implement mass element position. The initial dimensions of the raise and lowering chamber along the x-axis are indicated by x_{R0} and x_{L0} respectively. For this system, it is possible to write the equation of motion for the load as follows:

$$M_I \ddot{x} = \sum_i F_i \tag{3.1}$$

The force required to operate the implement is larger than the static friction between piston and cylinder, therefore, this term will be neglected. The motion equation can therefore be rewritten as follows:

$$M_I \ddot{x} + c_{PC} \dot{x} = p_R A_R - p_L A_L - M_I g \tag{3.2}$$

where: A_R and A_L represent the area of the raise and lowering sides of the actuator; c_{PC} represents the piston-cylinder viscous friction coefficient. Assuming p_R and p_L known for every time (e.g. measured), it is possible to express the dynamics relating the pressure in the cylinder chambers and the implement position:

$$x(s) = \frac{1}{s\left(M_I s + c_{PC}\right)}\left(p_R A_R - p_L A_L - M_I g\right) \tag{3.3}$$

Equation 3.3 is a result which will be used later but it is still not the most convenient way to explain the vibration in the system represented in Fig. 10a: rearranging the terms it is possible to obtain the analogous lumped parameter 1D mechanical system represented in Fig. 10b.

The pressure build-up equations for the two chambers of the actuator are:

$$\begin{cases} \dot{p}_R = \dfrac{B}{V_R}\left(Q_R - \dot{V}_R\right) \\ \dot{p}_L = \dfrac{B}{V_L}\left(Q_L - \dot{V}_L\right) \end{cases} \tag{3.4}$$

The volumes of each chamber respect to the implement position are

$$\begin{cases} V_R = V_{R0} + A_R x = A_R\left(x_{R0} + x\right) \\ V_L = V_{L0} - A_L x = A_L\left(x_{L0} + x\right) \end{cases} \tag{3.5}$$

where V_{R0} and V_{L0} represent the initial volumes. Then Eq. 3.4 becomes

$$\begin{cases} \dot{p}_R = \dfrac{B}{V_R}\left(Q_R - A_R\dot{x}\right) \\ \dot{p}_L = \dfrac{B}{V_L}\left(Q_L + A_L\dot{x}\right) \end{cases} \tag{3.6}$$

The pressure in each chamber can then by expressed as

$$\begin{cases} p_R = p_{R0} + \dfrac{B}{V_R}\int Q_R dt - A_R\dfrac{B}{V_R}x \\ p_L = p_{L0} + \dfrac{B}{V_L}\int Q_L dt + A_L\dfrac{B}{V_L}x \end{cases} \tag{3.7}$$

Multiplying both sides of the equations times the respective surfaces, it is possible to express Eq. 3.7 in terms of forces

$$\begin{cases} F_R = A_R p_{R0} + \dfrac{B}{x_{R0}+x}\int Q_R dt - \dfrac{A_R B}{x_{R0}+x}x \\ F_L = A_L p_{L0} + \dfrac{B}{x_{L0}-x}\int Q_L dt + \dfrac{A_L B}{x_{L0}-x}x \end{cases} \tag{3.8}$$

It is then possible to introduce the following terms:

Hydraulic stiffness (nonlinear):

$$\begin{cases} K_{HR} = \dfrac{A_R B}{x_{R0}+x} \\ K_{HL} = \dfrac{A_L B}{x_{L0}-x} \end{cases} \tag{3.9}$$

Forces due to flow entering the chambers (nonlinear):

$$\begin{cases} F_{QR} = A_R p_{R0} + \dfrac{B}{x_{R0}+x}\int Q_R dt = A_R p_{R0} + \dfrac{1}{C_{HR}}\int Q_R dt \\ F_{QL} = A_L p_{L0} + \dfrac{B}{x_{L0}-x}\int Q_L dt = A_L p_{L0} + \dfrac{1}{C_{HL}}\int Q_L dt \end{cases} \tag{3.10}$$

The terms C_{HR} and C_{HL} represent respectively the nonlinear hydraulic capacitance of the raise and lowering chambers. For the terms C_{HR} and C_{HL}, as well as terms K_{HR} and K_{HL}, the larger the cylinder dead volume and transmission lines volume are, the smaller the effect of the nonlinearity is. The linearization of Eq. 3.10 gives the terms indicated by the subscript "*o*"

$$\begin{cases} F_{QRo}(s) = A_R p_{R0} + \dfrac{1}{C_{HRo} s} Q_R \\ F_{QLo}(s) = A_L p_{L0} + \dfrac{1}{C_{HLo} s} Q_L \end{cases} \quad 3.11$$

The motion equation of the system in Fig. 10a (Eq. 3.2) can be rewritten for the analogous mechanical system in Fig. 10b:

$$M_I x s^2 + c_{PC} x s + x\left(K_{HLo} - K_{HRo}\right) = F_{QRo} - F_{QLo} - M_I g \quad 3.12$$

Rearranging the terms it is possible to show the position of the actuator can be controlled modulating the terms F_{QRo} and F_{QLo}

$$x(s) = \frac{1}{M_I s^2 + c_{PC} s + \left(K_{HLo} - K_{HRo}\right)} \left(F_{QRo} - F_{QLo} - M_I g\right) \quad 3.13$$

Equation 3.13 is the forced response of a second order system, whose natural frequency and damping ratio are respectively:

$$\begin{cases} \omega_N = \sqrt{\dfrac{K_{HLo} - K_{HRo}}{M_I}} \\ \zeta = \dfrac{c_{PC}}{2\sqrt{M_I\left(K_{HLo} - K_{HRo}\right)}} \end{cases} \quad 3.14$$

In case of *free response*, the oscillations are caused exclusively by the exchange of kinetic energy of the mass and the potential pressure in the hydraulic stiffness. Differently, in case of *forced response*, oscillations are depending on the hydraulic system as well, as it will be shown in the next section (Sect. 3.2).

Observing the expression of the damping ζ, it is possible to see that large M_I, which is typical in hydraulic machines, promotes vibrations. The natural frequency denotes the rate of most effective conversion between those two forms of energy. The considerations presented in this section are based on an extremely simplified case, however their validity is general. It is however important to at least mention the fact that hydraulic machines are typically composed by multiple actuators and multiple mechanical bodies: multiple natural frequencies and vibration modes can be observed.

Fluid power is typically used to handle large loads, and consequently the mass of the entire implement is large. The result is that the vibrations are characterized by large energy content and ω_N is typically low (in most applications it is less than 15Hz). The natural frequencies of the mechanical arms are typically larger and their energy content is lower. Consequently, vibration modes of the mechanical structure of the machine are excluded by considering the mechanical structure as it is composed by rigid bodies.

3.2 Attenuation/Amplification of Vibrations Caused by the Hydraulic Circuit

Assuming oscillations are occurring in the system in Fig. 10b (for example caused by the mechanism discussed in Sect. 3.1 or by an oscillating hanging load), the mechanical vibrations of x would be damped in case $F_{QR} - F_{QL}$ is 180deg out-of-phase with respect to the oscillation of x. A similar statement can be expressed with reference to the analogous system in Fig. 10a; Eq. 3.7 shows that two cases can occur:

- *Case 1 - vibration damping*: The mechanical vibration of x would be damped in case the oscillation of Q_R is +90deg out-of-phase with respect to the oscillation of p_R and the oscillation of Q_L is +90deg out-of-phase with respect to the oscillation of p_L.
- *Case 2 - oscillation amplification*: The mechanical vibration of x would be amplified in case the oscillation of Q_R is -90deg out-of-phase with respect to the oscillation of p_R and the oscillation of Q_L is -90deg out-of-phase with respect to the oscillation of p_L.

This work focuses on valve controlled hydraulic machines; therefore, the general valve controlled system hydraulic circuit can be represented in the simplified schematic in Fig. 11.

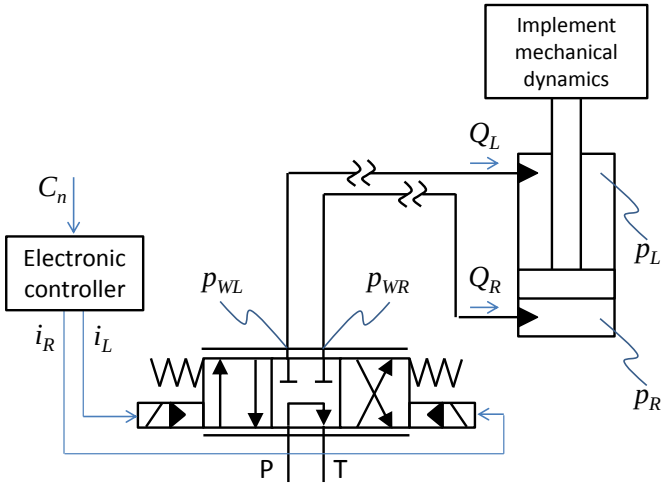

Fig. 11: General valve controlled actuator (e.g. open center spool).

In this example, a proportional directional valve (open center) is considered, however the next discussion applies even to other valve controlled architectures. The T port is connected to the tank. The P port is connected to the power supply and it is intentionally left unconnected because this discussion applies for any type of power supply unit.

Every possible combination of ports is characterized by specific metering area A_i, pressure drop Δp_i, and flow rate Q_i: from P to T port $(A_{PT}, \Delta p_{PT}, Q_{PT})$; from P to R port $(A_{PR}, \Delta p_{PR}, Q_{PR})$; from P to L port $(A_{PL}, \Delta p_{PL}, Q_{PL})$; from R to T port $(A_{RT}, \Delta p_{RT}, Q_{RT})$; from L to T port $(A_{LT}, \Delta p_{LT}, Q_{LT})$. The flow rates Q_R and Q_L are equal to:

$$\begin{cases} Q_R = Q_{PR} - Q_{RT} \\ Q_L = Q_{PL} - Q_{LT} \end{cases} \quad 3.15$$

In case of valve controlled systems, for a generic metering area A_i, the relationship between pressure drop Δp_i and the resulting flow Q_i is

$$Q_i = c_d A_i \sqrt{\frac{2\Delta p_i}{\rho}} \quad 3.16$$

If the pressure at the P port p_P were constant, then, according to Eq. 3.16, the flow rates and the pressure drops would be in-phase. This would be an intermediate situation between the case 1 (+90deg out-of-phase, vibration damping) and case 2 (-90deg out-of-phase, vibration amplification): vibrations would be governed exclusively by the mechanism described in the previous section (Sect. 3.1). However, in real applications, some additional dynamics may be present:

- Dynamics of the pressure p_P with respect to other variables (e.g. raise chamber cylinder pressure p_R)
- Dynamics between the pressures at the workports (p_{WR}, p_{WL}) and those in the cylinder chambers (p_R, p_L):
    - Long transmission lines;
    - Additional components on the transmission lines (e.g. counterbalance valves).

This additional dynamics might introduce phase shifts between the terms Q_i and Δp_i from Eq. 3.16. The phase shift may cause the occurrence of case 1 (vibrations damping) or case 2 (vibrations amplification).

A well-known problem of this sort is the vibrations during the operation of aiding loads in presence of counterbalance valves. In this example, oscillations of p_R and p_L produce the oscillations of the counterbalance metering area which, similarly to Eq. 3.16, gives rise to a oscillating flow which in some conditions might be consistent with case 2 (vibrations amplification). The solution to this problem is particularly complicated and it is still today solved in an ineffective way. In fact, the range of loads handles by these machines can be large, but the counterbalance valve design is optimal only for a specific load.

The oscillations mechanism due to the hydraulic circuit (forced response of the system in Fig. 10) is typically characterized by faster frequencies than the free response of the system in Fig. 10 (which was presented in Sect. 3.1). When the oscillation mechanism due to the hydraulic circuit occurs, it often becomes more relevant than the frequencies than the free response of the system in Fig. 10: the free response can only cause vibrations; the forced response theoretically can cause instabilities.

3.3 Machine Inputs and Disturbances

The step response of an underdamped system is oscillatory; however, a different input may not cause any oscillation in the system. Therefore, in order to discuss the vibrations in hydraulic systems it is not sufficient to focus exclusively on the system itself; a broader view has to include machine inputs as well.

Two types of machine inputs can be distinguished:

- The *operator command* C_n is an input provided to the machine to obtain a desired effect (e.g. user input to raise the boom of the crane);
- The *disturbance* W is an input which produces undesired dynamics. An example of disturbance W is presented in Fig. 12.

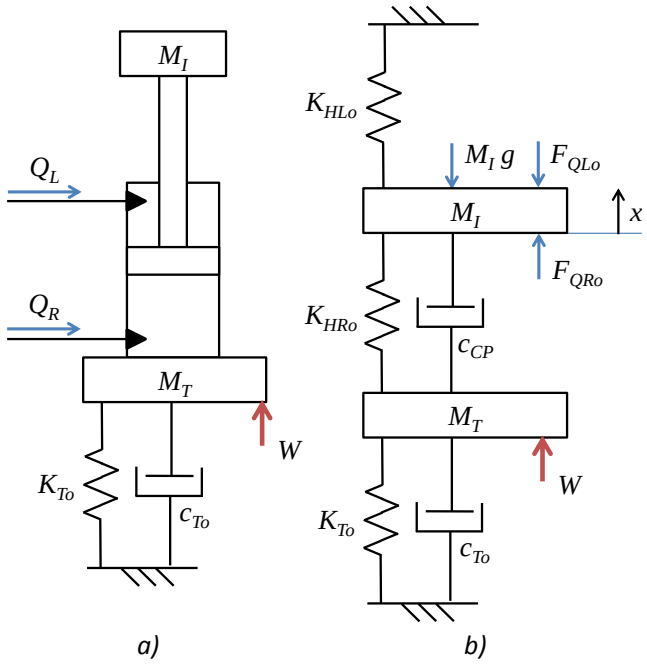

Fig. 12: Example of disturbance on the tractor of the machine: a) Elementary hydraulic system; b) Analogous mechanical system.

The example reported in Fig. 12 is similar to what is observed in case study 2: W consists in the forces exerted by the uneven road profile to the wheel loader tractor (whose mass is M_T) during the travel.

In hydraulic machines, both the operator command C_n and the disturbance W are often discontinuous (e.g. step, impulse…). Consequently, also the input to the system in Fig. 12b, namely F_{QRo} and F_{QLo}, are discontinues. In some cases, even smooth and continuous machine inputs determine discontinuous F_{QRo} and F_{QLo} because of the hydraulic system as well as the mechanical one are characterized by numerous discontinuous nonlinearities (e.g. saturations, dead-band, end-stop, backlash…).

CHAPTER 4. PROPOSED CONTROL METHOD

This section describes the proposed control method under a general perspective: the application to the case studies 1 (hydraulic crane) and 2 (wheel loader) will be presented in Chap. 5, 6, and 7 and Chap. 8, 9, and 10.

The proposed control method is based on the pressure feedback control principle: the hydraulic system will be shown to illustrate that no changes to the standard valve controlled layouts are required except for the addition of pressure sensors on the directional valve in correspondence of the workports of the controlled actuators.

Then, it will be demonstrated that the feedback signal from the proposed pressure sensors configuration may be sufficient to describe the vibrating body dynamics. In particular, the main challenge is here represented by the fact the observation is based exclusively on the measured signals (pressure at the workports and output electric current). The approximations introduced to make possible this indirect observation will be presented.

Previous pressure feedback control attempts on valve controlled systems showed limitations which prevented the diffusion in commercial machines. To overcome these problems, this work proposes a series of innovations which will be illustrated in this chapter. Firstly, the controller adaptation to the operating conditions of the machine is introduced to compensate the most relevant nonlinearities of the system. Second, the control parameters tuning is based on an innovative non-model-based optimization algorithm: being non-model-based it is suitable to return the best set of control parameters to reduce vibrations by means of an iterative routine which analyzes the actual machine dynamic response.

Finally, it will be shown how the proposed controller structure can be modified so it can be used in case of acceleration feedback. In the chapters relative to the case studies, pressure feedback and acceleration feedback based controller will be compared to outline which one of the two alternatives is more convenient in for those applications.

4.1 Pressure Feedback Control Principle

The proposed control method is designed in order to be applicable to all valve controlled mobile hydraulic machines. To fulfill this requirement, as pointed out in Chap. 2, the pressure feedback

control method was chosen among competing EH methods mainly for its reliability and simple hydraulic layout, which is shown in Fig. 13.

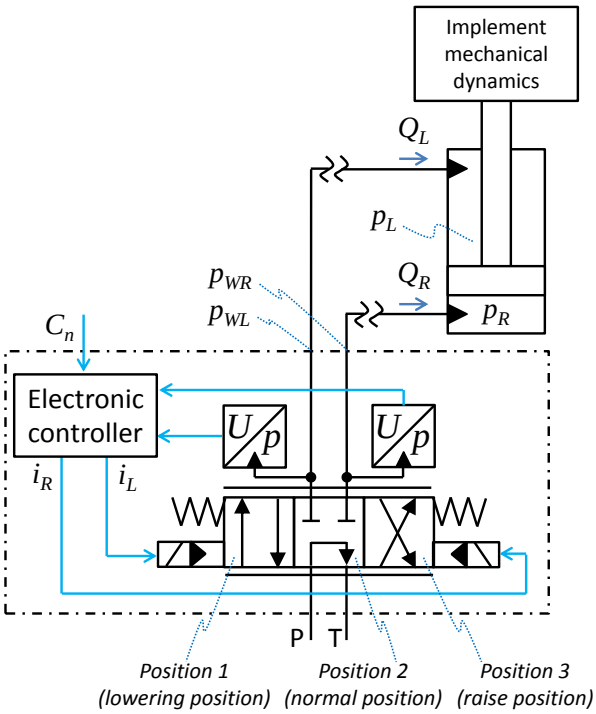

Fig. 13: Hydraulic circuit required to implement the proposed pressure feedback control method.

The operator command is indicated by C_n (normalized). The electric currents to the directional valve will be indicated by i_n (normalized). According to the sign of i_n, the actual current is sent to the raise solenoid (i_R) or to the lowering solenoid (i_L). The pressure in the raise and lowering side of the cylinder are p_R and p_L. P and T represent the power supply and return to tank port respectively. The pressure sensors can be located directly on the directional valve block, in correspondence of the workports. The pressures at the raise and lowering workports are indicated by p_{WR} and p_{WR}. This location protects the pressure sensors from environmental and mechanical stress, providing reliability and compactness to the assembly.

Different applications use specific components on the transmission lines from the directional valves to the actuator: the break lines in Fig. 13 indicate the proposed control can operate for any dynamics of these lines. In general, long lines might give raise to dynamics who can affect the system vibrations. Moreover, additional components can be located on those lines: in case study 1, counterbalance valves are typically flanged on the raise ports of the actuators of hydraulic cranes (Sect. 5.1); in case study 2, flow compensators are often mounted in proximity of the directional valve workports . For these reasons, the pressure in the cylinder (p_R, p_L) might differ from those at the workports , which are indicated by p_{WR} and p_{WR}.

It can be observed the pressure feedback control does not require any modification of the original hydraulic circuit, it just requires the addition of a pressure sensor on the workport of each controlled actuator. This simple hydraulic circuit can be easily applied to all valve controlled hydraulic machines. Moreover, industrial development of this method may lead to the production of specific valve blocks which integrate sensors and electronic controller: reliability, compactness and cost would benefit from this. Pressure feedback control method may also present a benefit in terms of system sizing effort. In fact, many alternative vibration damping methods are based on the use of additional hydraulic components which have to be properly sized for each application by means of a time consuming trial and error procedure.

From control perspective, the pressure feedback control method can be represented by the block diagram in Fig. 14.

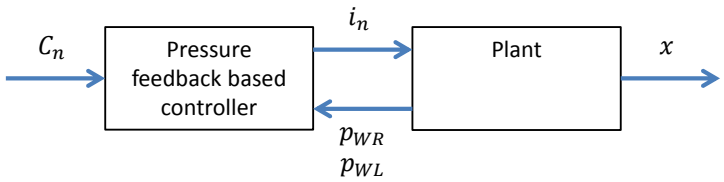

Fig. 14: Block diagram representing the pressure feedback control method inputs, outputs, and feedback signals.

Plant is a term often used in controls to refer to the entire system, except the controller. The vibrating body dynamics is represented by x: it can be a point of the implement, x_I (like in case study 1), or a point of the tractor, x_T (like in case study 2). It is possible to divide the vibrating body dynamics into two terms:

$$x = x_D + x_U \tag{4.1}$$

The term x_D represents the desired dynamics (ideal, in absence of vibrations), while the term x_U represents the undesired (oscillating) component. The feedback signals are p_{WR}, p_{WL} (measured by specific pressure sensors) and i_n (measured or evaluated by the electronic controller). The controller, in order to be effective, has to be able to perform two tasks:

- *Task 1 – estimation of the vibration*: The controller has to determine the dynamics vibrating body x (or at least x_U) on the basis of the available measurements: p_{WR}, p_{WL}, and i_n.
- *Task 2 – control action*: The controller has to command a control action i_n suitable to selectively reduce x_U.

In Sect. 3.1, it was shown that the pressure feedback control can perform task 2 (control action) by using i_n to modulate the flow entering the raise and lowering chamber of the actuator (Q_R, Q_L). Task 1 (estimation of the vibration) is the main challenge in the design of the pressure feedback control method. In fact, the estimation of the vibration would be straightforward in case it was directly measured through accelerometers or linear displacement sensor. Differently, in case of pressure

feedback control method, the vibrations have to be indirectly estimated from the available feedback signals, namely the measurements of p_{WR}, p_{WL}, and i_n.

4.2 Estimation of the Vibration with Pressure Feedback Method

In general, the estimation of the vibrations of x from the available measurements (p_{WR}, p_{WL}, from pressure sensors; i_n, controller output) introduces some approximations. Those approximations will be described in the next subsections. The exact (without approximations) model of the plant is represented in Fig. 15.

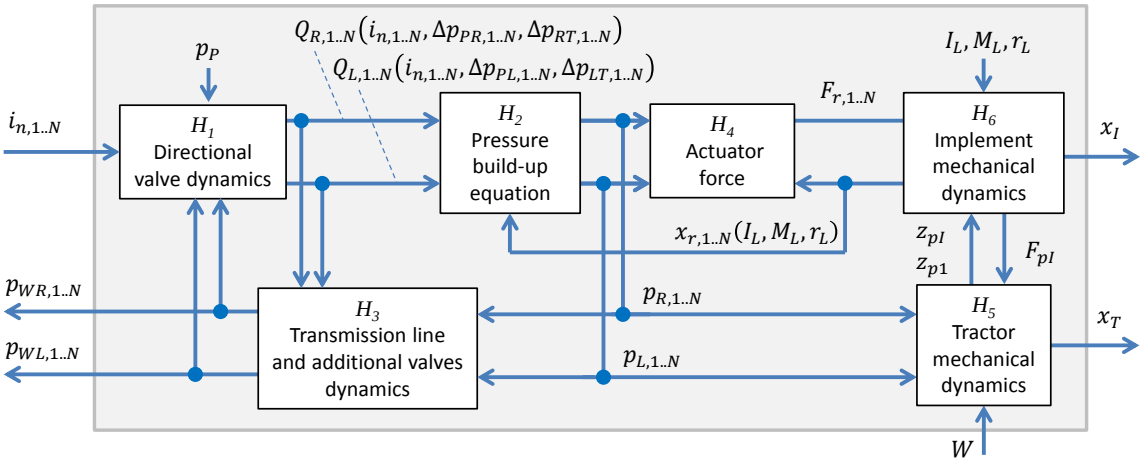

Fig. 15: Exact plant model in absence of approximations (traditional lumped parameters modeling approach).

The schematic is relative to a machine whose implement consists in N actuators. At this stage of the research, it is assumed that, among the N actuators of the machine, the motion of just one actuator at a time is performed.

The diagram is constituted by blocks representing the dynamics of different portions of the plant: H_1, directional valve dynamics; H_2, pressure build-up equation of the raise and lowering cylinder chamber fluid volumes; H_3, transmission lines and additional valve dynamics; H_4, actuator force; H_5, tractor mechanical dynamics; H_6, implement mechanical dynamics.

It is possible to observe that in the schematic in Fig. 15, the available measurements (p_{WR}, p_{WL}, and i_n) would not be sufficient to observe all states of the plant model. In fact, additional variables would be required to do so: p_P, directional valve P port pressure; I_L, inertia of the load respect to the axis through its center of mass; M_L, load mass; r_L, distance between the load center of mass and the implement pivot; W, disturbance acting on the tractor (as it was defined in Sect. 3.3). Among the previously listed variables, only W, being a disturbance, might remain unobserved by the controller, as it will be outlined in Sect. 9.3 for the case study 2 (wheel loader). The dependency of x on other variables (p_P, I_L, r_L) will be canceled by some specific assumptions, in order to make

all states on the plant identifiable to the controller on the basis of the available measurements (p_{WR}, p_{WL}, and i_n). Additionally, the available measurements (p_{WR}, p_{WL}, and i_n) will be used to observe the load mass M_L. The final model plant comprehending all the introduced approximation is showed in Fig. 16.

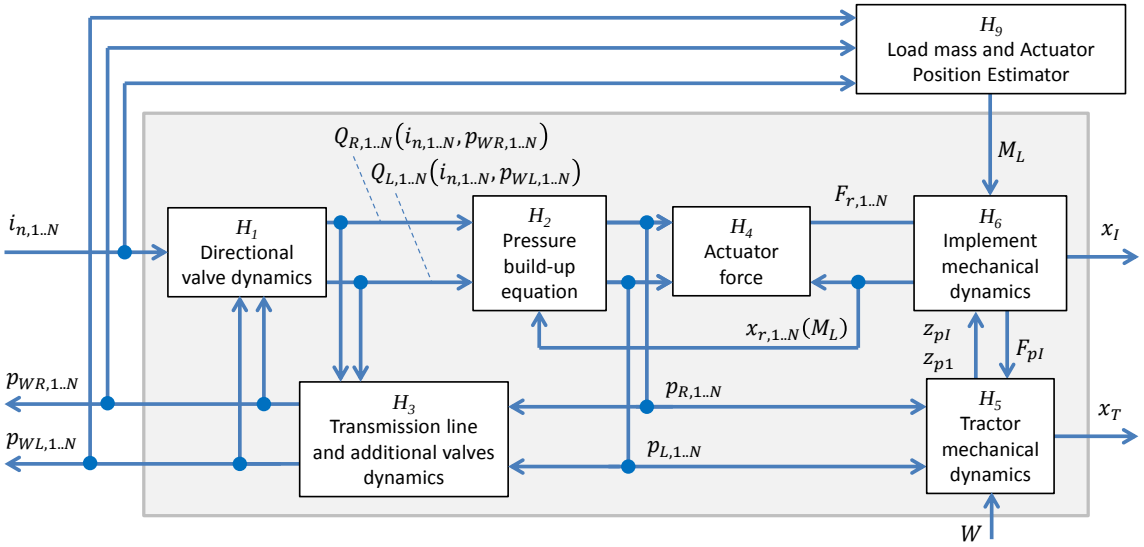

Fig. 16: Approximated plant model which allows the observation of all states of the system on the basis of the available measurements (p_{WR}, p_{WL}, and i_n).

In this case, unlike in Fig. 15, all states of the plant model (and consequently also the dynamics of x_I and x_T) are determined by the following variables: p_{WR}, p_{WL}, and i_n, which are measured; the load mass M_L, which can be estimated from the measured ones.

The next subsections will describe all approximations adopted to obtain the approximated plant model (Fig. 16) from the exact one (Fig. 15).

4.2.1 Directional valve dynamics (H_1)

The block H_1 represents the directional valve dynamics. This block determines the flow to the raise and lowering chambers of the actuator (Q_R, Q_L). This block is typically modeled according to Eq. 3.15 and 3.16. The metering areas A_i of the directional valve can be typically approximated by linear dynamics whose input is the current to the proportional solenoids of the directional valve i_n (Cristofori D., and Vacca A., 2011). Unlike i_n, the controller does not have a direct measure of the pressure drops Δp_i because p_P and p_T are not measured. It is possible to assume p_T=0 during the entire operation of the machine, however, another condition has to be added to have an estimate of p_P.

A solution would be represented by the addition of a further pressure sensor on the P port of the directional valve, like it was proposed by Garimella P., and Yao B. (2002). However, this research is aimed to obtain satisfactory control with the minimum number of pressure sensors; therefore in

this section the pressure sensor on the P port is not included. Since p_P is not directly measured, additional assumptions have to be made in order to find a relationship suitable to describe the flow rates Q_R and Q_L from the available measurements.

Two examples are represented by the two case studies of this work. In Sect. 6.2 it will be shown for case study 1 (crane) that the block H_1 can be approximated by the relationships: $Q_R(i_n, p_{WR})$ and $Q_L(i_n, p_{WL})$. In Sect. 9.2.2 it will be shown for case study 2 (wheel loader) that the block H_1 can be approximated by the relationships: $Q_R(i_n)$; $Q_L(i_n)$. Those approximate relationships are represented in Fig. 16 to replace the exact relationship in Fig. 15.

4.2.2 Raise and Lowering Chamber Pressure Build-Up (H_2)

The block H_2 represents the pressure build-up equation for the fluid volumes in the raise and lowering chamber of the actuator. The block H_2 is typically modeled according to Eq. 3.6, which is a linear combination of the flow rates (which the controller can estimate from block H_1) and the rod position x_r (which the controller can estimate from block H_3).

4.2.3 Transmission Lines Dynamics and Additional Valves (H_3)

The block H_5 represents the dynamics of the transmission lines (from the directional valve to the actuator) and the dynamics of additional valves located on those lines. For example, a linear modeling of the transmission lines dynamics is based on the hydraulic impedance model. In case of resistive-capacitive effect only, the pressure in the actuator chambers (p_R, p_L) can be obtained from the pressure at the workports (p_{WR}, p_{WL}) as follows:

$$\begin{cases} p_{WR} = R_{HR} Q_R + \dfrac{1}{C_{HR}} \dfrac{Q_{R,net}}{s} + p_R \\ p_{WL} = R_{HL} Q_L + \dfrac{1}{C_{HL}} \dfrac{Q_{L,net}}{s} + p_L \end{cases} \quad 4.2$$

Where: $Q_{R,net}$ and $Q_{L,net}$ are the net flows obtained by the difference of the flow entering and leaving the line; R_{Hi} is the hydraulic resistance and C_{Hi} is the hydraulic capacitance. The electronic controller can estimate the flows Q_R and Q_L from block H_1. An extension of this formulation suitable to take into account for additional valves on the transmission lines is presented in Sect. 6.4.2.

4.2.4 Actuator Force (H_4)

The block H_3 represents the actuator rod motion dynamics. This block basically evaluates the hydraulic force produced by the $i = 1..N$ actuator

$$F_{r,i} = p_{R,i} A_{R,i} - p_{L,i} A_{L,i} \quad 4.3$$

The electronic controller can estimate the pressure p_R and p_L from block H_2.

4.2.5 Tractor Mechanical Dynamics (H_5)

The block H_5 represents the tractor mechanical dynamics. The outputs from the tractor model are the position of the pivots of the implement (z_{pI}) and actuator (z_{p1}). The inputs for the tractor model are: F_{pI}, forces on the pivots of the implement; p_R and p_L which are used to determine the force on the pivot of the actuator F_{p1}. In many cases, including case study 1, those are the only relevant inputs. In fact, in case of hydraulic cranes, either they are mounted on a rigid support (like it is in case study 1) or on tractors provided with outriggers: in both cases, the tractor behaves like rigid constrain. Differently, in other cases (including case study 2, wheel loader), the tractor has its own dynamics during the machine operation. In those cases, the disturbance W becomes an which plays a relevant role as it will be shown in Sect. 9.3. With reference to case study 2, W is the uneven ground which produces oscillating forces acting on the tractor (Fig. 12). By definition, a disturbance is a system input which cannot be directly monitored and produces an undesired effect on the system output. There are two alternative ways to address W:

- The controller is designed to be insensitive to W. In this case it has to be verified the controller is stable and sufficiently effective ("robust") for all the expected values of W.
- The controller is designed to adapt itself to different values of W. It will be shown for this specific case the acceleration feedback may present advantages over the pressure feedback technique (see Sect. 9.3).

4.2.6 Implement Mechanical Dynamics (H_6)

The block H_6 represents the implement mechanical dynamics. It is recalled the assumption that only one actuator (among the N actuators) moves at a time.

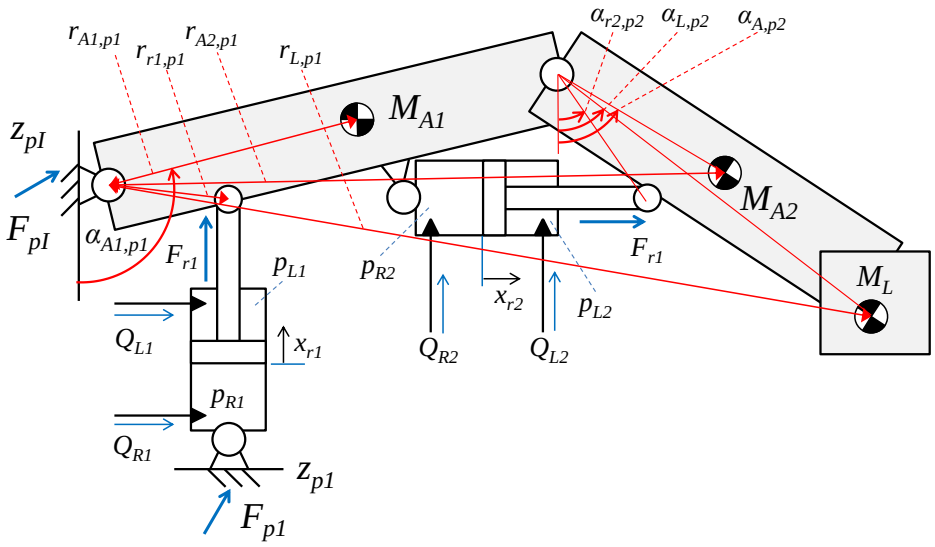

Fig. 17: Example of generic implement constituted by N=2 actuators and N mechanical arms.

Different hydraulic machines have different implements; however, a generic case can be discussed from the schematic in Fig. 17. To simplify the graphical representation, Fig. 17 is relative to the case $N = 2$, however, the following considerations are valid for any N.

The block H_6 basically solves the motion equation of the entire implement (rotation respect to the implement pivot, whose position is z_{pI}) as well as the $N - 1$ motion equations of the joints between the mechanical arms. The following subscripts will be used in this section: A, i mechanical arm; r, i actuator rod; p, i pivot ($i = 1..N$).

The motion equation for the rotation respect to the p, i pivot is:

$$\boldsymbol{I}_{p,i}\ddot{\boldsymbol{\alpha}}_{p,i} = \boldsymbol{T}_{Lp,i} + \boldsymbol{T}_{r,i} + \boldsymbol{T}_{A,i..N} + \boldsymbol{T}_{cp,i} \tag{4.4}$$

The overall inertia of the body respect to the pivot p, i is

$$I_{p,i} = \left(I_L + M_L r_{Lp,i}\right) + \sum_{j=i}^{N}\left(I_{A,j} + M_{A,j;p,i} r_{A,j;p,i}\right) \tag{4.5}$$

The load exerts the torque respect to the pivot p, i is

$$\boldsymbol{T}_{Lp,i} = \boldsymbol{r}_{Lp,i}\boldsymbol{g}\boldsymbol{M}_L \cos\boldsymbol{\alpha}_{Lp,i} \tag{4.6}$$

The actuators r, i exerts the torque respect to the pivot p, i

$$T_{r,i;p,j} = r_{r,i;p,j} F_{r,i;p,j} \cos\left(\alpha_{r,i;p,j}\right) \tag{4.7}$$

The forces of the actuators are known from Eq. 4.3. The mechanical arm A, i exerts the torque respect to the pivot p, i

$$T_{A,i;p,j} = r_{A,i;p,j} F_{A,i;p,j} \cos\left(\alpha_{A,i;p,j}\right) \tag{4.8}$$

Viscous friction respect to the pivot p, i is

$$\boldsymbol{T}_{cp,i} = \boldsymbol{c}_{p,i}\dot{\boldsymbol{\alpha}}_{p,i} \tag{4.9}$$

Two assumptions will be introduced at this point: the center of mass of the load is located in a specific point close to the mechanical arm end which is the farthest from the implement pivot; the inertia of the load with respect to its own axis I_L is exclusively function of the load mass M_L (the larger the mechanical arms with respect of the load dimensions are, the more accurate the approximation is).

After introducing those assumptions, it is possible to observe that the system has only N degrees of freedom, therefore N dimensions are sufficient to define its geometry in the plane. In this work, all angles α and all center of mass positions r will be defined according to the N actuator rod positions $x_{r,1..N}$. Considering the inertia respect to the center of mass $I_{A,1..N}$ as well as the masses $M_{A,1..N}$ of the mechanical arms are constant, the Eq.s 4.4..4.9 constitute a system of N equations in $N + 1$ variables ($x_{r,1..N}$,M_L). In order to solve for $x_{r,1..N}$ it is then necessary to have an estimate of M_L: for this purpose a specific algorithm was designed, as it will be described in the next section (Sect. 4.2.7).

4.2.7 Load Mass and Actuators Position Identification (H_9)

The load mass and actuators position identification algorithm (it will be referenced as block H_9) is formalized as it is described in this section. The block H_9 is obtained by the interaction of two blocks, as it is shown in Fig. 18: H_7, load mass estimator; H_8, actuators position estimator.

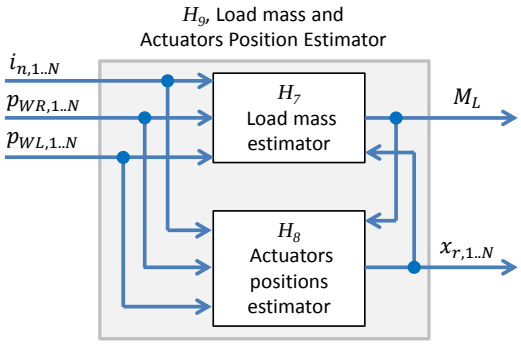

Fig. 18: Block diagram of the load mass and actuators rod position estimator (H_9).

Both the block H_7 and H_8 inputs are the pressure feedback method measurements: $(i_{n,1..N}, p_{WR,1..N}, p_{WL,1..N})$. Additionally, block H_7 receives as input $x_{r,1..N}$ (which is the output from block H_8). Similarly, block H_8 receives as input M_L (which is the output from block H_7).

The operation of the block H_9 is composed by a series of steps:

- Step 1: At the machine startup, it is assumed the machine is with no load: the block H_7 estimates $M_L = 0$.
- Step 2: The information collected by the block H_8 are sufficient to determine $x_{r,1..N}$ by solving N motion equations (Eq. 4.4).
- Step 3: As soon as $i_{n,1..N} = 0$ and the pressures $(p_{WR,1..N}, p_{WL,1..N})$ change, the machine is with load. The block H_7 solves Eq. 4.4 in steady-state conditions and determines the mass of the load M_L.
- Step 4: Block H_8 operates similarly to step 2 to determine $x_{r,1..N}$.
- Step 5: As soon as $i_{n,1..N} = 0$ and the pressures $(p_{WR,1..N}, p_{WL,1..N})$ change, the machine is with partial load or with no load. The block H_7 solves Eq. 4.4 in steady-state conditions and determines the residual mass of the load M_L.

After step 5, step 2 and next are repeated during the entire operation of the machine.

The procedure here described requires the controller performs the solution of N motion equations (Eq. 4.4). Although modern control units used in fluid power can handle this computation fast enough to avoid delaying the control, an alternative is represented by the implementation of look up tables of this type

$$x_{r,1..N} = f_{x_r}\left(M_L, p_{WR,1..N}, p_{WL,1..N}\right) \qquad 4.10$$

The function f_{x_r} is an interpolating function. A more complex function might be used to take into account the effect of the viscous friction ($i_{n,1..N}$ provide estimate of the each actuator velocity)

$$x_{r,1..N} = h_{x_r}\left(i_{n,1..N}, M_L, p_{WR,1..N}, p_{WL,1..N}\right) \tag{4.11}$$

Relationship in Eq.s 4.10 and 4.11 can be also determined experimentally for a sufficiently fine grid of values $x_{r,1..N}$ where the motion of the machine is possible. This implementation does not require any modeling of the implement mechanical dynamics, and it is therefore non-model-based.

In cases in which it may happen accidental loss of load, the identification performed by block H_9 might become non reliable. For example, in case study 2, during the travel of the wheel loader loss of material may occur; however, in these machines angular sensors on the implement pivot are often present. Therefore, with no need to add any extra-sensor to the machine, these angular sensors can be used to guide the identification of block H_9 and make it more reliable.

4.3 Pressure Feedback Based Controller Implementation

Several controller implementations are possible: it will be first shown the most intuitive and then, all the steps will be presented to finally arrive at the innovative pressure feedback control implementation developed in this work. The most intuitive is presented in Fig. 19.

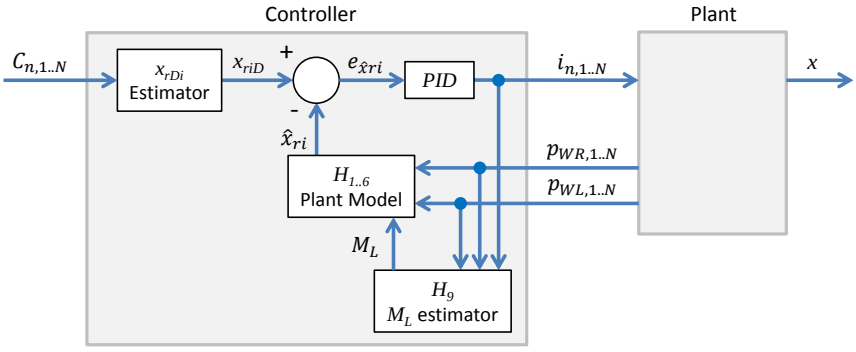

Fig. 19: Simplest implementation of the pressure feedback control method: tracking of the vibrating part position.

This implementation basically consists in the tracking control of the vibrating part position x. This implementation requires the definition of x_{riD} which is representative of the ideal (desired) motion of the rod of i −actuator the machine in absence of vibrations

$$x_{rDi} = \int Q_{\max}\left(\frac{C_{Rni}}{A_{Ri}} - \frac{C_{Lni}}{A_{Li}}\right)dt \tag{4.12}$$

where Q_{max} represents the maximum flow provided by the power supply and the normalized operator command C_{ni} is broken into its two summands: if $C_{ni} \geq 0$, $C_{Rni} = C_i$ and $C_{Lni} = 0$; if $C_{ni} <$

0, $C_{Rni} = 0$ and $C_{Lni} = C_{ni}$. Equation 4.12 is implemented in the block which will be indicated as the "x_{rDi} *estimator*".

In the previous section the approximate plant model constituted by the blocks $H_1..H_6$ was introduced. This approximate model is suitable to determine all the states of the plant and the oscillating body dynamics x from the information coming from the measurements ($p_{WR,1..N}, p_{WL,1..N}, i_{n,1..N}$) and from the estimate of M_L performed by the block H_9. The approximate plant model will be used to estimate the state representative of the position of the i −actuator rod, which will be indicated by $\hat{x}_{ri}$.

The difference between x_{rDi} and $\hat{x}_{ri}$ will be called position error and it will be indicated by $e_{\hat{x}ri}$. A compensator tries to minimize $e_{\hat{x}ri}$ controlling the flow rates across the directional valve Q_R and Q_L to apply the damping action F_{QR} and F_{QL} to the system (as it was shown in Fig. 10b). In this example, the simple case of a PID compensator is presented, whose well known transfer function is

$$P + \frac{I}{s} + Ds \qquad 4.13$$

where P, I, and D represent the proportional, integral and, derivative gain respectively.

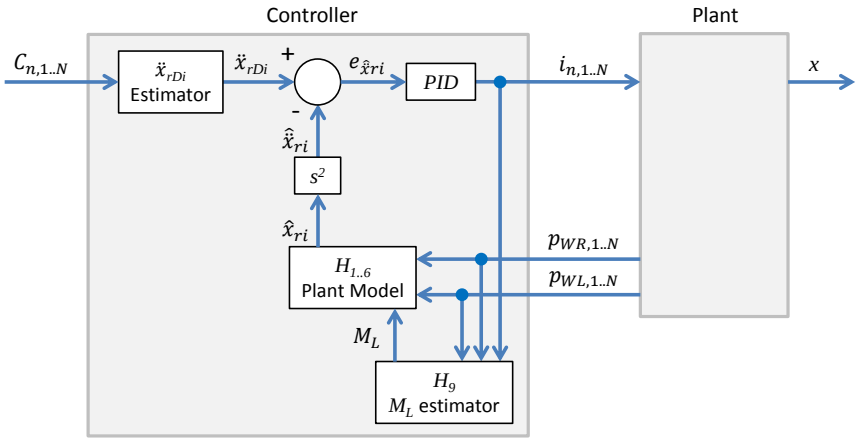

Fig. 20: Alternative implementation of the pressure feedback control method: tracking of the vibrating part acceleration.

An implementation similar to the one in Fig. 19 is the one shown in Fig. 20. In this case, the tracking control rather than being performed on the vibrating part position x is performed on its acceleration $\ddot{x} = xs^2$.

This implementation requires the use of a second order differentiator which transforms the approximate plant model output into $\hat{\ddot{x}}_{ri}$. Additionally, this implementation requires the definition of a new estimator, indicated in Fig. 20 as "$\ddot{x}_{rDi}$ *estimator*", suitable to derive the desired (no oscillations) acceleration $\ddot{x}_{rDi}$. Although the modeling of the $\ddot{x}_{rDi}$ estimator is theoretically feasible, a further implementation presents the advantage of not requiring it, as it is shown in Fig. 21.

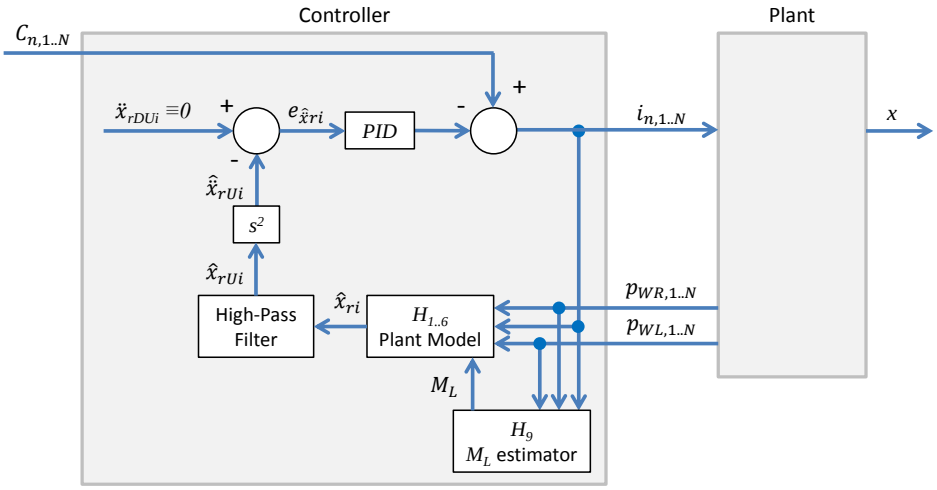

Fig. 21: Alternative implementation of the pressure feedback control method: tracking of a specific acceleration profile.

This implementation uses a high pass filter which can for example be modeled according the following transfer function

$$\frac{s}{s + \omega_{HP}} \qquad 4.14$$

in which ω_{HP} represents the cut-off pulsation. The purpose of the high pass filter is to remove the steady-state component of the signal and just keep the transient (oscillatory in this case) part of it, as it is shown in the example in Fig. 22.

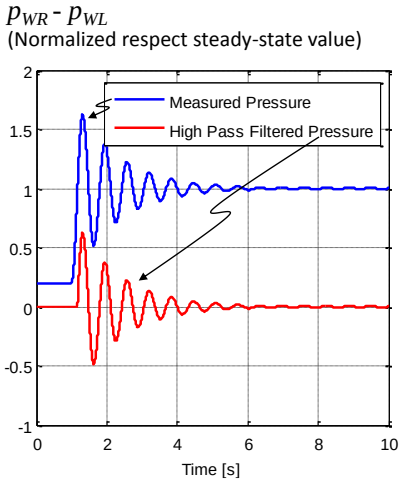

Fig. 22: Example of high pass filter operation to remove the steady-state component of a signal: only the oscillating part is left.

The output from the high pass filter is the undesired (oscillatory) dynamics of the i −actuator rod $\hat{x}_{rUi}$, which is derived into the undesired acceleration $\hat{\ddot{x}}_{rUi}$. The presence of the high-pass filter makes the controller output oscillatory across zero, and it does not affect the steady state valve of

x_{ri}. Consequently, the integral term of the compensator, which is the one used to compensate for offset in the controlled output respect to the desired value, becomes unnecessary.

Additionally, in this implementation, the desired dynamics is in this case: $\ddot{x}_{rDUi} \equiv 0$. This allows removing one summing junction and the simplified block diagram is shown in Fig. 23.

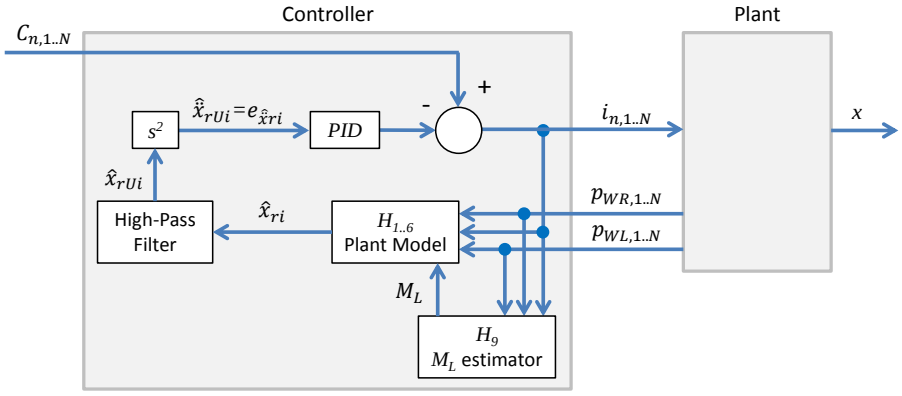

Fig. 23: Simplification of the block diagram in Fig. 21.

The plant model is strongly non-linear, as it was pointed out in the previous section. However, vibrations can be considered a small signal with respect to the steady-state operating point. The steady-state operating point can be identified by using the measurements $(p_{WR,i..N}, p_{WL,i..N}, i_{n,i..N})$ combined with the load estimation (M_L). A linear dynamics in correspondence of the identified operating point can then be used to determine the variations in the plant output for small variations of the states respect to the identified operating point. The plant which adapts its dynamics (from a set of linear dynamics) to the identified operating point will be called adaptive plant, and it is represented in Fig. 24.

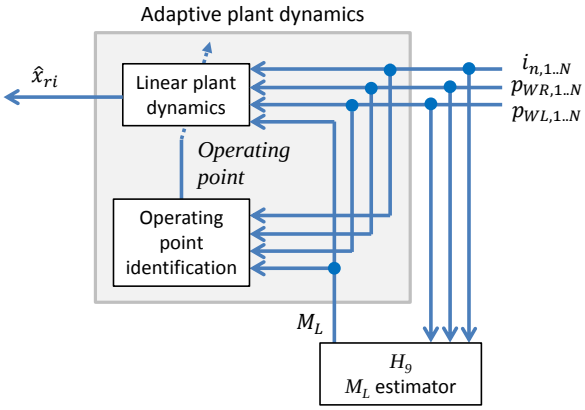

Fig. 24: Representation of the adaptive plant whose dynamics is selected from a set of linear dynamics according to the identified operating point.

Since the linear plant dynamics is changing with the identified operating point, the controller should also change accordingly; therefore the entire controller should become adaptive, as it is represented in Fig. 25.

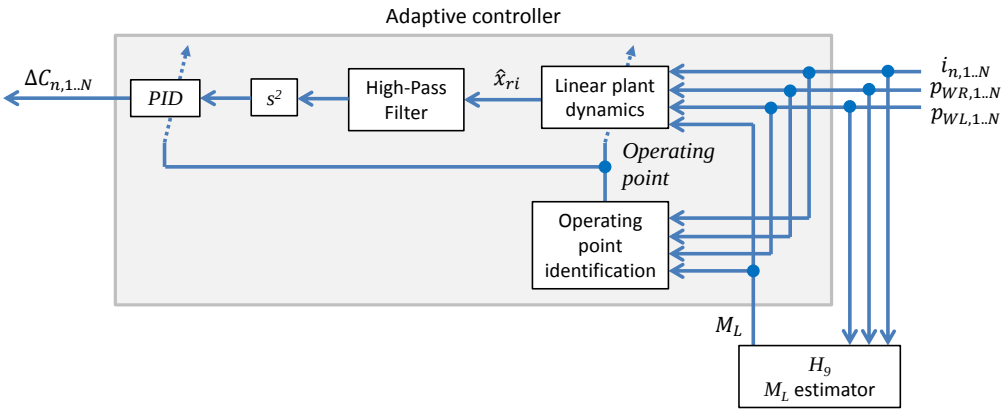

Fig. 25: Block diagram of the adaptive controller in which both the plant dynamics and the PID compensator parameters are adapted with respect to the identified operating point.

The high pass filter is designed to remove the frequencies which are lower than the slowest vibration expected; therefore it does not need to be adapted to the identified operating point. The four consecutive linear blocks (linear plant dynamics, high-pass filter, second order differentiator, and PID controller), can be multiplied together to make a unique block, which will be called H_{10} (adaptive controller and model), as it is shown in Fig. 26.

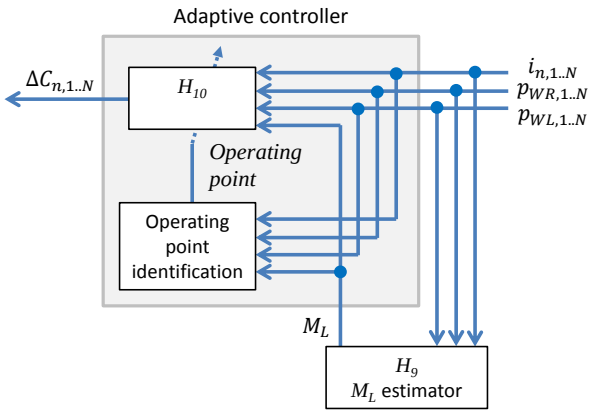

Fig. 26: Block diagram of the adaptive controller in which the linear dynamics are grouped into a unique block (H_{10})

Therefore the final implementation of the controller can be represented as in Fig. 27.

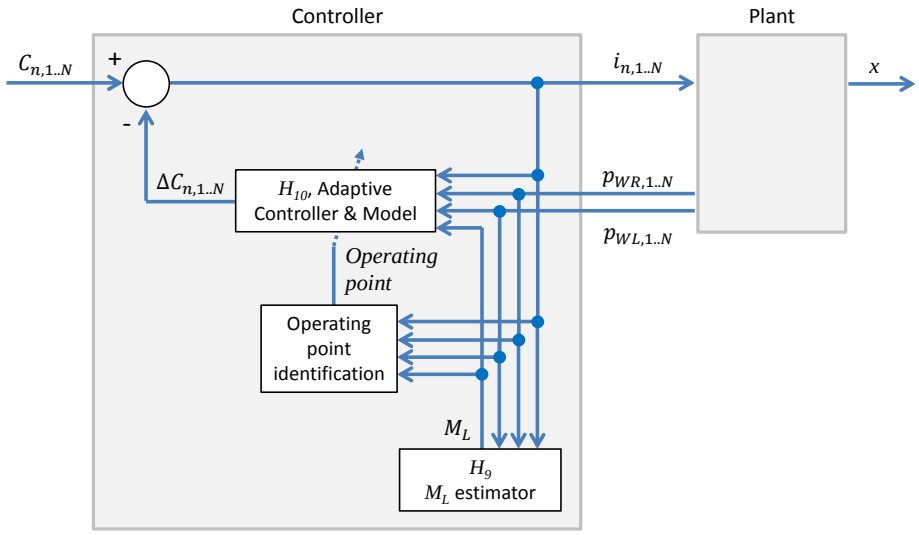

Fig. 27: Final implementation of the proposed method: it is suitable for implementation of adaptive control algorithm and non-model-based tuning.

The expression of the block H_{10} is

$$H_{10} = (P + \delta P) + \frac{(I + \delta I)}{s} + (D + \delta D)s = P^* + \frac{I^*}{s} + D^* s \qquad 4.15$$

Basically, the block H_{10} has two purposes:

- It includes the PID compensator (P, proportional term; I, integral term; D, derivative term).
- It includes the terms δP, δI, δD which are used to model the dynamics of the plant, filter and differentiator. It has to be observed that these parameters are suitable to take into account for a 3rd order plant. In case even larger order plant dynamics is expected, additional terms can be added to H_{10} in order to make it a higher order polynomial. For example, 4th order can be achieved by adding $\left({I_2^*}/{s^2}\right)$. Nevertheless, so far in this work H_{10} has been used in the simplified form: $H_{10} = P^* + D^* s$.

Although it might appear confusing the idea of grouping those two purposes together in the same block, there are two specific reasons behind it:

- *Adaptive control algorithm*: The block H_{10} is structured in order to make it possible to adapt its parameters to the varying operating conditions of the machine which are identified by the measurements ($p_{WR,1..N}, p_{WL,1..N}, i_{n,1..N}$) and from the estimate of M_L performed by the block H_9. This adaptation algorithm represents one of the principal innovations of the proposed control method and it will be described in the next section (Sect. 4.4).
- *Non-model-based controller tuning algorithm*: The block H_{10} is structured in order to make it possible to run an automatic tuning algorithm based on the analysis of the experimental response of the real machine to specific inputs. Since the tuning is performed on the

analysis of experiments and no model is involved, it is called non-model-based controller tuning algorithm, and it represents one of the principal innovation of the proposed control method, as it will be described in Sect. 4.5.

4.4 Adaptive Control Algorithm

The block H_{10} includes terms depending on the measurements ($p_{WR,1..N}, p_{WL,1..N}, i_{n,1..N}$) and on the estimate of M_L performed by the block H_9: P^*, I^*, D^*. This makes it possible to adapt the expression of H_{10} respect to the measurements ($p_{WR,1..N}, p_{WL,1..N}, i_{n,1..N}$) and the estimate of M_L. A controller which does not adapt itself with respect to varying operating condition (such as a linear controller) would have satisfactory performances only in correspondence of the design operating condition. Differently, the innovative adaptive controller presented in this work, automatically adapts H_{10} to ensure optimal performances over the entire range of operating conditions of the machine.

The adaptation algorithm implemented into the controller is based on the *Gain-Scheduling* technique (Åström K. J., and Wittenmark B., 2008). The gain scheduler is a nonlinear feedback of special type; it has a linear controller whose parameters are changed in a preprogrammed way as a function of one or more *scheduling variables*, which in this work consist in the measurements ($p_{WR,1..N}, p_{WL,1..N}, i_{n,1..N}$) and the estimate of M_L performed by the block H_9. Ultimately, the gain scheduler parameters can be expressed as

$$\begin{cases} P^* = f_P\left(M_L, p_{WR,1..N}, p_{WL,1..N}, i_{n,1..N}\right) \\ I^* = f_I\left(M_L, p_{WR,1..N}, p_{WL,1..N}, i_{n,1..N}\right) \\ D^* = f_D\left(M_L, p_{WR,1..N}, p_{WL,1..N}, i_{n,1..N}\right) \end{cases} \quad 4.16$$

The resulting gain scheduler can be implemented in the controller as an actual function or as an interpolated lookup table.

In some specific cases the gain scheduler might be simplified. For example in case study 2, the position of the wheel loader actuator can be measured by an angular sensor which is typically installed on the implement pivot. In that case: the scheduling variables can be limited to M_L and i_n (assuming W can be estimated, it can be included); the controller still needs all measurements $p_{WR,1..N}, p_{WL,1..N}, i_{n,1..N}$ and the estimated M_L.

The general procedure to determine the values of the gain scheduler parameters for each combination of the scheduling variables will be explained in the next section (Sect. 4.5).

4.5 Non-Model-Based Controller Tuning Algorithm

In the implementations from Fig. 19 to Fig. 23, the approximate plant model and the PID compensator were two separate blocks. Consequently, errors in the approximate plant model would lead to a poor tuning of the PID compensator, resulting in low control performance. Differently, the

structure of H_{10} is designed in order to combine the approximate plant model and the PID compensator making it possible to perform together two procedures:

- *Experimental system identification of the plant dynamics*: with reference to the notation from Eq. 4.15, it consists in the identification of the parameters: $\delta P, \delta I, \delta D$.
- *Experimental PD compensator tuning*: with reference to the notation from Eq. 4.15, it consists in the tuning of the parameters: P, I, D.

Those two procedures can be performed simultaneously by analyzing the experimental response of the actual machine to specific inputs: in this way all the parameters (P, I, D) and $(\delta P, \delta I, \delta D)$ can be determined at the same time by determining the parameters (P^*, I^*, D^*). The combination of the experimental system identification and the experimental PD compensator tuning will be indicated in this document by the name of *non-model-based controller tuning*. The adjective non-model-based remarks the fact that the procedure does not require any model of the machine; indeed, it can be performed directly on the actual machine. At the current level of the research, however, the non-model-based controller tuning has been tested for simplicity only on the numerical models of case study 1 and 2: the testing on the experimental equipment of case study 1 represents one of the future developments.

The non-model-based controller tuning is performed through the iterative optimization depicted in Fig. 28 (in this framework only P^*, D^* are determined, while I^* was excluded).

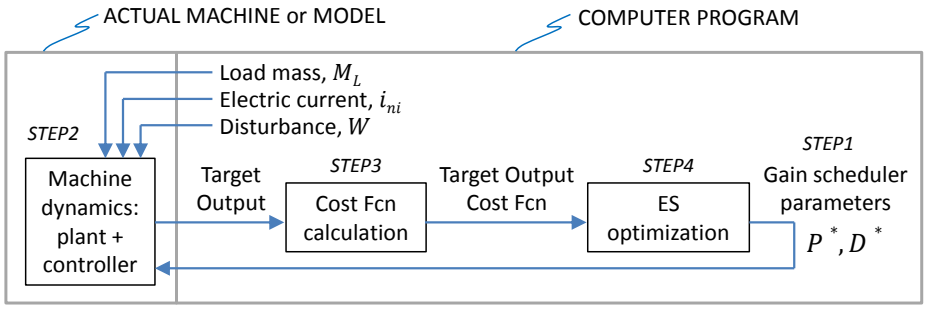

Fig. 28: Block diagram representing the iterations of the non-model-based controller tuning procedure.

Each combination of scheduling variables $(M_L, p_{WR,1..N}, p_{WL,1..N}, i_{n,1..N})$ will give a different set of the parameters (P^*, I^*, D^*), which will be then stored into the gain scheduler from previous section (Sect. 4.4). The iterative optimization is repeated until the convergence of the parameters (P^*, I^*, D^*), namely those parameter suitable to minimize the cost function which quantifies the undesired vibration. For example, in the case study 1 (crane), the undesired vibration is the one measured by the accelerometer at the end of the main boom (Fig. 35,1).

Table 3 describes the iterative procedure, with reference to Fig. 28, as it was implemented in a Matlab® program:

Table 3: Description of the steps constituting the non-model-based controller tuning algorithm.

Iteration $k =$	Step	Description
1	1	*Initialization* It is first necessary to specify the combinations of scheduling variables $(M_L, p_{WR,1..N}, p_{WL,1..N}, i_{n,1..N})$ for which the non-model-based controller tuning will be performed. Eventually, if the disturbance W can be estimated, it becomes a scheduling variable as well. The first iteration initialized by imposing the control parameters P^* and D^* equal to zero, which corresponds to the case of standard machine without the proposed control.
1	2	*Machine dynamics* The method requires the knowledge of the profile over time of a determined target output. The target output has to be representative of the quantity whose vibration has to be minimized. For example, in case study 1 (crane), the main boom oscillations are those who were to be minimized. In that case, the target output was chosen to be the rotation of the main boom ψ. The target output is evaluated for a set of P^* and D^* parameters imposed at the previous step as well as the scheduling variables imposed at step 1. Note that the controller parameters P^* and D^* will be updated at each iteration k, while the scheduling variables defined at iteration 1 step 1 will be constant for the entire non-model-based controller tuning procedure. Being the controller tuning method non-model-based, the machine dynamics can be measured directly from the actual machine, alternatively, it can be applied to a numerical model as well. In case study 1 an accurate nonlinear model of the crane (described in Sect. 6.1) was used. Similarly, in case study 2 an accurate nonlinear model of the wheel loader (described in Chap. 9) was used[1].

[1] The use of the experimental set-up of case study 1 (described in Chap. 5) to perform the controller tuning were later on performed within an associated research project at Purdue University and results will be subject for a future publication.

1	3	*Cost function calculation* The target output is used to compute a cost function representative of the vibration which has to be minimized. For each machine, several formulations for the cost functions can be used for this purpose. With reference to case study 1 (crane), the cost function was determined as the difference between the ideal rotation of the main boom $\psi_D(t)$ in absence of oscillations and the actual one $\psi(t)$ from previous step (see Sect. 7.2).
1	4	*Extremum-seeking optimization algorithm* The cost function is the input for the optimization algorithm whose output is a new set of parameters P^* and D^*. The proposed method applies an innovative formulation of the *extremum seeking optimization algorithm* (Ariyur K. B., and Krstić M., 2003), whose basic functioning principle is illustrated in the block diagram in figure Fig. 29. 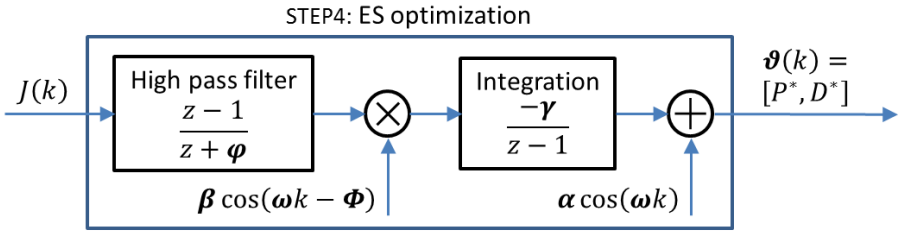 *Fig. 29: Block diagram of the single parameter extremum-seeking optimization algorithm used in step 4 of the non-model-based controller tuning algorithm.* The ES algorithm basically consists in an iterative search for the extremum (the minimum in this case) of a function (the cost function J in this case). This search is performed by iteratively modifying $\boldsymbol{\vartheta}$, which is a vector which includes one or more parameters of the system ($\boldsymbol{\vartheta} = [P^*, D^*]$ in this case) through two harmonic perturbations: $\boldsymbol{\beta}\cos(\boldsymbol{\omega}k - \boldsymbol{\Phi})$, and $\boldsymbol{\alpha}\cos(\boldsymbol{\omega}k)$. For a given iteration k, the closer the cost function J is to its extremum; the smaller is the effect of the perturbations is: this ensures the convergence of the algorithm to a unique solution. Analytical proof of convergence is presented by Ariyur K. B., and Krstić M. (2003). In more detail, the cost function is firstly high pass filtered in order to remove frequencies lower than $\boldsymbol{\varphi}$ and then multiplied times the perturbation signal $\boldsymbol{\beta}cos(\boldsymbol{\omega}k - \boldsymbol{\phi})$. The resulting signal, $\boldsymbol{\xi}(k)$ is then integrated and multiplied times $-\boldsymbol{\gamma}$ (where $\boldsymbol{\gamma} > 0$). The resulting signal $\widehat{\boldsymbol{\vartheta}}(k)$ is finally added to the perturbation signal $\boldsymbol{\alpha}cos(\boldsymbol{\omega}k - \boldsymbol{\phi})$ to get the new set of control parameters $\boldsymbol{\vartheta}(k) = [P^*, D^*]$.

2..end	1..4	For all remaining iterations (from $k = 2$ to convergence): • Iteration k, step 1: the set of control parameters is determined by the extremum-seeking optimization (Iteration $k - 1$, Step 4). • Iteration k, steps 2, 3 and 4 are analogous to those described for iteration $k = 1$. The iterative procedure is repeated until the final iteration, which is the one for which the set of parameters $[P^*, D^*]$ converges to the best value, namely the one which minimizes the cost function J which is representative of the oscillations extent. The resulting set of parameters $[P^*, D^*]$ is then stored in the gain scheduler for the specific combinations of scheduling variables specified at iteration $k = 1$, step 1.

The non-model-based controller tuning procedure has to be repeated for all the specific combinations of $(M_L, p_{WR,1..N}, p_{WL,1..N}, i_{n,1..N})$ and eventually W in which vibrations are expected to be relevant.

An example of non-model-based control parameters tuning is represented in Fig. 30. The figure is obtained by applying the non-model-based control parameters tuning to the model of case study 1 (crane model, Sect. 6.1). The scheduling variables for this optimization are: M_L=1000kg; i_{n1} step from 0% to 100% (representative of a full speed raise); $p_{WR1} \cong$35bar; $p_{WR1} \cong$4bar (all other variables =0). The disturbance, for the crane is typically W=0 (it will be shown in Sect. 10.1 that the disturbance has to be considered in case study 2, wheel loader). It is possible to observe that the first iteration k=1, the control parameters P^*, D^* are initialized to zero. In the next iterations, they oscillates towards the direction which minimizes the cost function J, which at iteration k=1000 has reached the convergence to its minimum. Consequently, the parameters P^*, D^* corresponding to the iteration k=1000 will be stored in the gain scheduler in correspondence of the above specified scheduling variables.

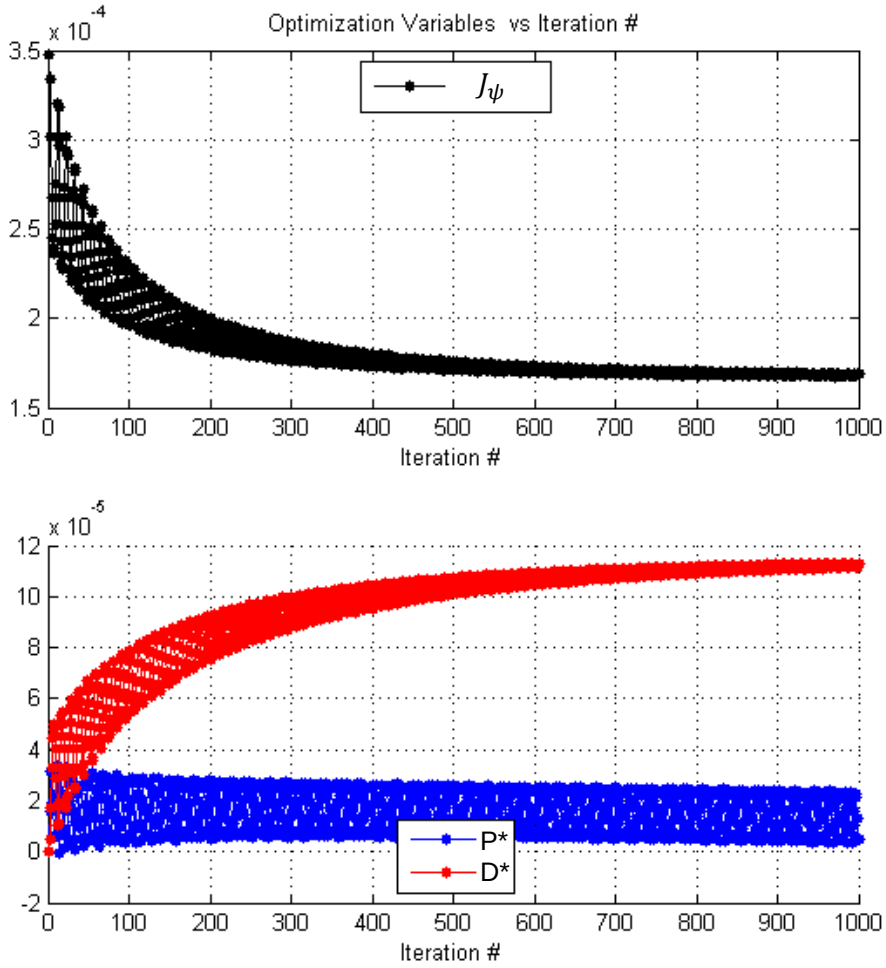

Fig. 30: Example of non-model-based controller parameters tuning relative to case study 1 (crane). After an adequate number of iterations the control parameters P and D converge to the values which minimize the vibrations quantified by the cost function. The example is relative to M_L=1000kg and i_n is a step from 0 to 100%.

4.6 Acceleration Feedback Based Control Implementation

This section describes how the pressure feedback based controller described in Sect. 4.3 can be modified to be applied to the case of acceleration feedback. Adaptive control algorithm and non-mode-based controller tuning algorithm are still applicable as respectively described in Sect. 4.4 and Sect. 4.5.

The schematic represented in Fig. 23 for the pressure feedback can be simplified in case of acceleration feedback as it is represented in Fig. 31.

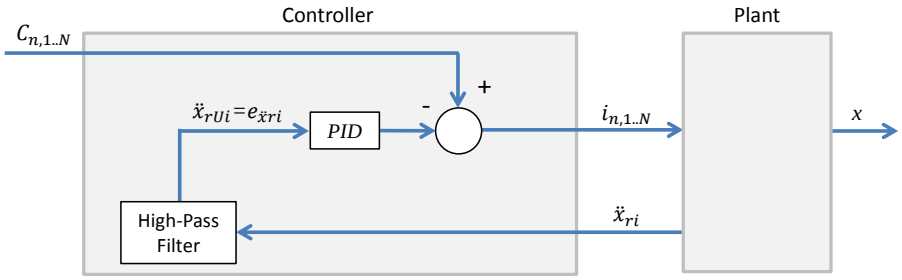

Fig. 31: Schematic of a vibration damping controller in case of acceleration feedback which is analogous to the one presented in Fig. 23.

By considering a gain scheduled structure of the controller, the schematic in Fig. 31 can be represented with the final block diagram used in case of pressure feedback which was represented in Fig. 27. In the case of acceleration feedback, however, the load mass estimator and the operating point identification would require a different formulation which is not subject of this research.

In this document the results of the acceleration feedback controller will be presented (see Sect. 10.4) with the goal to provide a comparison with the pressure feedback controller. In particular, these results will be relative to a specific operating condition with constant load mass and therefore a constant parameters controller will be sufficient for the study.

CHAPTER 5. CASE STUDY 1: CRANE: REFERENCE MACHINE

The goals for the research on case study 1 were detailed in the specific section (Sect. 1.3.1), together with a brief description of the reference crane. The present chapter describes the main features of the reference crane hydraulic circuit (Sect. 5.1). Then, in Sect. 5.2, it will be presented an overview of the main features of the instrumented experimental crane which was installed at Maha Fluid Power Research Center to serve as experimental test bench for this research. Finally, the details of the data acquisition and control system will be described.

5.1 Hydraulic System

The simplified hydraulic schematic of the standard commercial crane is shown in Fig. 32 and the components are listed in Table 4. The telescopic stages will not be addressed in this work. The crane is originally intended to be supplied by a fixed displacement pump providing approximately 45 l/min. To adjust to this value the flow from the power supply available at the Maha Fluid Power Research Center, the system represented by the components 1 to 4 were used. The electric motor 1 is a standard three phase asynchronous motor spinning at 1185 rpm. The pump 2 is an axial piston pump whose maximum displacement is 80 cc. The pressure relief valve 4 is used prevent over pressurization of the pump delivery line. Component 3 is a two-way pressure compensated flow control valve. Acting on the knob of this component it is possible to adjust the internal flow area and consequently set the maximum flow rate at its output port, regardless the value of the inlet and outlet pressures.

The directional valve block (model P70, Parker-Hannifin®, 2006) includes several sections: inlet section, mid-sections, and end section. The inlet section (components 5 to 7) contains the pressure port of the valve block P and it allow to discharges flow in case the pressure overcomes the set value. The end section (components 22 to 24) contains the return port R and drain port D. The main function of the end section is to adjust the pressure of the inlet line of the proportional pilot valves 13, 14, 20 and 21. The mid-sections represented in Fig. 32 are those relative to outer boom and telescopic boom: they include the proportional pilot valves and the main spools 12 and 19 who deliver the flow to the actuators. Additionally, the mid-sections contain the anti-cavitation valves (10, 11, 17, and 18) which accomplish a double function: they prevent excessive pressure in the

transmission lines of the actuators; in case of sudden motion of the actuator, they prevent cavitation by allowing a backflow from the return line.

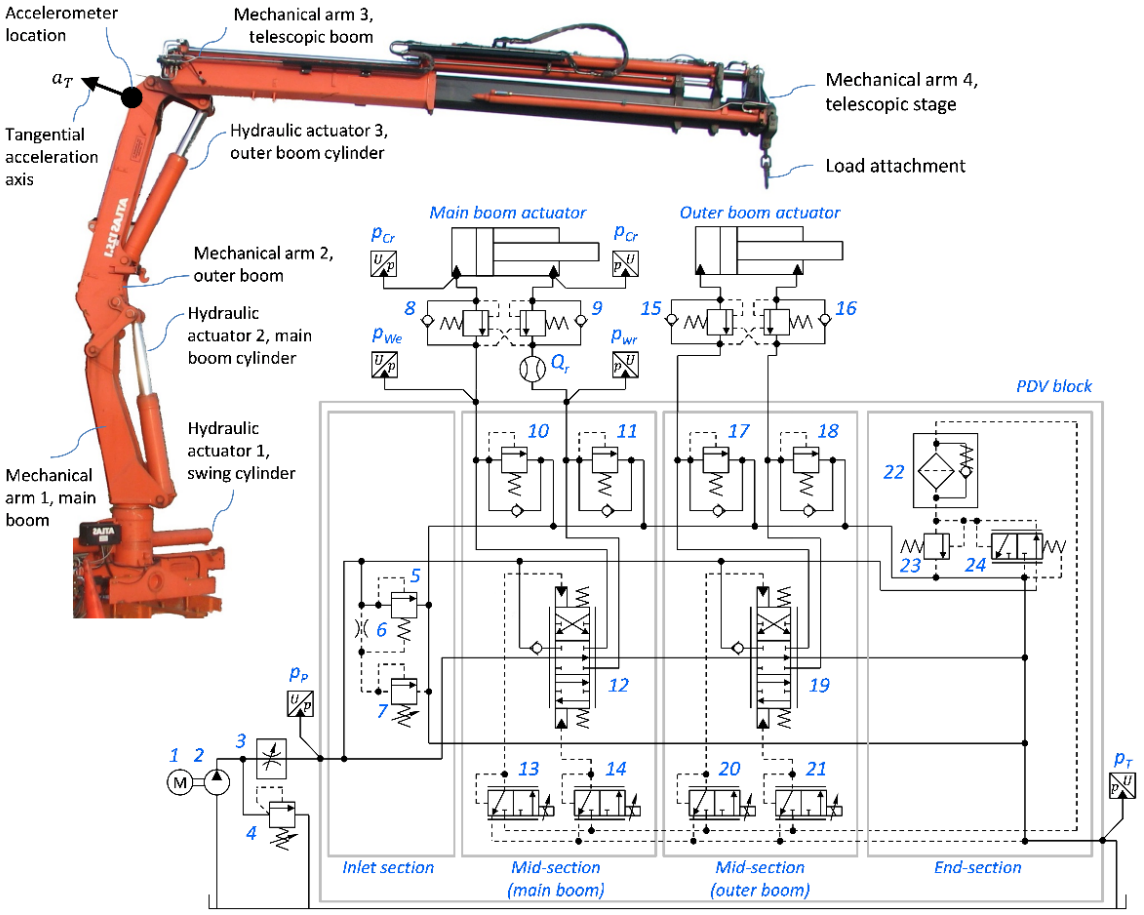

Fig. 32: Simplified hydraulic circuit of the crane (only outer boom and telescopic boom are represented).

Table 4: List of the components of the hydraulic circuit of the experimental crane.

Reference to Fig. 32	Description	Reference to Fig. 32	Description
1..3	Constant flow rate power supply.	10, 11, 17, 18	Anticavitation valve on the working port of the directional valve.
4	Pressure compensated flow control valve.	22..24	Pressure reducing system which determines the inlet pressure of the pilot stage.
5, 6, and 7	Pressure limiter integrated in the directional valve inlet section.	8, 9, 15, 16	Counterbalance valves.
13, 14, 20, 21	Pilot stage of the directional valve.	pP, pT, p_{We}, p_{Wr}	Pressure sensors (Parker IQAN SP500).
12, 19	Main stage of the directional valve.	Q_r	Flow meter (Parker SCFT-0380-PD).

The counterbalance valves (8, 9, 15, 16) have three main functions: they prevent excessive pressure in the transmission line; they hold the load in position when no flow is directed to the actuator; they prevent the load from falling in case of aiding loads. The settings of the counterbalance valves which would ensure those three functions however might give rise to vibrations; therefore, more energy dissipative settings are used to damp oscillatory dynamics (Handroos H., et al., 1993). The crane is equipped with the pressure sensors indicated in Fig. 32 as p_P, p_T, p_{We}, p_{Wr} as well as the flow meter Q_r.

5.2 Instrumented Experimental Crane

The reference crane is the model Atlas® 125.1 A5 (Atlas Maschinen Gmnh®, 1996). The reference hydraulic crane was introduced in Sect. 1.3.1. In particular, in Fig. 1 the technical drawings of the crane were presented, including dimensions and load weight limitations. Additionally, Fig. 1 indicated next to representation of the crane parts, the nomenclature used in this document. The crane was originally designed for truck mounting, as it is shown in Fig. 33.

Fig. 33: Truck mounting of the reference crane from manufacturer documentation (Atlas Maschinen Gmnh®, 1996).

The crane used for this project was disassembled from the truck and then mounted on a specific stand firmly grounded on a concrete pad at Maha Fluid Power Research Center, as it is shown in Fig. 34. The hydraulic flow is generated by the central hydraulic power supply of the Maha Fluid Power Research Center and by means of metal pipes (inside the building) and flexible hoses (outside the building) it is taken to the directional valve block. The electronic controller is installed in a portable enclosure (Fig. 35, 2) which also holds the emergency stop and the control levers.

The portable enclosure allows operating the crane either from outside the building or from inside the building, as it is shown in Fig. 35. The portable enclosure can be interfaced to a laptop (Fig. 35, 3) to perform the following operations: real-time monitoring of all sensors through graphical and numerical indicators; measurements acquisition; measurement post processing; controller programming.

Fig. 34: Picture of the experimental crane installed at Maha Fluid Power Research Center (Purdue University): 1) telescopic stages; 2) telescopic boom; 3) telescopic boom actuator; 4) outer boom; 5) outer boom actuator; 6) main boom; 7) load (barrel of concrete, 1000kg).

Besides the pressure sensors and flow meter described in the previous section, the experimental setup is suitable to handle additional signals. Several wireless sensors were installed: among those, the most relevant for the goals of this case study is the one installed on at the outer boom end, as it is shown in Fig. 35-1. The experimental set up has also the capability of monitoring the electrical signals (voltage and current) provided to the directional valve sections.

The schematic in Fig. 36 shows the structure of the control and data acquisition hardware system, while Table 5 reports the specifications of the components. The data acquisition functions and system control functions are all performed by the same electronic controller (Parker-Hannifin® IQAN MC-2). This electronic controller is a standard industrial unit and it operates at a maximum frequency of 333Hz which is way above the maximum frequency of the vibrations observed on the

crane (typically below 20Hz). The programming of the electronic controller was performed by connecting a laptop where the IQAN Design® software was installed. The same laptop was used for real-time monitoring of all signals and (using again IQAN Design®) and post-processing (using purposely coded Matlab® scripts).

Fig. 35: Picture of the experimental crane from the measurement room of the Maha Fluid Power Research Center (Purdue University). The crane can be controlled from the portable control enclosure (2). The laptop (3) can be used to configure the control unit e perform real-time acquisition. The point 1 indicates the location of the outer boom accelerometer.

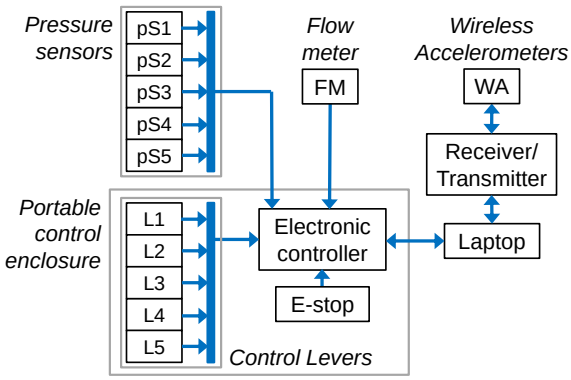

Fig. 36: Block diagram representing the control and data acquisition hardware system.

Table 5: Specifications of the sensors and the control unit used for the acquisition.

Component	Description	Code	Measurement Range	Full scale error	Response time [ms]
Electronic controller	Programmable real-time input/output unit	Parker® IQAN MC-2	0 – 10 A; ±30 V	1.0%	3.00
Pressure sensor (pS)	Piezo-resistive type	Parker® IQAN SP500	0 – 500 bar	4.0%	5.00
Flow meter (FM)	Turbine type	Parker® SCFT-0380-PD	10 – 300 l/min	1.0%	50.00
Wireless Accelerometer	Wireless accelerometer with transmitter/receiver base	MicrtoStrain ® *Sensor*: G-Link-mXRS-2G *Base*: WSDA	± 20 m/s^2	1.0%	0.25

CHAPTER 6. CASE STUDY 1: CRANE: MODELING AND STABILITY ANALYSIS

The goals of case study 1 were described in the specific section (Sect. 1.3.1). This chapter will describe the simulation model of the reference hydraulic crane and the stability analysis.

Firstly, the crane non-linear model will be described in Sect. 6.1 and Sect. 6.2. The model was developed to accomplish the following purposes: tool for the testing different control algorithms prior to their implementation on the actual experimental machine; deepen the understanding of the system by studying all those quantities it would not be convenient to directly measure. Even if the non-model-based controller tuning algorithm can be directly implemented on the actual machine, this chapter shows the application on the nonlinear model (application on the actual machine is currently under investigation by the research partner).

Then, in Sect. 6.3 the stability analysis for the pressure feedback based controller is shown for case study 1. A linear model was derived from the nonlinear one to use root locus technique to show the stability of the proposed method as well as its capability to introduce system damping.

Finally, the analytical formulation of a model suitable to accurately estimate the mechanical arms acceleration from the pressure measurements will be presented in Sect. 6.4 (experimental validation will be provided in Sect. 7.5). The goal for this model is to provide a comparison between pressure feedback and acceleration feedback controller for the case study 1.

6.1 Nonlinear Model

The model includes different physical domains, as represented in Fig. 37: the hydraulic model, the planar mechanical model and the electronic controller model. All models follow a lumped parameter approach, and the overall model is implemented combining two simulation environments: the plant model (hydraulic model and planar mechanical) in LMS Imagine.Lab AMESim®, while the electronic controller is implemented in MathWorks Simulink®. This section is only intended to provide the description of the modeling approach, validation and results will be provided in Chap. 7.

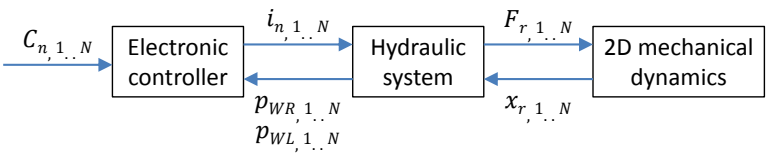

Fig. 37: Nonlinear crane model: representations of the models and variables.

6.1.1 Hydraulic Model

As represented in Fig. 37, the hydraulic model receives as input from the electronic controller model the current i_n to the directional valve proportional solenoids and from the planar mechanical model the position of the hydraulic actuators rods x_r. The outputs of the hydraulic model are the pressures at the directional valve block workports (p_{WR}, p_{WL}) and the forces on the hydraulic actuator rods (F_r). The description of the hydraulic model references to the hydraulic circuit represented in Fig. 32. It will be presented below the modeling approach for all components as well as a table of the parameter values (Table 6).

6.1.1.1 Proportional directional valve

The technical drawing of the mid-section of the reference proportional directional valve of case study 1 is presented in Fig. 38 (Parker-Hannifin®, 2006).

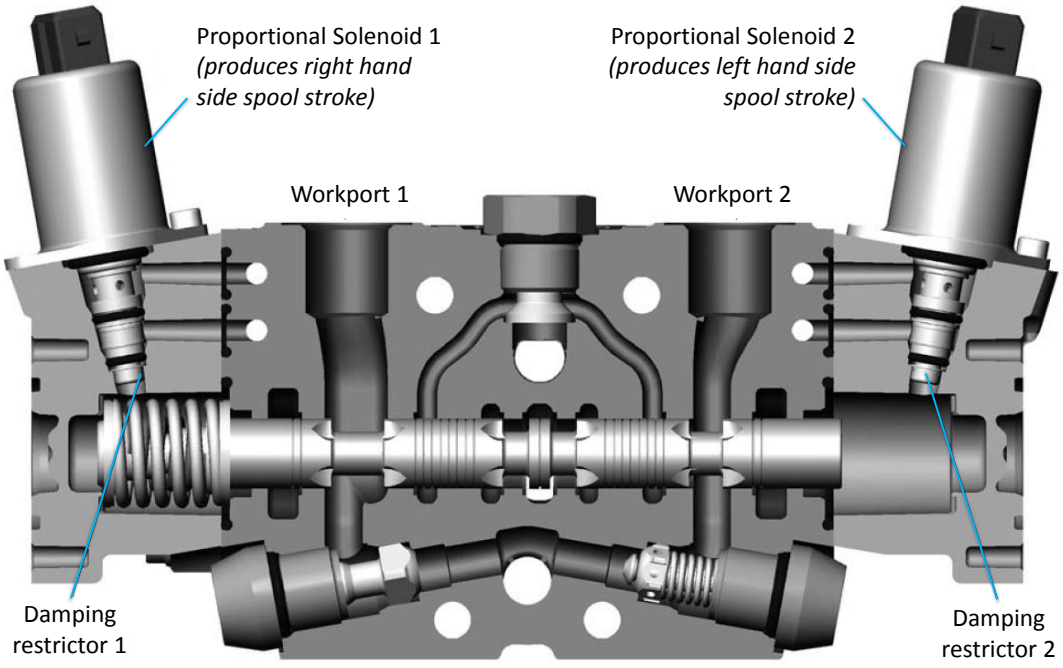

Fig. 38: Technical drawing of the mid-section of the reference proportional directional valve of case study 1 (Parker-Hannifin®, 2006).

The main stages (12, 19) of the proportional directional valve are piloted by means of electrically operated valves (13, 14, 20, 21). For the pilot stages, the pressure in the pilot chambers (p_{pR}, raise, p_{pL}, lowering) depends on the electrical current i_n according to the following relationship: if $i_n \geq 0$

$$\begin{cases} p_{pR} = p_{p,\max} H_p(s) i_n \\ p_{pL} = p_T \end{cases} \quad 6.1$$

Otherwise, if $i_n < 0$

$$\begin{cases} p_{pR} = p_T \\ p_{pL} = p_{p,\max} H_p(s) i_n \end{cases} \quad 6.2$$

Where $p_{p,\max}$ is the maximum pilot pressure (determined by the valve 37) and the dynamics is determined by

$$H_p(s) = \frac{\omega_{pn}^2}{s^2 + 2\zeta_p \omega_{pn} s + \omega_{pn}^2} \quad 6.3$$

The directional valve main stage is a proportional open-center valve having six ports and three positions. The main stage spool position is obtained by solving its dynamic equation along its axis:

$$M_m \ddot{x}_m = F_{Sm} + F_{Fm} + F_{fm} + F_{pm} \quad 6.4$$

The spring force F_{Sm} is modeled according the linear Hooke's law. The friction force F_{Fm} is computed according to the Karnopp's friction model (Garcia C., 2008) where the viscous friction coefficient is calculated according to

$$c_m = \frac{2\pi\mu l_m}{R_m - r_m} \quad 6.5$$

Following a quasi-steady state approach, the flow force F_{fm} includes only the steady-state term

$$F_{fm} = \sum_i F_{fm,i} = 2c_d \cos\alpha_m \sum_i A_{m,i} \Delta p_{m,i} \quad 6.6$$

where the subscript i indicates the different metering areas. The term F_{pm} represents the net sum of all the pressure forces acting on the spool, evaluated by multiplying the pressure acting on each volume of fluid (including the pilot chambers) times the spool surfaces perpendicular to its axis

$$F_{pm} = \sum_i \pm p_{m,i} S_{m,i} \quad 6.7$$

The $\pm$ sign indicates that, according to the orientation of $S_{m,i}$, the force may be towards the positive or negative direction of the spool axis. The pressure in the pilot chambers are evaluated as described in Eq. 6.1 and Eq. 6.3, while in the other volumes of fluid (which are represented in Fig. 39), pressures are evaluated according to the pressure build-up equation, which according to this notation becomes

$$\dot{p}_{m,i} = \frac{B}{V_{m,i}} \sum_i \left(Q_{m,i} \pm \dot{V}_{m,i} \right) \quad 6.8$$

The $\pm$ sign indicates that, according to the orientation of the i-control volume, the pressure variation may increase or decrease be towards the positive or negative velocities of the spool axis.

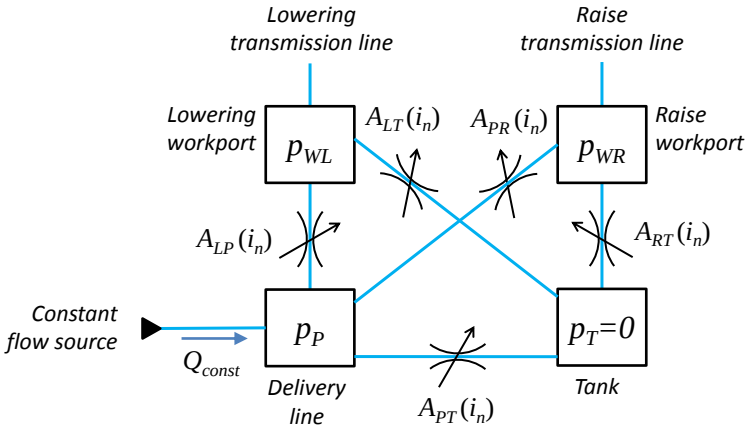

Fig. 39: Simplified representation of the metering areas of the directional valve in case study 1.

Equation 6.8 keeps into account the flow leakages between fluid volumes

$$Q_{ml,i} = \frac{\pi R_m \left(R_m - r_m\right)^3 \Delta p_m}{6\mu l_m} \tag{6.9}$$

The flow rate across the metering sections can be evaluated according to the orifice equation

$$Q_{m,i} = c_d A_{m,i}\left(i_n\right)\sqrt{\frac{2\Delta p_{m,i}}{\rho}} \tag{6.10}$$

By measuring the geometry of the metering edges, which as it is shown in Fig. 6 contains several notches, it was determined the nonlinear relationship between each metering area $A_{m,i}$ and the position of the spool x_m. According to Eq. 6.1 through 6.4 it is possible to relate x_m to i_n, therefore the metering area from in Eq. 6.10 can be expressed as

$$A_{m,i} = f_{1,i}\left(x_{m,i}\right) = f_{2,i}\left(i_n\right) \tag{6.11}$$

Beside the directional valve, the other components of the system in Fig. 32 are modeled according the following approach.

6.1.1.2 Orifice

The flow across the orifices is determined through the orifice equation (Eq. 6.10), where the value of $A_{m,i}$ is constant.

6.1.1.3 Check valve

Check valves are modeled similarly to the orifices, but an “if-statement” is added to permit the flow on yin one direction.

6.1.1.4 Relief valve

The flow rate across the relief valve is computed according the following piecewise equation

$$\begin{cases} Q_{RV} = 0 \quad (\Delta p_{RV} \le 0) \\ Q_{RV} = K_{PF}\Delta p_{RV} \quad (\Delta p_{RV} > 0) \end{cases} \tag{6.12}$$

where Δp_{RV} is defined as

$$\Delta p_{RV} = p_{RVin} - p_{RVs} \tag{6.13}$$

and K_{PF} is the pressure-flow coefficient, obtained by linearization of the orifice equation for the nominal operating condition

$$K_{PF} = \left.\frac{\partial Q}{\partial \Delta p}\right|_0 \tag{6.14}$$

6.1.1.5 Hydraulic linear actuator

The net force produced by the hydraulic linear actuator is obtained by solving the dynamic equation of the piston

$$F_r = p_R A_R - p_L A_L + \dot{x} c_{PC} + F_C \tag{6.15}$$

where F_C is the reaction force acting when the piston is in contact with the end stops and c_{PC} is the viscous friction coefficient evaluated applying Eq. 6.5 to the actuator geometry. The leakage flow rate is computed from Eq. 6.9 by using the actuator geometry. The pressure in the actuator chambers is the integral of the pressure build-up equation, and it is equal to Eq. 3.7.

6.1.1.6 Flow control valve

In this work a two way pressure compensated flow control valve is used. The schematic of the valve is presented in Fig. 40.

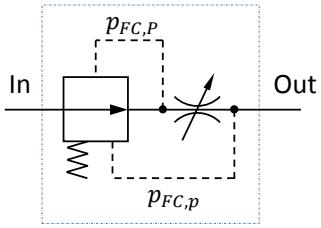

Fig. 40: Schematic of the pressure compensated flow control valve.

The adjustable orifice is modeled according to the orifice equation, while the flow rate across the normally open valve is modeled according the following piecewise equation

$$\begin{cases} Q_{FC} = K_{PF,FC}\Delta p_{FC} \quad (\Delta p_{FC} < 0) \\ Q_{FC} = 0 \quad (\Delta p_{FC} \ge 0) \end{cases} \tag{6.16}$$

where Δp_{FC} is equal to

$$\Delta p_{FC} = p_{FCs} + p_{FCp} - p_{FC,P} \tag{6.17}$$

6.1.1.7 Counterbalance valves

The counterbalance valve schematic is shown in Fig. 41.

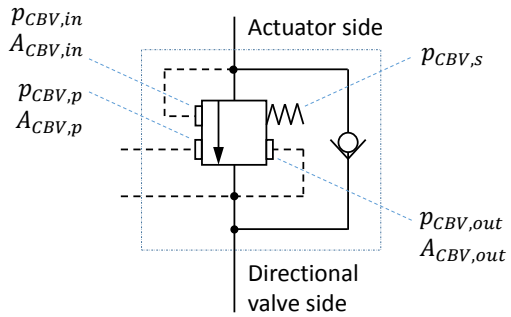

Fig. 41: Schematic representing the generic counterbalance valve.

It includes a check valve and a normally closed valve modeled according to the piecewise equation

$$\begin{cases} Q_{OVC} = 0 \quad (\Delta p_{OVC} \le 0) \\ Q_{\mathrm{OVC}} = K_{OVC,PF}\Delta p_{OVC} \quad (\Delta p_{OVC} > 0) \end{cases} \tag{6.18}$$

where Δp_{OVC} is equal to

$$\Delta p_{OVC} = A_{OVCin}\, p_{OVCin} + A_{OVCp}\, p_{OVCp} - p_{OVCs} - A_{OVCs}\, p_{OVCout} \tag{6.19}$$

where the areas $A_{OVC,in}$, $A_{OVC,p}$, and $A_{OVC,out}$ are normalized with respect to the maximum value.

6.1.1.8 Hydraulic line and fluid properties

The hydraulic lines are modeled as a transmission line having impedance formed by a series of capacitive-resistive-capacitive elements. Additional details regarding the line modeling are reported in: LMS.Imagine.Lab AMESim®, 2010.

Table 6: Parameters used in the hydraulic model.

Parameter	Value	Unit	Parameter	Value	Unit
$p_{p,max}$	30	bar	p_{RVs}	270	bar
p_T	0	bar	p_{OVCs}	300	bar
ω_{pn}	300	rad/s	ς	0.8	–
c_d	0.7	–	α_m	69	deg
B	1.6e9	Pa	μ	4e-2	kg/ms
ρ	870	kg/m^3	A_{OVCin}	1	–
A_{OVCout}	0.5	–	A_{OVCp}	4	–

6.1.2 Planar Mechanical Model

The planar mechanical model computes the motion of the reference crane structure. The model input are the forces generated by the hydraulic actuators, and the output is the instantaneous position of the hydraulic actuators. As previously stated, the test cycle operates the main boom only; therefore the reference crane motion can be simplified according to the following considerations:

- The swing motion is not modeled because it does not affect the overall crane dynamics (consequently the crane will be modeled according to a planar model rather than a tridimensional one).
- The telescopic stage is considered as a single rigid body.
- The counterbalance valves on the outer boom cylinder keep it retracted during the entire test cycle. For this reason, the outer boom planar mechanical cylinder is set completely retracted as initial condition. However, during the test cycle, oscillations in its position are made possible by the compressibility of the fluid in the outer boom cylinder.

The planar mechanical model is developed in absolute coordinates and it is constituted basically by three models:

- Rigid body submodel represents the different parts of the crane structure. Main parameters of the submodel are the real dimension and masses of the reference crane.
- Pivot joint submodel constrains two rigid bodies allowing only one degree of freedom, namely the rotation respect to the axis perpendicular to the plane.
- Prismatic joint submodel is used to simulate the linkage between the cylinder rod and one or two rigid bodies. This submodel constrains the cylinder, allowing its translation along its axis only.

The model was implemented using blocks from the AMESim® planar mechanical library (LMS.Imagine.Lab AMESim®, 2010), which uses a Lagrange multiplier based method to determine the forces and torques acting on each rigid body.

6.1.3 Electronic Controller Model

The electronic controller model allows simulating the directional valve current i_n for a given operator command C_n (which can be read directly from the actual C_n measurement). This model can simulate both the original open loop control system and the proposed control method in order to compare them. The model is implemented in Simulink® and its solvers runs in parallel with the AMESim® one, which evaluates the plant dynamics.

6.2 Approximate Directional Valve Dynamics

In Sect. 4.2.1, the formulation of the proposed control method was based on the assumption that it is possible to determine an approximate relationship to approximate the directional valve dynamics which is based exclusively on plant model states which can be identified from the measurements which are available in case of pressure feedback control method (namely: p_{WR}, p_{WL}, and i_n, which are measured, and the load mass M_L, which can be estimated from the measured ones).

In the case of the hydraulic crane, the power supply provides approximately constant flow, therefore the pressure is determined by the load. It is recalled the assumption only one actuator is moving at a time. Therefore, the resulting situation can be represented in the schematic in Fig. 39. At first approximation, the flow will be divided according to the following pattern:

- Flow from P port to T, R, or L:
  - If the valve is in normal position all the flow goes from P to T.
  - If the valve is in raise position: the flow is divided into two: from P to T and from P to R. The two flows are divided in a proportion depending on the value of the metering areas A_{PT} and A_{PR} (which can both be approximates as a linear function of i_n) and the pressures at the T port and R workport (both known: $p_T = 0$; p_{WR} is measured).
  - If the valve is in lowering position: it is similar to the previous case.
- Flow from a workport to T: The flow is determined by the metering area (which can be approximate as a linear function of i_n), the workport pressure (which is measured) and the tank pressure ($p_T = 0$).

6.3 Stability Analysis of Pressure Feedback Control

This section shows the stability of the proposed control method with reference to case study 1. Additionally, a comparison between the system damping of the original machine and the version which uses the proposed control method will be presented.

Like all hydraulic system, case study 1 is strongly nonlinear. A rigorous analysis would require applying nonlinear system stabilities theories. Several levels of complexity characterize the different nonlinear systems stability theories (Franklin G. F., et al., 2009). *Linearization by nonlinear feedback* method can be applied in case all the nonlinearities can be measured and subtracted to the desired output. In this case, only the linear part of the output dynamics is left and a linear controller can be designed. Since this technique was not applicable in case of pressure feedback control (many nonlinearities cannot be directly measured by pressure measurement), this technique was not used for design purpose and it cannot be applied to analyze the system stability. *Linearization by inverse nonlinearity* method can be applied only in case all the nonlinearities occur on the control term, which in the pressure feedback control case is i_n. This method cannot be

applied because nonlinearities occur on other variables as well (e.g. the square root of the pressure drop is computed in the orifice equation). *Equivalent gain analysis* method can be applied only in case the nonlinearities are al on the feedback signals. This method cannot be applied since because nonlinearities occur on other variables as well (e.g. nonlinearities in the machine mechanical dynamics). *Circle criterion* can be applied only in case only one nonlinearity is present in the system, which is an extremely unlikely condition for hydraulic machines. *Lyapunov's first and second stability methods* impose very few conditions and they are applicable in most of the cases. The drawback of this freedom is that also the guidelines to apply the methods are weak. A function derived from the set on equations of the nonlinear system, is called Lyapunov function in case it satisfied specific properties. In case the Lyapunov function is determined, then it is possible to determine whether the system is stable or not. However, the Lyapunov stability methods have a series of drawback: no specific guidelines for the determination of the Lyapunov functions are available yet, therefore it is in most of the cases a time consuming trial-and-error process; the only information given by the Lyapunov methods is whether the system is stable or asymptotically stable, therefore there is no chance to proof whether the system is unstable.

The comparison of the features of the above methods suggests a different approach would fit better for case study 1. The *small signal approach* is based on the linearization of all the equations (typically according to first order Taylor series method) in correspondence of a nominal operating point. Being the crane model strongly nonlinear, it is not possible to use the small signal approach to infer conclusion from the overall machine dynamics. However, it can be used to test every set gain scheduled control parameters (P^*, I^*, D^*) for any specific combination of scheduling variables. Since the procedure has to be repeated for any specific combination of scheduling variables it might be time consuming, however, computational software (e.g. Matlab®) offer specific tools to linearize a nonlinear model in user defined operating conditions. The automatic linearization process results in the state space description of the linearized system or in the overall transfer function. Setting C_n as system input and ψ (velocity of rotation of the outer boom) as system output, the numerical linearization tool was applied to the nonlinear model of the crane and for several combinations of scheduling variables were obtained as many transfer functions.

As already stated, the Lyapunov stability methods can just provide information about the system stability, differently; the chosen approach is also able to indicate how well the controller is operating in order to stabilize the system versus the standard system which does not use any active damping method. An example of this is proposed in Fig. 42: C_n is a step from 0 to 100%; M_L=200kg; the initial position of the outer boom is ψ_0=0deg.

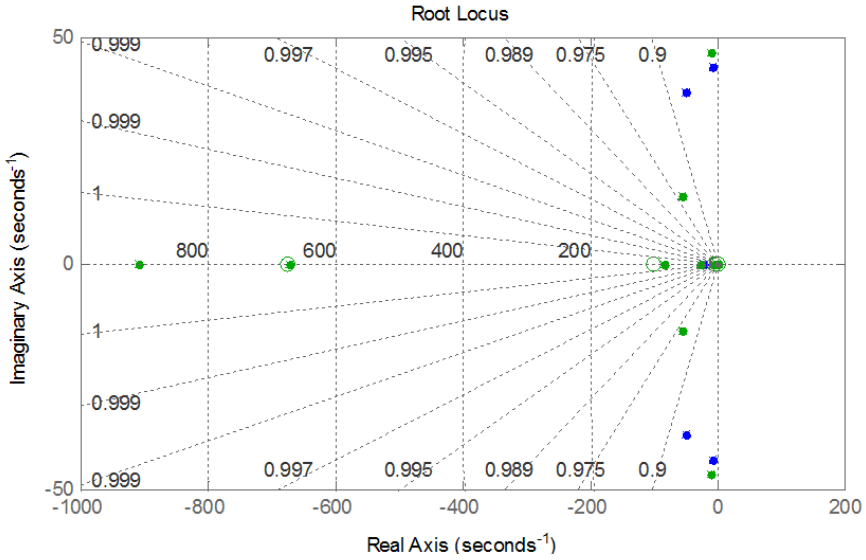

Fig. 42: Root loci of the system (input: operator command; output: outer boom rotation): blue dots represent the original crane dynamics; green dots represent the crane using the proposed vibration damping method.

Fig. 42 shows the entire root loci of the system: solid circles represent the pole; the colors blue and green are respectively used to represent the standard crane and the crane using the proposed damping method. It is possible to observe several high frequency poles on the real axis, meaning those poles are exponentially stable and their associate dynamics will decay to zero very fast. Those poles have a negligible effect on the machine vibrations; therefore it is convenient to focus on the poles closer to the right half plane of the root loci (where eventual unstable poles would be located).

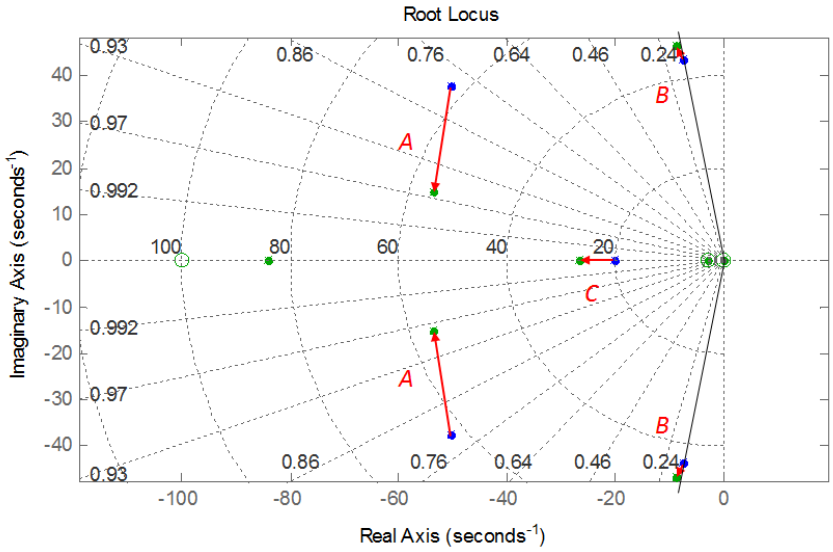

Fig. 43: Zoom of the root loci in correspondence of the dominating poles.

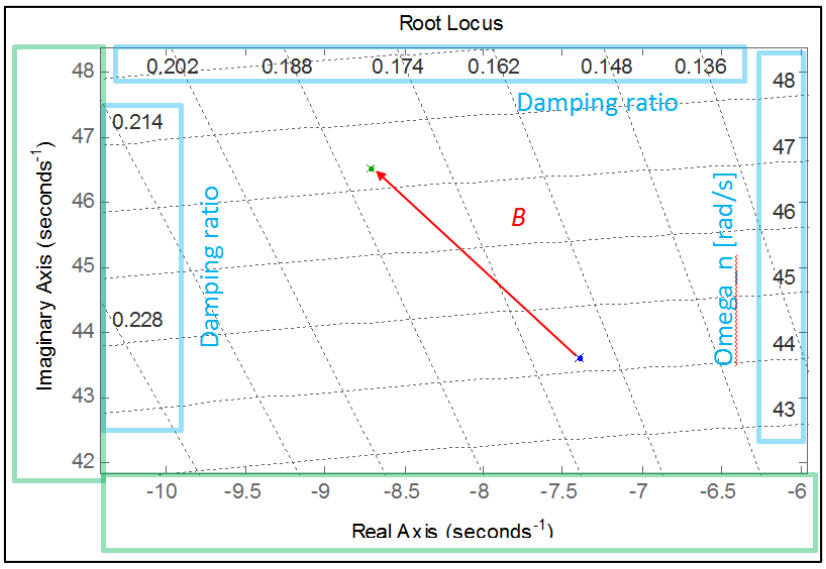

Fig. 44: Zoom of the root loci in correspondence of the high frequency poles.

From Fig. 44 it is possible to observe no poles are located on the right half plane, and the only poles on the imaginary axis are distinct (no repeated poles): this allows concluding the system is stable, and specifically, it is marginally stable. In particular, it was expected to obtain this conclusion, since the step response to the input C_n of the system output $\dot{\psi}$ (velocity of rotation of the outer boom) will not decay to zero, but will stabilize to the steady-state value of $\dot{\psi}$.

It is then focusing on the dominant poles (indicated in Fig. 43 with A, B, C) which is possible to conclude the effect of the proposed controller on the standard system

- A moves towards the real axis and consequently it significantly increases its damping (and slightly reduces the natural frequency): damping goes from about 0.80 to 0.97.
- B slightly increases the damping (and slightly increases the natural frequency): damping goes from 0.164 to 0.184.
- C is already on the imaginary axes; however it increases the frequency making its exponential stability faster.

It is possible to conclude then that the introduction of the proposed vibration damping system does not compromise the stability of the system, which remains marginally stable. On the contrary, the introduction of the proposed control method increases the damping of all dominant poles and increases their natural frequency (consequently settling time reduces).

The complete stability analysis would require the analysis of all combinations of scheduling variables and this task will be performed as a future work.

6.4 Pressure Feedback vs. Acceleration Feedback: Analytical Modeling

The aim of this section is to present a comparison between the proposed control method in case of pressure feedback and in case of acceleration feedback. The goal is pursued by presenting the analytical formulation of a model to estimate the mechanical arms acceleration based on pressure measurements only. The validation of this model will be presented in Sect. 7.5.

Also, the method presented in this section requires in addition to the pressure sensors on the workports, as it was described in Sect. 4.2.1, additional pressure sensors on the power supply and return ports. These additional sensors allow to extend even further the generality of the pressure feedback control method since the estimation of the mechanical arms acceleration is now applicable in case of: any configuration of the power supply; in presence of any additional valve in the transmission line from the directional valve to the actuator.

The estimate of the mechanical arms dynamics is obtained through a model composed by four elements as represented in the schematic of Fig. 45.

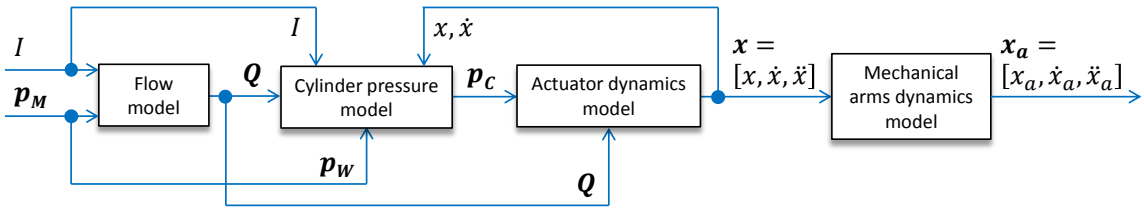

Fig. 45: Block diagram representing the model to estimate the mechanical arms dynamics.

The block diagram in Fig. 45 will be presented following the order from left to right. The first block calculates the flow in the transmission lines $\boldsymbol{Q} = [Q_e, Q_r]$ from the value of the electric current I and the measured pressures $\boldsymbol{p_M} = [p_P, p_T, p_{We}, p_{Wr}]$. The second block calculates the cylinder pressure $\boldsymbol{p_C} = [p_{Ce}, p_{Cr}]$. This model requires the value of $\boldsymbol{Q}$, the current I, and the pressures measured at the workports $\boldsymbol{p_W} = [p_{We}, p_{Wr}]$. Then, the third block calculates $\boldsymbol{x} = [x, \dot{x}, \ddot{x}]$ from the values of $\boldsymbol{p_C}$ and $\boldsymbol{Q}$. Finally, the fourth block calculates the mechanical arms dynamics $\boldsymbol{x_a} = [x_a, \dot{x}_a, \ddot{x}_a]$. A detailed description of the overall model is provided in the following subsections.

6.4.1 Flow at the Workports

The electric current I to the PDV solenoids is typically a known quantity since it is the output from the control unit. The spool of a 4/3 open center PDV is schematically represented in Fig. 46 along with the indication of the flow rates across each metering area.

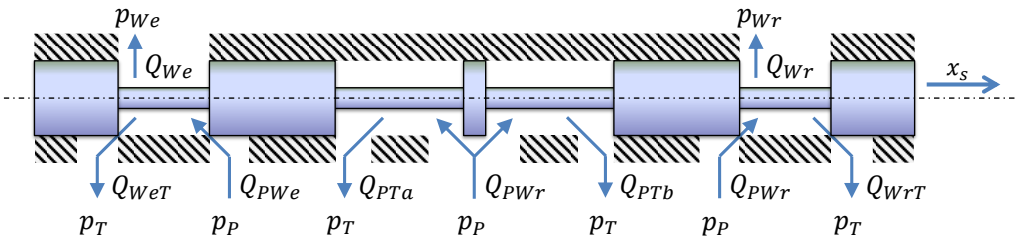

Fig. 46: Schematic representing the metering areas determined by the position of the spool of a 4/3 PDV.

The current I causes the translation x_s of the PDV spool along its own axis with a dynamics that can be approximated by the second order transfer function below:

$$H(s) = \frac{x_s(s)}{I(s)} = \frac{\omega_n^2}{s^2 + 2\varsigma\omega_n s + \omega_n^2} \tag{6.20}$$

The spool position x_s determines the metering areas of each PDV port. According to the lumped parameters modeling approach, metering areas can be described by set of variable orifices whose amplitude depends on the spool position (see Fig. 47).

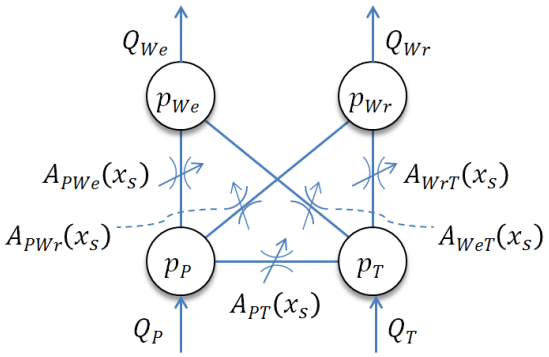

Fig. 47: Representation of the lumped parameters model of the valve in.

The flow rates across the different metering areas can be evaluated from the orifice equation (Eq. 6.6). Considering the relationship between the metering areas $\boldsymbol{A}$ and the spool position x_s to be approximately linear during the control of the actuator velocity (region between the valve saturation and the deadband), then Eq. 6.6 can be rewritten to determine the flow rates from the pressure source port to the workports

$$\begin{cases} Q_{PWe}(I, p_P, p_{We}) = sign(p_P - p_{We})\, c_d\, A_{PWe}(I)\, H(s) \sqrt{\dfrac{2|p_P - p_{We}|}{\rho}} \\ Q_{PWr}(I, p_P, p_{Wr}) = sign(p_P - p_{Wr})\, c_d\, A_{PWr}(I)\, H(s) \sqrt{\dfrac{2|p_P - p_{Wr}|}{\rho}} \end{cases} \tag{6.21}$$

Similarly, the flow from the workport to the return is represented by

$$\begin{cases} Q_{WeT}\left(I, p_{We}, p_T\right) = sign\left(p_{We} - p_T\right) c_d A_{WeT}\left(I\right) H\left(s\right) \sqrt{\dfrac{2\left|p_{We} - p_T\right|}{\rho}} \\ Q_{WrT}\left(I, p_{Wr}, p_T\right) = sign\left(p_{Wr} - p_T\right) c_d A_{WrT}\left(I\right) H\left(s\right) \sqrt{\dfrac{2\left|p_{Wr} - p_T\right|}{\rho}} \end{cases} \quad 6.22$$

The metering areas as a function of the electric current I in Eq. 6.21 and Eq. 6.22 can be collected in the vector: $\boldsymbol{A_{PDV}}(I) = [A_{PWe}(I), A_{WeT}(I), A_{PWr}(I), A_{WrT}(I)]$. The value of all areas in $\boldsymbol{A_{PDV}}(I)$ can be obtained according to the experimental procedure described in Sect. 7.5.1.

With reference to the schematic of Fig. 47 it is then possible to express the final equation for the estimate of the flow rates at the workports

$$\begin{cases} Q_{We}\left(I, p_P, p_{We}, p_T\right) = Q_{PWe} - Q_{WeT} \\ Q_{Wr}\left(I, p_P, p_{Wr}, p_T\right) = Q_{PWr} - Q_{WrT} \end{cases} \quad 6.23$$

In the present study it will be assumed that the flow entering the cylinder is in phase with the one leaving the respective workport. Consequently, Q_{Ce} will be considered to be approximately equal to Q_{We} and both quantities will be indicated by Q_e (transmission line relative to the extension of the actuator). Similarly, Q_{Cr} will be considered to be approximately equal to Q_{Wr} and both quantities will be indicated by Q_r (transmission line relative to the retraction of the actuator). This assumption implies the inductive and capacitive effect of the volume of fluid inside the transmission lines are limited. This assumption is reasonable for many applications, like for the hydraulic crane taken as reference in this work, because of the limited diameter and length of the transmission lines connecting the PDV to the actuators.

6.4.2 Pressure in the Cylinder Chambers

In general, the pressure in the cylinder chambers differs from the respective pressure at the PDV workports. For this reason, the cylinder pressure model is formulated to determine the cylinder chambers pressure from the values measured at the PDV workports.

6.4.2.1 Simple Transmission Lines

This case is relative to those machines where no additional elements (e.g. valves, accumulators) are installed on the lien between the PDV and actuator.

The formulation in this case is based on linear impedance model for hydraulic transmission lines. Assuming lines of limited length, the flow rate at the workport can be considered only the resistive effect will be considered so that the resulting equations are:

$$\begin{cases} p_{Ce}\left(p_{We}, Q_e\right) = p_{We} - R_{Le} Q_e \\ p_{Cr}\left(p_{Wr}, Q_r\right) = p_{Wr} - R_{Lr} Q_r \end{cases} \quad 6.24$$

where R_{Le} and R_{Lr} represent the resistance on the transmission lines (extension and retraction side respectively). Similarly, V_{Lr} and V_{Le} represent the fluid volumes of the transmission lines (extension and retraction side respectively).

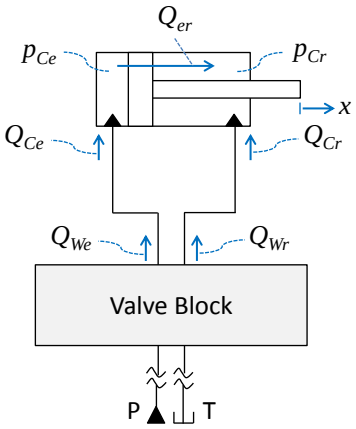

Fig. 48: Example of simple transmission lines.

6.4.2.2 Additional Valves on the Transmission Lines

In the cases where additional valves are introduced in the transmission line to obtain specific functionalities the model considers a set of equations relative to different modes of operation of the machine. The following description takes as reference the case of where counterbalance valves are used to handle aiding loads and meet safety requirements of the system.

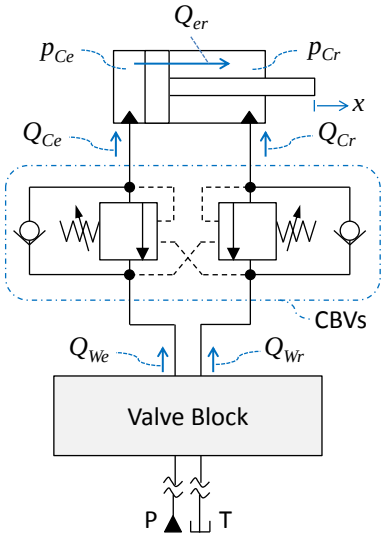

Fig. 49: Example of additional valve on the transmission lines (counterbalance).

The system architecture of Fig. 49 is used in several hydraulic machines, and in particular in the experimental setup considered in this work. Unlike other previous works in which the counterbalance valve dynamics is accounted through detailed modeling of the valve itself (Ritelli G.

F., and Vacca A., 2013), the present formulation describes an innovative approach. In particular, the proposed method requires only one parameter describing the counterbalance valve (namely the hydraulic resistance representative of the flow through the unidirectional valve integrated in the counterbalance valve).

Case 1: Extension of the hydraulic cylinder $(I > 0)$

In this case the flow goes through the unidirectional valve from the extension workport to the extension chamber of the cylinder. The pressure in the extension chamber of the cylinder can be still evaluated with the linear impedance model for hydraulic transmission lines, by means of the following equation

$$p_{Ce}\left(p_{We}, Q_e, \left(I > 0\right)\right) = p_{We} - R_{CBVe} Q_e \tag{6.25}$$

The hydraulic resistance R_{CBVe} is representative of the pressure drop across the transmission line and the unidirectional valve of the CBV on the extension side.

The pressure build up equation (derived from continuity and the state equation for the fluid) can be used to determine the pressure in the retraction chamber of the cylinder.

$$\dot{p} = \frac{\beta}{V}\left(\sum_i Q_i + \dot{V}\right) \tag{6.26}$$

In Eq. 6.26: V is the volume of the fluid; β is the bulk modulus of the fluid; and Q_i is the generic flow entering the control volume net of leakages. Flow leakages represented in Fig. 49 by Q_{er} could be included in the summation term, but in several applications like the one described in this work can be neglected. The pressure in the retraction side of the cylinder can therefore be expressed as

$$p_{Cr}\left(p_{Cr}, Q_r, \left(I > 0\right)\right) = p_{Cr}\left(t_{I>0}\right) + \frac{\beta}{V_{Cr}} \int_{t_{I>0}} \left(Q_r - \dot{V}_{Cr}\right) dt \tag{6.27}$$

In Eq. 6.27, $p_{Cr}(t_{I>0})$ represents the initial value of the pressure in the retraction side of the cylinder. This value has to be stored in the control unit as soon as the condition $I > 0$ takes place and has to be reset when the condition $I < 0$ (which defines case 2) occurs. The value of the retraction side cylinder volume V_{Cr} and its derivative $\dot{V}_{Cr}$ can be evaluated by from $\boldsymbol{x}$ calculated as described in the next section.

Solutions of the impedance model and pressure build up equations describe all cases of the model to estimate the pressure in the cylinder chambers, but separate sub-sections are presented to formalize the switching logics.

Case 2: Retraction of the hydraulic cylinder $(I < 0)$

Case 2 can be treated with the same approach of case 1, however this time the pressure build up equation is solved for the extension side whereas the impedance model is solved for the retraction side of the cylinder:

$$p_{Ce}\left(p_{Ce},Q_e,\left(I<0\right)\right)=p_{Ce}\left(t_{I<0}\right)+\frac{\beta}{V_{Ce}}\int_{t_{I=0}}\left(Q_e-\dot{V}_{Ce}\right)dt \quad 6.28$$

$$p_{Cr}\left(p_{Wr},Q_r,\left(I<0\right)\right)=p_{Wr}-R_{CBVr}Q_r \quad 6.29$$

Case 3: Stop of the hydraulic cylinder motion $(I=0)$

With reference to the system of Fig. 49 two sub-cases can be identified: stop after extension and stop after retraction. These two cases differ because of a series of reasons including: the hydraulic circuit often differs from the extension to the retraction side; typically these machines operate large inertial loads whose force of gravity is oriented in specific directions.

Case 3A: Stop after retraction

In case of stop after retraction, the inertia of the machine will promote the retraction of the actuator even after the PDV reaches normal position: with reference of Fig. 41, oil in the transmission line is moved from the volume of fluid adjacent to the retraction workport into the volume of fluid of the retraction side of the cylinder chamber. The presence of the unidirectional valve on the transmission line – retraction side – forces this flow to be always directed from the workport to the cylinder: this causes a pressurization of the retraction chamber of the cylinder. As a consequence, also the extension chamber of the cylinder pressurizes, reaching values high enough to open the counterbalance valve (this will be found in the results, section 4). Eventually, both the counterbalance valves on the system of Fig. 41 open, and consequently:

$$p_{Ce}\left(p_{We},\left(I=0\right)\right)=p_{We} \quad 6.30$$

$$p_{Cr}\left(p_{Wr},\left(I=0\right)\right)=p_{Wr} \quad 6.31$$

Case 3B: Stop after extension

In case of stop after extension, the inertia of the machine will promote the extension of the actuator even after the PDV reaches normal position: with reference to Fig. 41, oil in the transmission line is moved from the volume of fluid adjacent to the extension workport into the volume of fluid of the extension side of the cylinder chamber. The presence of the unidirectional valve on the transmission line –extension side – forces this flow to be directed always from the PDV workport to the cylinder. Eventually the pressure at the extension workport becomes decoupled with respect to the value in the respective cylinder chamber. The pressure in the extension camber can be evaluated similarly to Eq.6.28 by considering $Q_e=0$

$$p_{Ce}\left(p_{Ce},Q_e,\left(I=0\right)\right)=p_{Ce}\left(t_{I<0}\right)+\frac{\beta}{V_{Ce}}\int_{t_{I=0}}\dot{V}_{Ce}dt \quad 6.32$$

The pressure in the transmission line –extension side – has to hold the load and it is typically large enough to produce the complete opening of the counterbalance valve on the retraction line, making the pressure measured at the retraction port coincident with the one at the respective cylinder chamber:

$$p_{Cr}\left(p_{Wr},\left(I=0\right)\right)=p_{Wr} \tag{6.33}$$

6.4.3 Hydraulic Actuator Mechanical Dynamics

The estimation of the actuator mechanical dynamics is based on the pressure build up equation at the chambers of the cylinders. The general formulation in Eq.6.26 can be rewritten as:

$$\begin{cases}\dot{p}_{Ce}=\dfrac{\beta}{V_{Ce}}\left(Q_e-\dot{V}_{Ce}\right)\\ \dot{p}_{Cr}=\dfrac{\beta}{V_{Cr}}\left(Q_r+\dot{V}_{Cr}\right)\end{cases} \tag{6.34}$$

In Eq. 6.34, the volumes are given by

$$\begin{cases}V_{Ce}=V_{Ce,min}+xA_e\\ V_{Cr}=V_{Cr,max}-xA_r\end{cases} \tag{6.35}$$

By rearranging the terms of Eq. 6.34 it is possible to obtain the following differential equations for the pressure in the two cylinder chambers

$$\begin{cases}\dot{p}_{Ce}=\dfrac{\beta}{V_{Ce,min}+A_e x}\left(Q_e-A_e\dot{x}\right)\\ \dot{p}_{Cr}=\dfrac{\beta}{V_{Cr,max}-A_r x}\left(Q_r+A_r\dot{x}\right)\end{cases} \tag{6.36}$$

The flow rates and the pressures in the cylinder are obtained according to the method described in Sect. 6.4.1. The parameters A_e, A_r, $V_{Ce,min}$ and $V_{Cr,max}$ are constants related to the actuator geometry. Each one of the differential Eq. 6.36 can be numerically solved to obtain x: for this study, a finite difference solution in the time domain was chosen. The time domain is divided in time intervals ($j=1..k..m$). The interval amplitude corresponds to the sampling time Δt of the data acquisition system. The initial value of the actuator position, x_0, has to be set (it also corresponds to the last position at the end of the previous cycle of operation, or it can be set to a known value every time the actuator reaches an end stop). For many machines, such as the hydraulic crane used for the experiments of this research, the actuators at rest are typically fully retracted ($x_i=0,\forall i$) so mechanical constrains can be engaged as safety measures to prevent undesired movements of the mechanical arms.

Once the initial time step is defined, the motion of the actuator at each time step can be evaluated according to:

$$\begin{cases} x_k\left(p_{Ce},Q_e\right)=+\dfrac{\beta_{e,k}\left(p_{Ce,k}\right)\Delta t}{D_{e,k}}\left(Q_e+\dfrac{A_e}{\Delta t}x_{k-1}\right)-\dfrac{p_{Ce,k}-p_{Ce,k-1}}{D_{e,k}}V_{e,min} & \text{(a)} \\ x_k\left(p_{Cr},Q_r\right)=-\dfrac{\beta_{r,k}\left(p_{Cr,k}\right)\Delta t}{D_{r,k}}\left(Q_r-\dfrac{A_r}{\Delta t}x_{k-1}\right)+\dfrac{p_{Cr,k}-p_{Cr,k-1}}{D_{r,k}}V_{r,max} & \text{(b)} \end{cases} \quad 6.37$$

The denominator terms $D_{e,k}$ and $D_{r,k}$ group the following variables

$$\begin{cases} D_{e,k}=A_e\left(p_{Ce,k}-p_{Ce,k-1}+\beta_{e,k}\left(p_{Ce,k}\right)\right) & \text{(a)} \\ D_{r,k}=A_r\left(p_{Cr,k}-p_{Cr,k-1}+\beta_{r,k}\left(p_{Cr,k}\right)\right) & \text{(b)} \end{cases} \quad 6.38$$

The pressure dependency of the bulk modulus is considered according to a linear relationship (Ivantysyn J., and Ivantysynova M., 2001):

$$\begin{cases} \beta_{e,k}\left(p_{Ce,k}\right)=K_\beta p_{Ce,k}+\beta_{p=0} \\ \beta_{r,k}\left(p_{Cr,k}\right)=K_\beta p_{Cr,k}+\beta_{p=0} \end{cases} \quad 6.39$$

Where: $K_\beta={}^{\partial\beta}/_{\partial p}$ is the angular coefficient of the linearized curve bulk modulus with respect to the pressure at a specific temperature, and $\beta_{p=0}$ is the bulk modulus at the same temperature and 0bar. The applicability of Eq. 6.37a and Eq. 6.37b is guaranteed as long as a sufficiently fine sampling time Δt is used so that:

$$\begin{cases} \left[\left|p_{Ce,k}-p_{Ce,k-1}\right|<\beta_{e,k}\right] \\ \left[\left|p_{Cr,k}-p_{Cr,k-1}\right|<\beta_{r,k}\right] \end{cases} \Rightarrow \begin{cases} D_{e,k}>0 \\ D_{r,k}>0 \end{cases} \quad 6.40$$

A sampling frequency of 600Hz was observed to largely satisfy this condition. The availability of two equations to determine x_k (namely Eq. 6.37a and Eq. 6.37b) is convenient since it gives the possibility to estimate the actuator dynamics by using the equation corresponding to the most accurate cylinder pressure estimate.

6.4.4 Mechanical Arms Dynamics

In this work it is assumed the mechanical arms can be modeled as rigid bodies since their deformations are typically negligible. Consequently, the mechanical arms dynamics can be obtained from the actuators dynamics by means of a set of trigonometric equations representative of the machine kinematics. The set of equations is specific to the geometry of the machine. In case the proposed method is used in a vibration damping controller, the estimate of the mechanical arms

dynamics is not strictly necessary since according to the assumption in his section there is a direct correspondence between vibrations of the mechanical arms and those of the actuator.

CHAPTER 7. CASE STUDY 1: CRANE: RESULTS

The goals of case study 1 were described in the specific section (Sect. 1.3.1). This chapter describes the results of the case study 1.

Firstly, the comparison between simulation results and experimental results will be presented to validate the crane nonlinear model (Sect. 7.1). Then, it will be presented an example of result obtained from the non-model-based controller parameters tuning for a specific combination of scheduling variables and a specific expression for the cost function (Sect. 7.2). The effectiveness of the pressure feedback vibration damping method will be presented through simulation results (Sect. 7.3) and through experiments (Sect. 7.4). Finally, the method to estimate the mechanical arms acceleration from pressure measurements will be validated to provide a comparison between the pressure feedback and acceleration feedback based control methods (Sect. 7.5).

7.1 Nonlinear Model Validation

The validation of the nonlinear model presented in Sect. 6.1 was performed by comparing, for a specific reference cycle, the simulation results and the experimental results. In particular, the test cycle is represented in Fig. 50. The test cycle was chosen for its simplicity: the crane is with no load; the outer booms as well as all telescopic stages are retracted. The test cycle is constituted by four steps based on the motion of the outer boom at its maximum speed: step 1 is the outer boom lowering from ψ=90deg to ψ_{min} (mechanical end-stop); step 2 is the outer boom sudden stop after the lowering (stop at ψ_{min}); step 3 is the outer boom raise from ψ_{min} to ψ=90deg; step 4 is the outer boom sudden stop after the raise (stop at ψ=90deg). The operator command C_n required to perform this cycle is shown in Fig. 51a, while Fig. 51b shows the resulting pressure in the raise workport p_{WR}. Additionally, Fig. 51c and Fig. 51d show zooms of Fig. 51b in correspondence of the areas where p_{WR} oscillates the most.

The general trend as well as the oscillations in the highlighted areas are captured by the simulation model with a level of accuracy consistent with the purpose of the model. The validation of the nonlinear model justifies its use as tool for: stability analysis by small signal approach linearization (Sect. 6.3); non-model-based controller parameters tuning (next section).

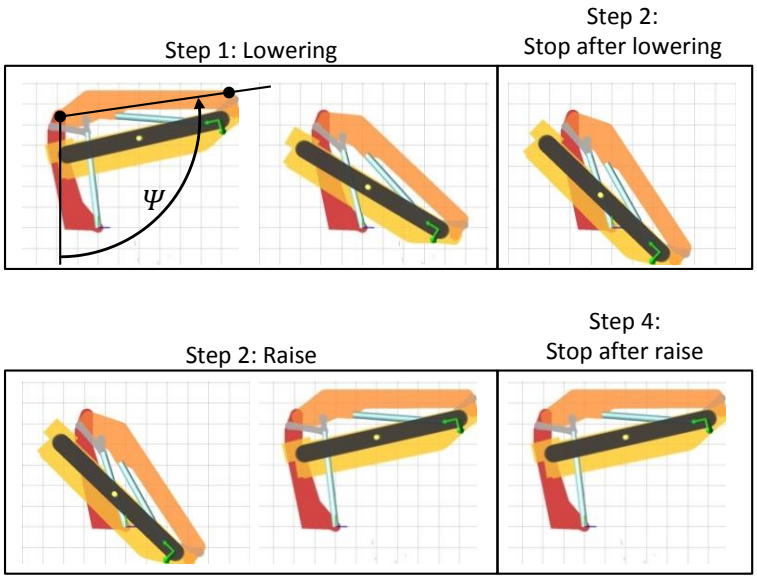

Fig. 50: Schematic representing the steps of the test cycle for the validation of the crane nonlinear model.

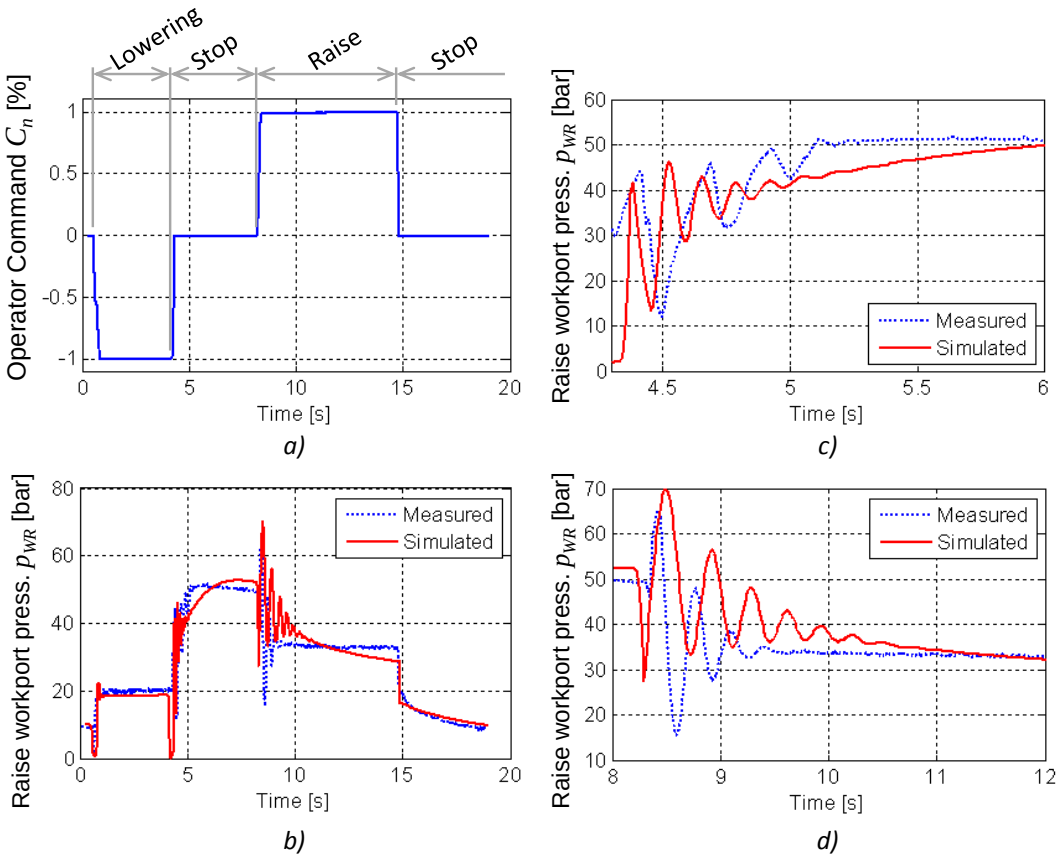

Fig. 51: Nonlinear model validation: a) Operator command test cycle; b) Resulting pressure profile measured at the raise workport; c) Zoom in correspondence of the oscillation during the stop after lowering; d) Zoom in correspondence of the oscillation during the raise.

7.2 Non-Model-Based Controller Parameters Tuning

The general concept behind the non-model-based controller parameters tuning was introduced in Sect. 4.5. In this section, the general concept will be applied to case study 1.

First of all it is necessary to define the target output, namely the output from the machine dynamics which will be used to evaluate the cost function. The cost function is a number which quantifies the extent of the vibrations which have to be damped. Many combinations of target output and cost functions formulations have been tested, however it has been observed that among those properly defined, the results are pretty much consistent. In this section, just one alternative will be presented, namely the one which is most intuitive and turned out to be also effective in all tested conditions. The target output boom angle ψ was used to evaluate the cost function J_ψ representative of the extent of the vibrations on the outer boom:

$$J_\psi(k) = \int_{t_1}^{t_2} \left| \psi(k,t) - \psi_D(k,t) \right| dt \qquad 6.41$$

where: t_1 is the time of the reference step input of i_n; t_2 is the time in which the vibrations of iteration 1 are small enough to be negligible; $\psi_D(t)$ is the polynomial fitting curve of the angle $\psi(k,t)$ from t_1 to t_2 for the iteration 1. The physical meaning of $\psi_D(t)$ is the representation of the desired motion of the crane with no oscillations and no delays. Fig. 52 (top) shows the overlap of $\psi(t,1)$ and $\psi_{PF}(t)$; figure Fig. 52 (bottom) shows $J_\psi(1)$ represented by the area underneath the curve (cost function in correspondence of the iteration k=1, namely the oscillations of the standard crane without the proposed control method).

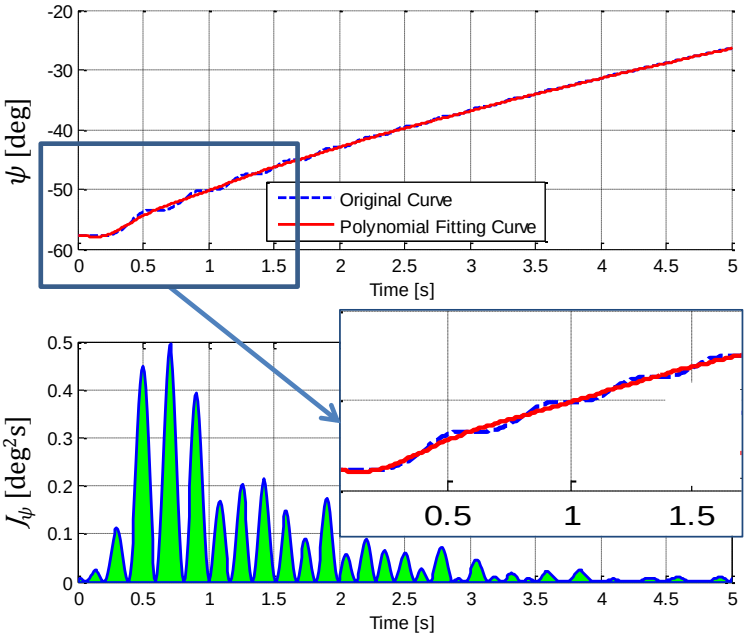

Fig. 52: Rotation of the outer boom (top) and computation of the relative cost function (bottom).

The order of the polynomial fitting curve was chosen on the basis of the following principle: the polynomial order is the smallest order which ensures the following condition:

$$\begin{cases} \psi_{PF}(t)|_{t_1} = \psi(t,1)|_{t_1} \\ \psi_{PF}(t)|_{t_2} = \psi(t,1)|_{t_2} \end{cases}$$

This condition means that the polynomial fitting curve $\psi_{PF}(t)$ has to be equal to the actual curve at iteration 1 ($\psi(t,1)$) in correspondence of the two points identified by t_1 and t_2. The resulting cost function J_ψ is a scalar representative of the oscillation amount for the specific k: combination of control parameters set (P^*, I^*, D^*), load mass M_L, and electric current i_n. Once J_Ψ is determined, it is possible to run the iterative algorithm described in 4.5: the resulting convergence of the parameters was shown in Fig. 30. For each set of control parameters (P^*, I^*, D^*) obtained thorugh this method, it is possible to test their effectiveness in the relative operating condition defined by the scheduling variables: this test will be performed through simulation results first (Sect. 7.3), and through experiments after (Sect. 7.4).

7.3 Pressure Feedback: Simulation Results

In correspondence of a specific set of scheduling variables (mass M_L=0kg, and electric current i_n= raise step from 0 to 100%) and for an initial position of the outer boom identified by ψ_{min}, the controller parameters obtained as described in the previous section simulated were used to evaluate the effectiveness of the proposed control. The results are showed in Fig. 53.

Fig. 53a shows the outer boom rotation ψ in the standard case (indicated by the label “undamped”) and the proposed control method case (indicated by the label optimum): a zoom of the initial area were the vibrations are the largest is shown in Fig. 53b. It has to be specified that Fig. 53b show the comparison between the standard crane and the one controlled with the proposed method, and therefore they substantially differ from Fig. 52 (previous section) where it was shown the comparison between the standard crane and the desired (ideal in absence of oscillations) motion of the crane. Finally, Fig. 53c shows the pressure profile in the raise workport: being in this case the oscillations amplified with respect to Fig. 53b, it is more evident the action of the proposed control on the system.

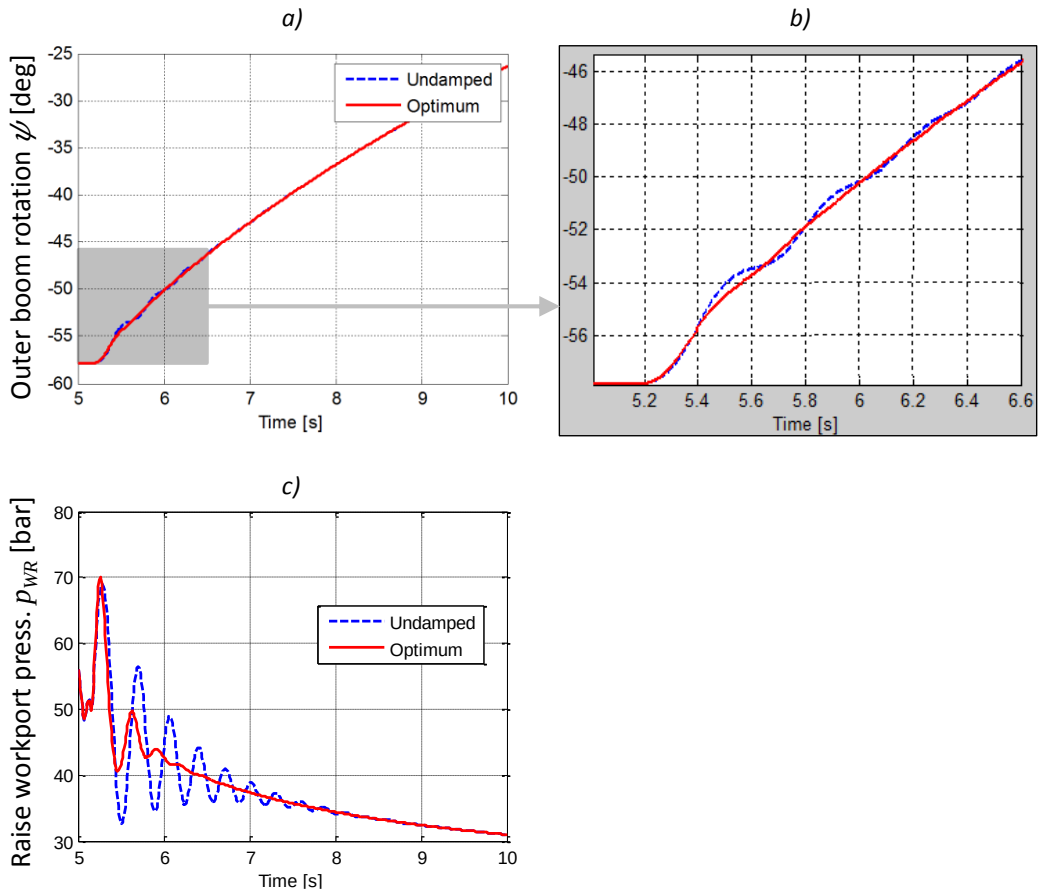

Fig. 53: Simulation results for the hydraulic crane: a) rotation of the outer boom as response of a step input of the operator command; b) zoom in correspondence of the initial motion, when the vibrations are more relevant; c) pressure in the raise workport relative to the motion in figure a).

7.4 Pressure Feedback: Experimental Results

This section shows the experimental results obtained from measurement of the instrumented crane described in Chap. 5. Four configurations of the crane characterized by specific features are considered in this section (see Fig. 54):

- *Configuration 1 (commercial machine)*: The proposed control is not used, and the machine operates according an open-loop strategy. System damping is introduced through the energy dissipative settings of the counterbalance valves.
- *Configuration 2*: The machine operates according a closed-loop strategy based on the proposed method. System damping is introduced through the energy dissipative settings of the counterbalance valves.
- *Configuration 3*: The proposed control is not used, and the machine operates according an open-loop strategy. The counterbalance valve settings are energy efficient and consequently the machine is affected by much higher vibrations than configuration 1 (commercial machine).

- *Configuration 4*: The machine operates according a closed-loop strategy based on the proposed method. System damping is not introduced through the energy dissipative settings of the counterbalance valves. However, system damping is introduced by the proposed control method. This configuration offers potential for energy efficiency and desirable dynamics.

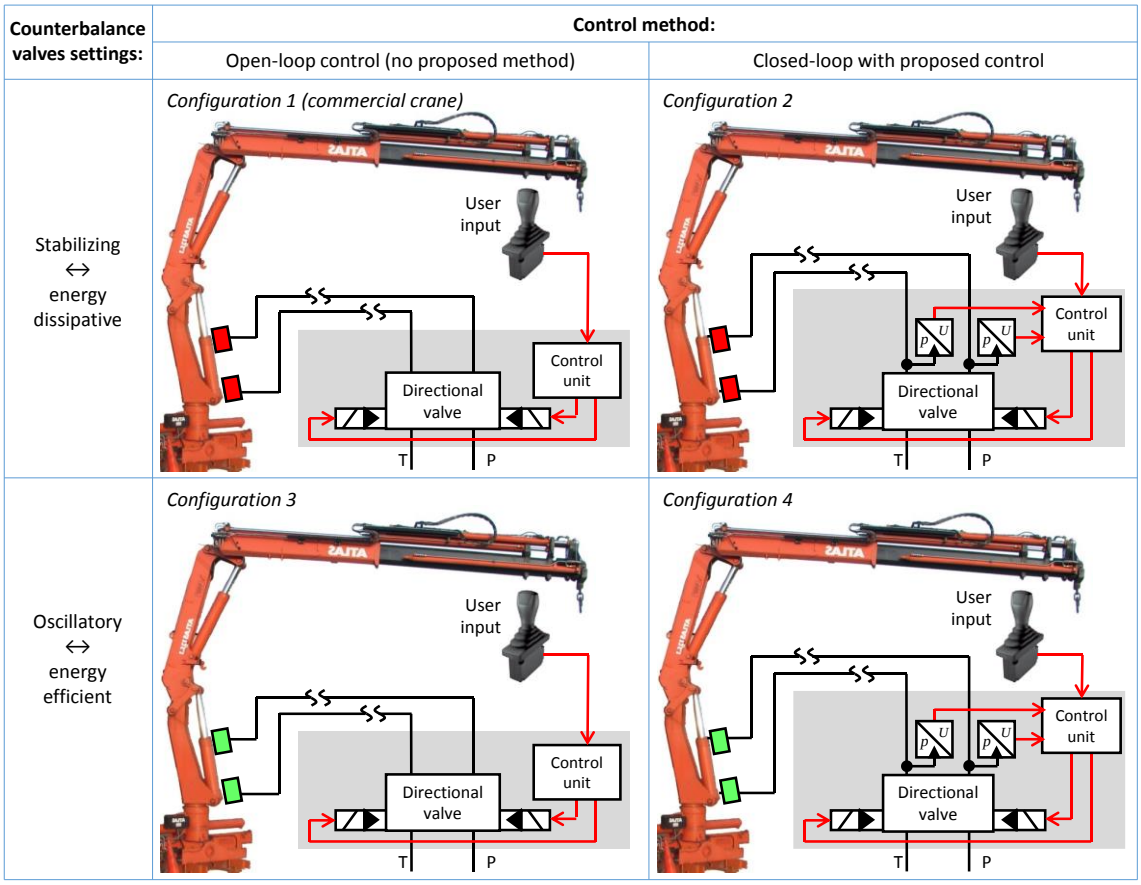

Fig. 54: Summary of the four configurations of the crane experiments.

The first test regards the comparison of the crane results in configuration 1 and configuration 2. The goal of this test is to prove the capability of the proposed vibration damping method to improve the machine dynamics even further than what an energy dissipative setting of counterbalance valve could do. Several operating conditions were tested:

- Test condition 1: maximum speed outer boom raise (C_n is a step from 0 to 100%); the telescopic boom and all telescopic stages are retracted; no load is applied (M_L=0); initial outer boom position is ψ_{min}.
- Test condition 2: sudden stop after raise of the outer boom raise (C_n is a step from 100% to 0%); the telescopic boom and all telescopic stages are retracted; no load is applied (M_L=0); initial outer boom position is ψ_0=105deg.

- Test condition 3: maximum speed outer boom raise (C_n is a step from 0 to 100%); the telescopic boom is extended (all telescopic stages are retracted); no load is applied (M_L=0); initial outer boom position is ψ_0=105deg.

The result of the comparisons are shown in Fig. 55 for the three test conditions and for the following measurements:

- a_T, tangential acceleration of the outer boom end (Fig. 35,1)
- a_C, centripetal acceleration of the outer boom end (Fig. 35,1)
- p_{WR}, pressure at the raise workport (Fig. 32)

All measurements in Fig. 55 show the proposed control method is suitable to reduce the vibrations of the outer boom either as direct measurement performed by the accelerometer or as indirect measurement of the pressure sensor. The reduction of the vibration can be quantified in about 30% reduction of the settling time and overshoot.

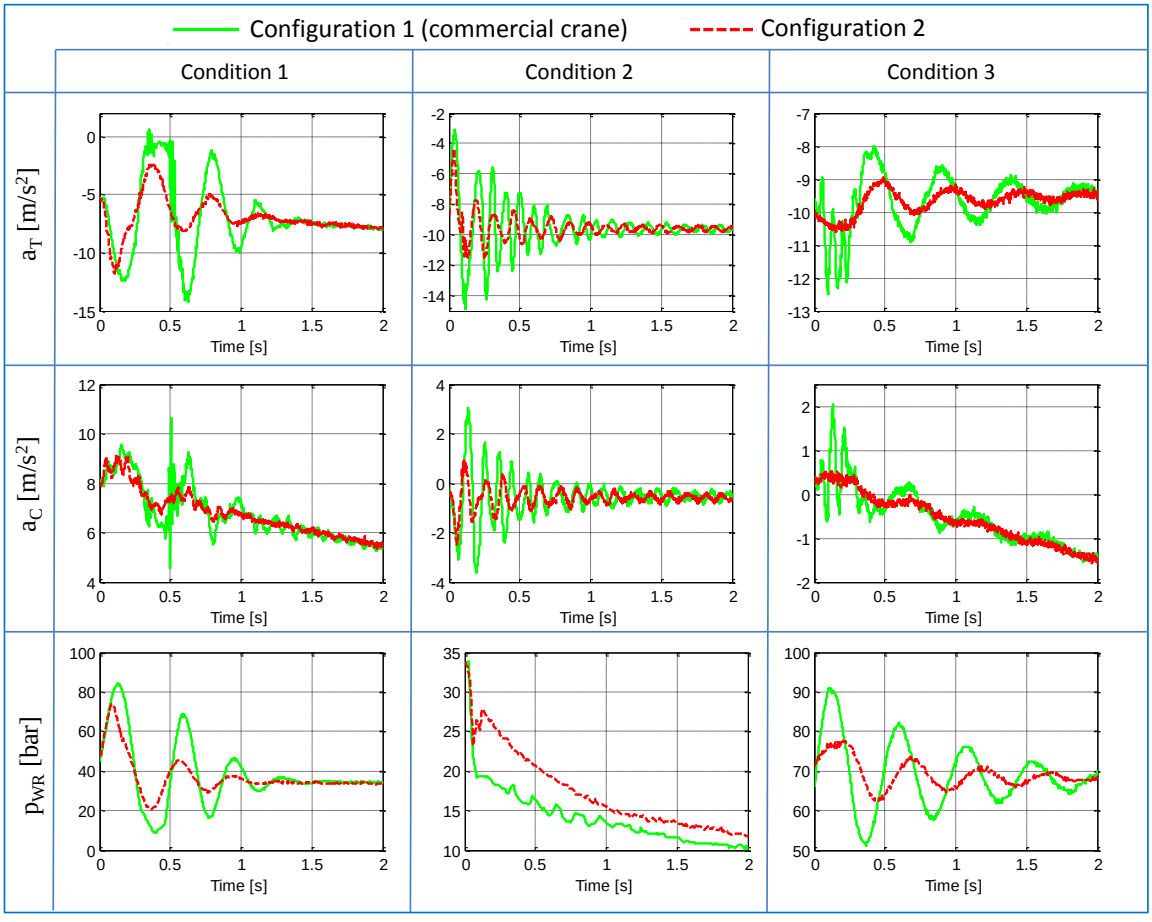

Fig. 55: Comparison between standard crane and the crane using the proposed vibration damping method. The figures reports measurements in terms of tangential and centripetal acceleration (outer boom end) and pressure (raise workport) for the three different test conditions defined in this section.

The second type of test is based on the comparison between the configurations 1 and 3. The goal of this test is to quantify the potential energy savings which can be accomplished by using energy efficient settings of the counterbalance valves. The second type of tests were later on carried out within an associated research project at Purdue University and results were published by Ritelli G. F., and Vacca A. (2013). A summary of those results is reported in Fig. 56. In particular, Fig. 56 represents the positions of the crane over time and defines the test working cycle. This test cycle and four different configurations of the counterbalance valves (in terms of pilot ratio α and spring pressure setting p_s) were used to obtain the curves in Fig. 56. Those curves show up to 42.7% of energy savings can be achieved. A positive trend of the energy saving was observed with larger load mass.

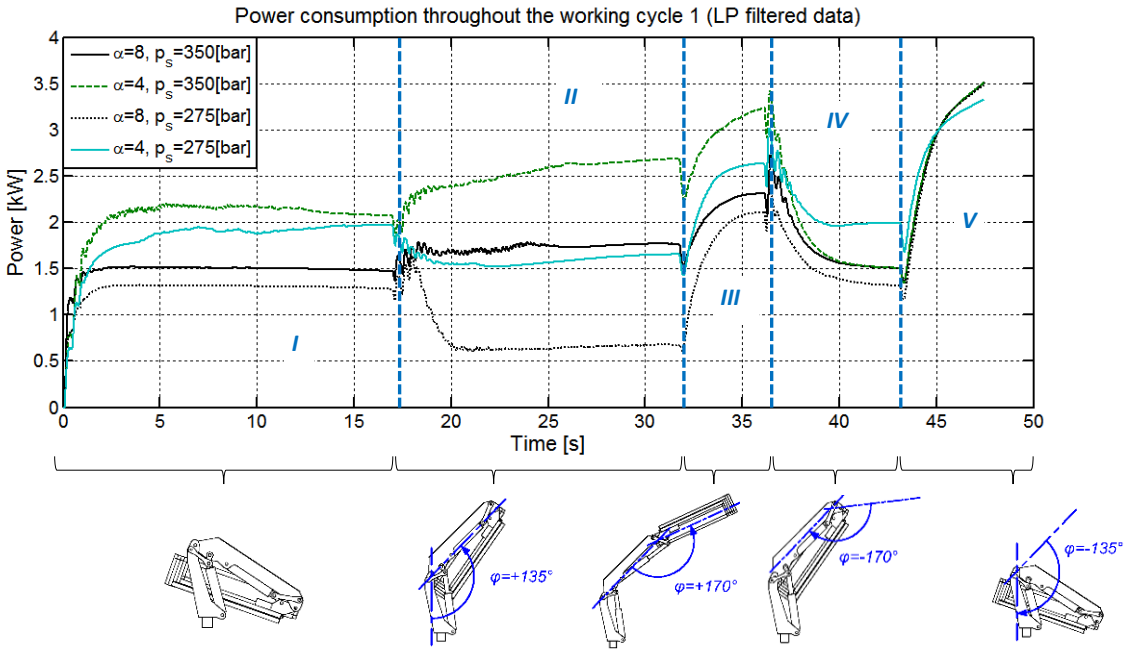

Fig. 56: Power consumption through the working cycle represented by the crane positions indicated with reference to the time axis (Ritelli G. F., and Vacca A., 2013).

The third type of test is based on the comparison between the configurations 3 and 4. The goal of this test is to quantify the actual performance of the proposed controller in terms of vibration damping as well as energy savings. The third type of tests were later on carried out within an associated research project at Purdue University and results were published by Ritelli G. F., and Vacca A. (2013). A summary of those results is reported in Fig. 57. In particular, Fig. 57 is relative to the step II indicated in in Fig. 56, namely the lowering of the outer boom. In this condition, up to 80% vibration reduction was achieved.

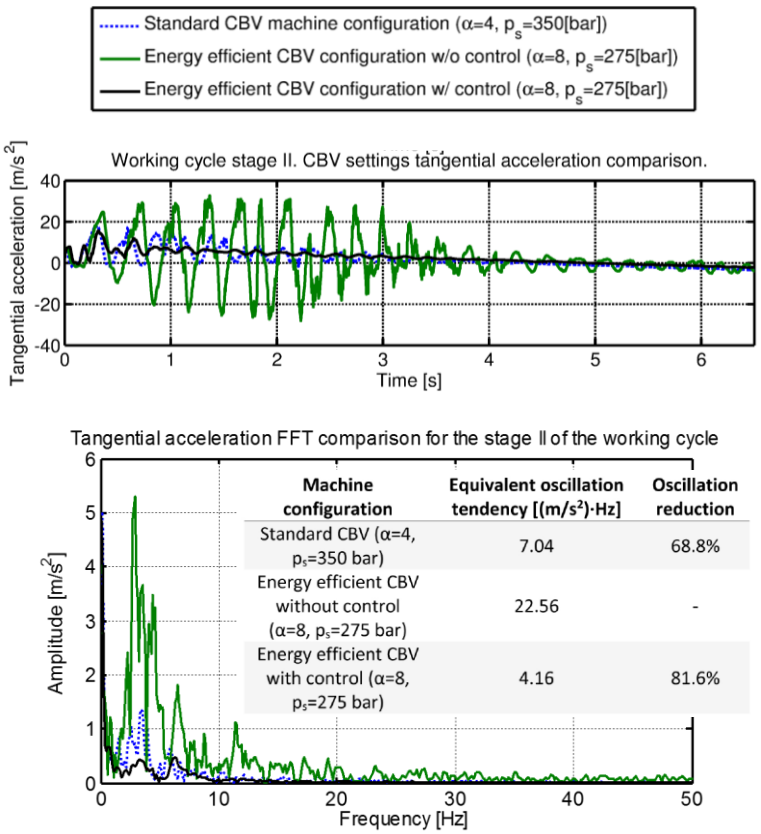

Fig. 57: Time and frequency domain plots obtained during the step II represented in Fig. 56 (Ritelli G. F., and Vacca A., 2013).

7.5 Pressure Feedback vs. Acceleration Feedback: Experimental Results

This section presents the validation of every single part of the method presented in Sect. 6.4 to estimate the mechanical arms acceleration from pressure measurements. The goal is to demonstrate the pressure measurements are sufficient to have accurate estimate of the undesired vibration the proposed control method aims to cancel.

For this purpose two particular test cycles operated on the main boom cylinder were considered. These cycles are composed by four phases: raise (extension); stop after raise; lowering (retraction); stop after lowering. It has to be observed the raise phases are representative of a resistive load operation while the lowering phases are representative of assistive load operation.

In particular, test cycle 1 (represented in Fig. 58) was obtained by operating the main boom cylinder at full speed. In case of test cycle 2 (represented in Fig. 59) the main boom cylinder is operated at 75% speed. In order to introduce a variability of the inertia of the machine, in case of test cycle 1 the main boom cylinder is operated while the outer boom cylinder is completely retracted, whereas in case of test cycle 2 the outer boom cylinder is extended so that outer boom and telescopic boom are aligned. The different geometrical configuration causes a much larger inertia of the machine in

the case of test cycle 2 compared to the test cycle 1 (this will also result in a different pressurization of the main boom actuators, as it will appear clearly from the plots described below).

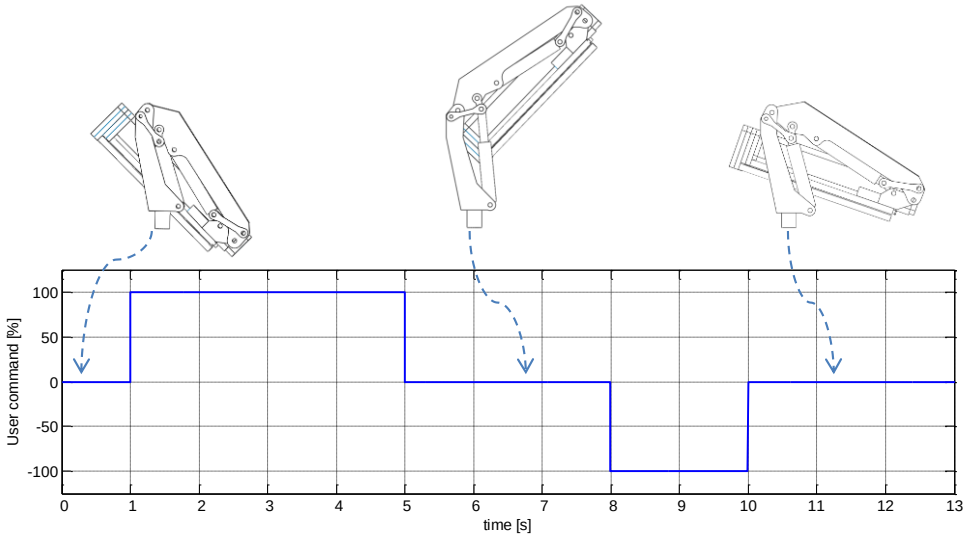

Fig. 58: Test cycle 1: outer boom cylinder is completely retracted; main boom cylinder is operated at full speed.

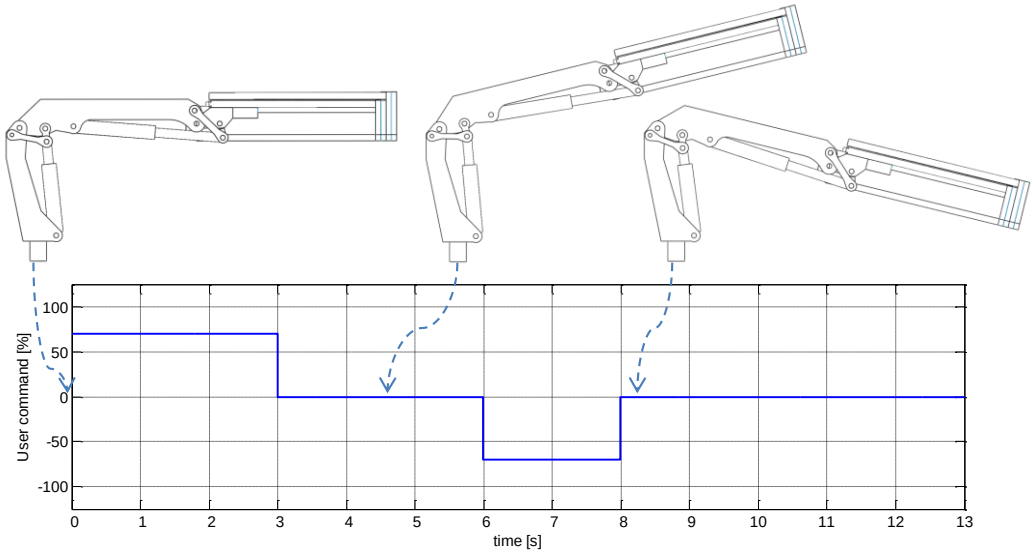

Fig. 59: Test cycle 2: outer boom is extended so that outer boom and telescopic boom are aligned; main boom cylinder is operated at 75% speed.

The temperature was monitored during the tests to be approximately equal to 30 °C. Although this temperature may appear low, respect to other fluid power applications, it is reasonable for truck mounted hydraulic cranes. In fact, the operation of those machines can occur in discontinuous fashion and for short periods of time with consequent limited oil heat up.

7.5.1 Experimental Characterization of the Proportional Valve

As described in Sect. 6.4.1, the model which computes the flow rate at the PDV workports requires the characterization of the steady-state metering area as functions of the electric current. For this purpose, tests were performed using the configuration to acquire simultaneously: electrical current; flow rate; pressure. The measurements were used in Eq. 6.20 to calculate the curves represented in Fig. 60 (normalized metering areas as a function of the normalized electric current on the proportional directional valve). The curves were implemented as a set of piecewise curves into Eq. 6.21 and Eq. 6.22. The metering areas are equal to zero for current below 42% (representative of the spool overlap deadband limit). A 4th order polynomial fitting was used to interpolate the curves in the interval from 42% to 87% (representative of the saturation limit). Within the interval between deadband and saturation limits, all curves are characterized by an R-squared values above 0.90 (which justifies the linearity assumption presented in Sect. 6.4.1). Above 87% of the current, the metering areas are equal to the maximum values. The terms of the transfer function in Eq. 6.20 were obtained from linear analysis of the model presented in Eq. 6.20 resulting in ω_n=15Hz and ς=0.85.

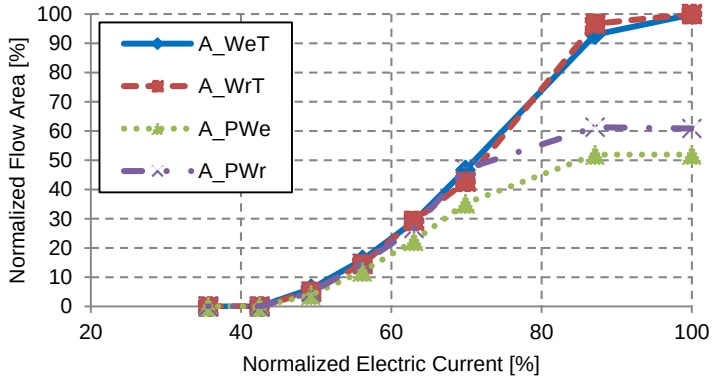

Fig. 60: Normalized metering areas of the PDV for the reference hydraulic crane obtained experimentally as a function of the normalized electric current.

7.5.2 Validation of the Cylinder Pressure Model

The validation of the cylinder pressure estimate is provided with the results in Fig. 61 (relative to test cycle 1) and in Fig. 62 (relative to test cycle 2). The two plots report the pressure measured at the PDV workport, the pressure measured in the cylinder chamber and the estimate of the pressure in the cylinder obtained using the proposed method. Fig. 61a and Fig. 62a are relative to the extension side of the cylinder whereas Fig. 61b and Fig. 62b are relative to the retraction side of the cylinder.

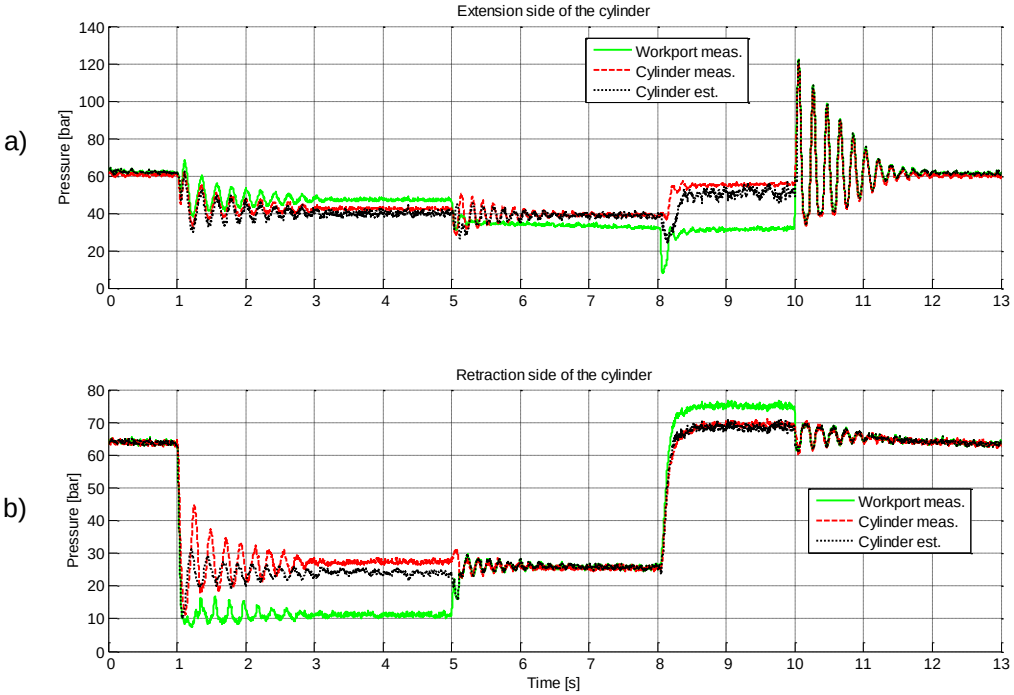

Fig. 61: Validation of the estimate of the cylinder pressure for test cycle 1: a) extension side of the cylinder; b) retraction side of the cylinder.

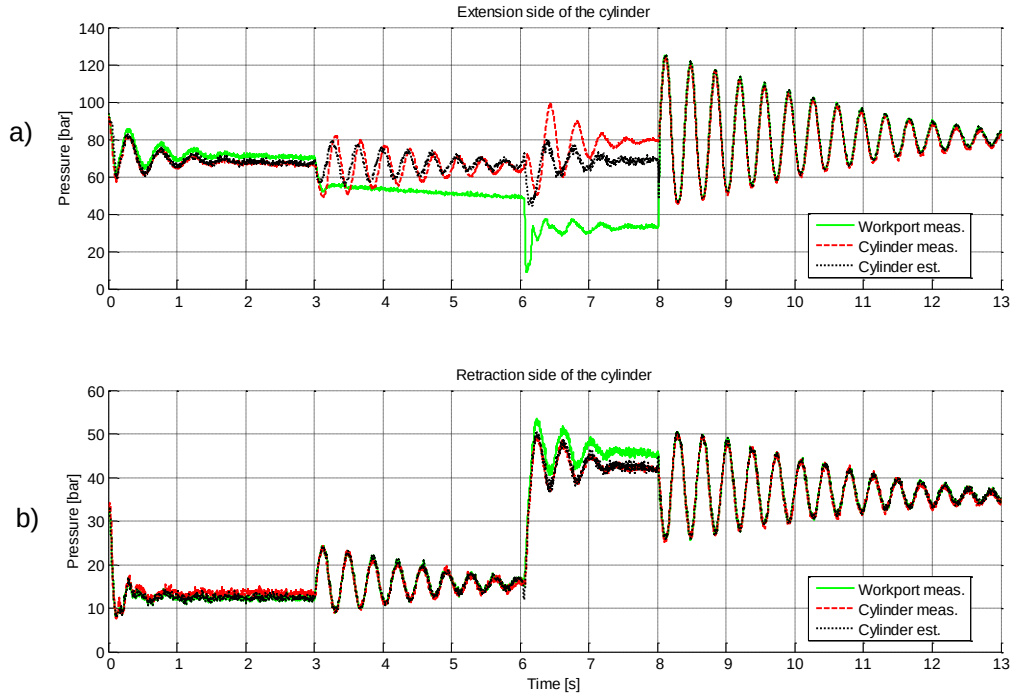

Fig. 62: Validation of the estimate of the cylinder pressure for test cycle 2: a) extension side of the cylinder; b) retraction side of the cylinder.

These pressure comparisons show that for all test cycle intervals of both cycles, the estimated pressure accurately approximates the measured one. It can be observed that few intervals show less accurate results, but for those intervals the opposite side is still very accurate. As it was described in Sect. 6.4.3, the availability of two equations to determine x_k (namely Eq. 6.37a and Eq. 6.37b) is convenient since it gives the possibility to estimate the actuator dynamics by using the equation corresponding to the most accurate cylinder pressure estimate. The switching logic was implemented so that the equation based on the most accurate pressure estimate is used: Eq. 6.37a will be used in case of raise and stop after lowering, while in the remaining cases Eq. 6.37b will be used.

7.5.3 Validation of the Mechanical Arms Dynamics Estimate

This section presents the validation of the model to estimate the hydraulic actuator dynamics (Sect. 6.4.3) and the model to estimate the mechanical arms (Sect. 6.4.4). In particular, the model of the mechanical arms dynamics is based on a set of trigonometric equations to transform the main boom cylinder motion $\boldsymbol{x} = [x, \dot{x}, \ddot{x}]$ into the motion of the point of the outer boom where the accelerometer is located $\boldsymbol{x}_a = [x_a, \dot{x}_a, \ddot{x}_a = a_T]$ (see Fig. 63).

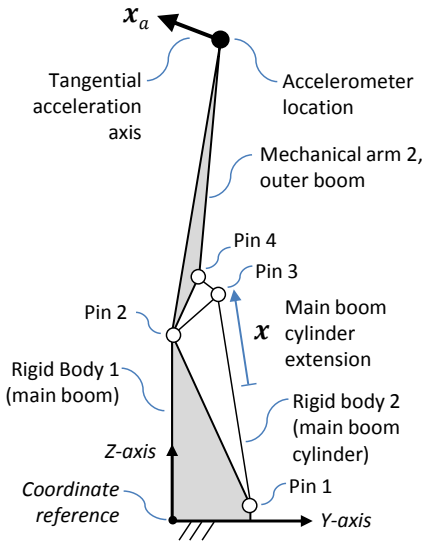

Fig. 63: Schematics of the kinematics of the reference machine.

The validation is based on the comparison between the tangential acceleration a_T from the model with the measured one. The results are presented for test cycle 1 in Fig. 64 and for test cycle 2 in Fig. 65. Fig. 64a and Fig. 65a are relative to the case the measured cylinder pressure is used in Eq. 6.37a and Eq. 6.37b whereas Fig. 64b and Fig. 65b are relative to full application of the proposed method, when the case the estimated cylinder pressure is used in Eq. 6.37a and Eq. 6.37b.

These comparisons show how the estimated acceleration accurately approximates the measured acceleration in all tested conditions. In particular, it is possible to notice how the prediction of the arm acceleration is accurate in case the cylinder pressure is estimated rather than measured: this confirms the accuracy of the cylinder pressure model for the considered application.

Looking closely at the results presented in Fig. 64 and Fig. 65 it can be observed the estimated curve appears to present a certain extent of phase delay with respect to the measured one. In these plots, the phase delay is amplified with respect to Fig. 62 and Fig. 63 since the estimated cylinder stroke is low pass filtered and differentiated twice to obtain the acceleration. A simple low-pass Butterworth low pass filter was used for this purpose. In case this phase lag is critical for the control application of the presented method, this could be reduced by developing more sophisticated filtering techniques.

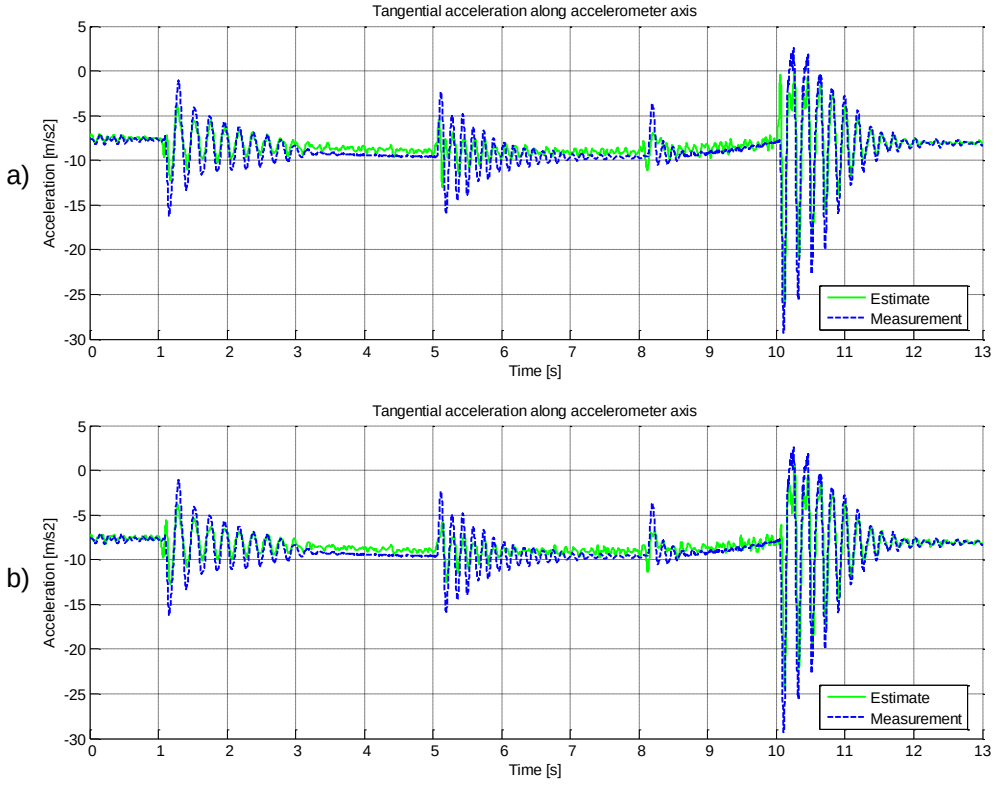

Fig. 64: Comparison between measured and estimated tangential acceleration of the outer boom for test cycle 1: a) estimate from cylinder pressure measurement; b) estimate from cylinder pressure estimate.

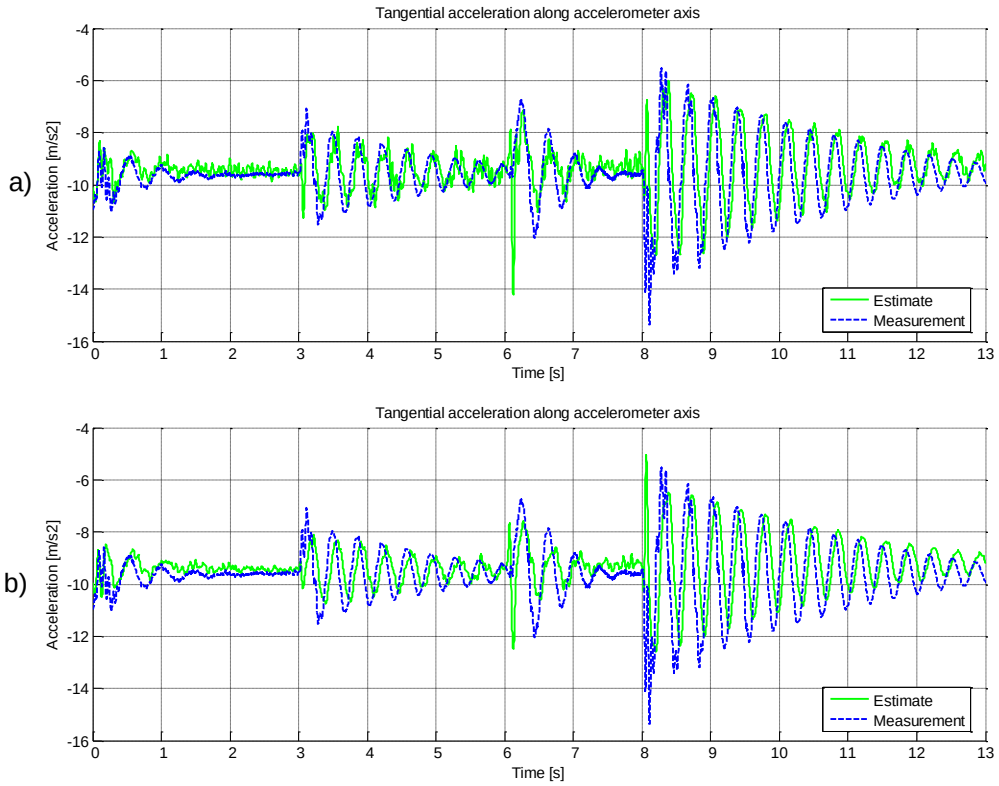

Fig. 65: Comparison between measured and estimated tangential acceleration of the outer boom for test cycle 2: a) estimate from cylinder pressure measurement; b) estimate from cylinder pressure estimate.

7.5.4 Dynamic Effect of Fluid Compressibility

This section illustrates how the compressibility of the fluid affects the mechanical dynamics of the hydraulic actuator. In particular, the simulation results presented in this section are relative to the extension chamber of the cylinder (similar considerations can be formulated for the retraction side). With reference to Eq. 6.6, the velocity of the actuator can be rewritten as

$$\dot{x} = \frac{Q_e}{A_e} - \dot{p}_{Ce} \frac{V_{Ce,min} + A_e x}{\beta A_e} \tag{6.42}$$

In case of incompressible fluid, the velocity will be equal to $\dot{x} = Q_e / A_e$. The comparison between the estimate of the actuator velocity in case of compressible and incompressible fluid is shown in Fig. 66a for test cycle 1 and in Fig. 66b for test cycle 2. The comparison shows the compressibility amplifies the mechanical vibrations and therefore the incompressible fluid assumption would lead to inaccurate results. Additionally, the vibrations during the stop phases of the machine operation are entirely governed by the fluid compressibility since no flow is entering or leaving the cylinder chambers. For these reasons the value of the bulk modulus used in the actuator mechanical dynamics model (Eq. 6.37a and Eq. 6.37b) has to be as accurate as possible.

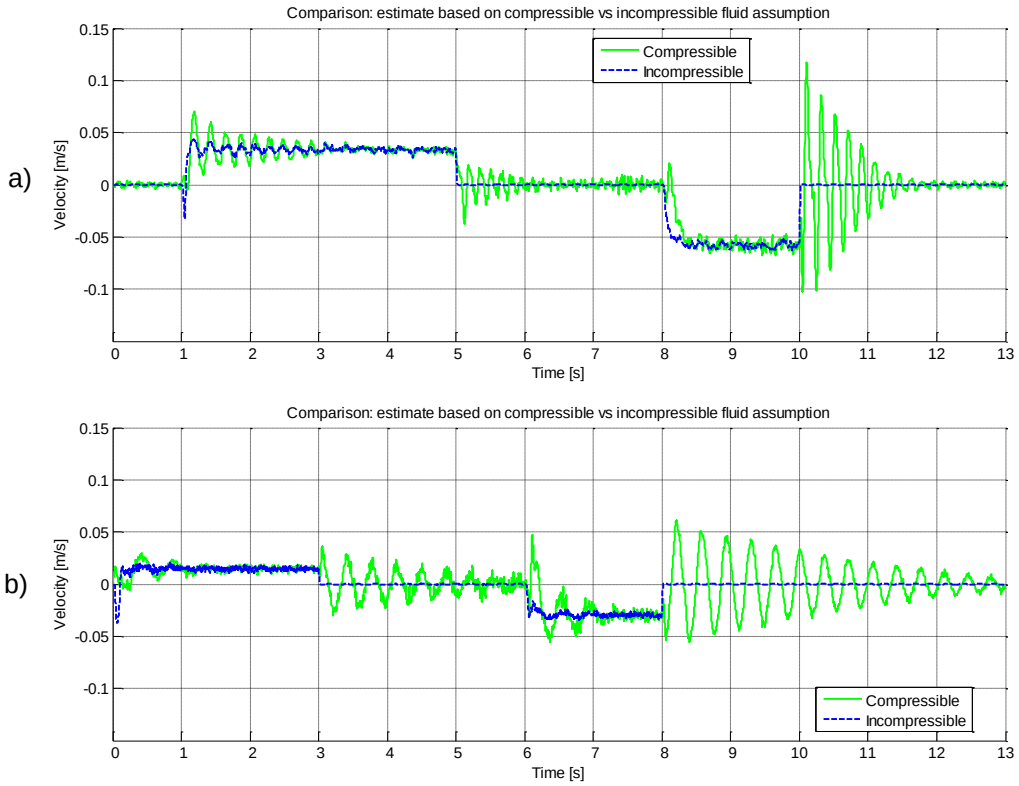

Fig. 66: Comparison between the estimate of the actuator velocity in case of compressible and incompressible fluid: a) test cycle 1; b) test cycle 2.

As it was illustrated above, one of the innovations of the proposed method is the capability to use a value of the bulk modulus dependent on the operating conditions of the machine. In particular, the influence of the cylinder pressure variation on the bulk modulus can be observed in Fig. 67a for the test cycle 1 and in Fig. 67b for the test cycle 2. In both cases the variation of the bulk modulus reaches 10% of the constant value at 30degC and 100bar, justifying therefore the modeling of this phenomena.

a)

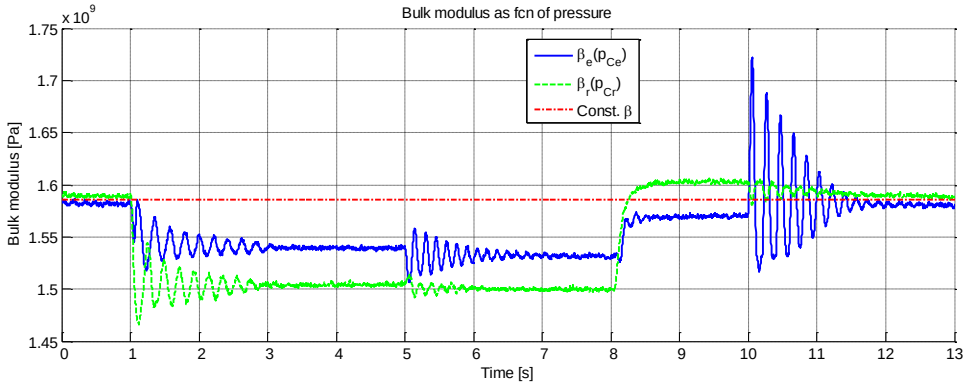

b)

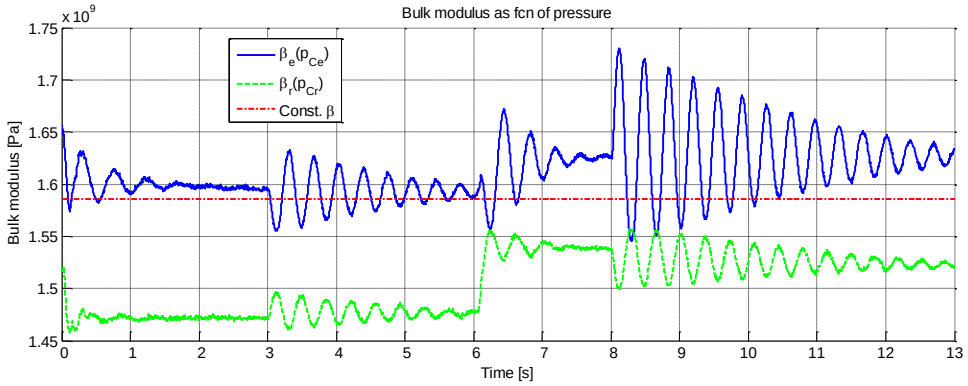

Fig. 67: Variation of the bulk modulus as a function of the pressure: a) test cycle 1; b) test cycle 2.

CHAPTER 8. CASE STUDY 2: WHEEL LOADER: REFERENCE MACHINES

The goals of case study 2 were detailed in Chap. 1 (Sect. 1.3.2), together with a brief description of the reference wheel loaders. In particular, in this study two wheel loaders were considered: the CNH Case Construction 621F and the 1021F (CNH America LLC ©, 2012). The initial part of the research consisted in testing the proposed vibration damping method through a series of simulations performed with a numerical model of the machine 1021F provided by an industrial sponsor of this research. The numerical model was previously developed and experimentally validated by the research sponsor, but within this research additional features were added into it, as described in Sect. 9.2. The simulated performance of the proposed control technique to reduce machine vibrations convinced the research sponsor to test the proposed control method. However, a different machine was available for this second phase of the research. In particular, the tests were performed on an electrohydraulic prototype of the machine 621F, equipped with additional sensors and a control/acquisition hardware specifically developed within this research were added, as described in Sect. 8.2.

There is no significant difference between the hydraulic circuits of the models 621F and 1021F, therefore the description presented in Sect. 8.1, inclusive of the Passive Ride Control system (PRC), is applicable to both machines.

8.1 Hydraulic System

A simplification of the hydraulic schematic representative of both wheel loaders is presented in Fig. 68. In this section, the numbers in Fig. 68 will be used as reference for the components of the hydraulic circuit.

Large wheel loaders use two boom actuators connected in parallel; in that case the box indicated as “boom section” should be repeated twice. The box indicated as “additional sections” represents the additional functions of the machine which do not take part into the vibration damping (such as bucket tilting, steering, etc…). The layout of the additional sections is similar to the one represented in the boom section box.

The research sponsor converted the pure-hydraulic commercial machine into an electro-hydraulic prototype. In particular, in the original machine, a pilot operated directional valve was controlled by a specific hydraulic joystick. In the prototype, the pilot operated directional valve was replaced by

the electro-hydraulic proportional directional valve indicated by 5 in Fig. 68. Also, the hydraulic joystick is replaced by an analog joystick connected via CAN-bus to the digital electronic controller represented by 4 in Fig. 68. The electronic controller manages several functions of the machine, including the current to the solenoids of the proportional directional valve 5.

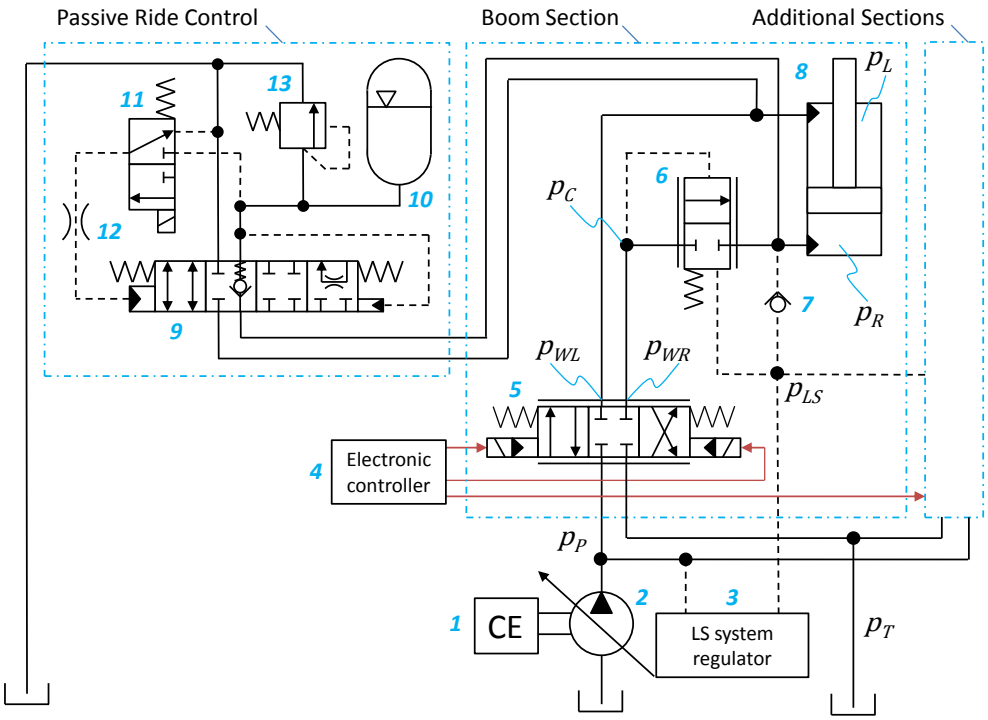

Fig. 68: Simplified schematics of the typical wheel loader hydraulic circuit.

The flow is typically provided by the variable displacement pump 2 which is driven by the combustion engine of the machine 1. The pump displacement is controlled by the displacement control system 3 according to the load-sensing configuration. The load-sensing principle basically consists in the continuous adaptation of the pump displacement to match the flow demand. In practice, the system 3 modifies the pump displacement to maintain a constant difference between the delivery pressure p_P and the pressure in the actuator whose load is the highest (p_{LS}, load-sense pressure). Additionally, a flow compensator is typically used to ensure the velocity of all actuators is exclusively determined by the command to its relative control spool 5, even in case of pump saturation (flow-sharing principle). In Fig. 68, the example of the post-compensator 6 is presented: it increases the pressure at its inlet port p_C in order to equalize the pressure drops across the control spools 5 of all sections: $p_P - p_C$, constant for all sections. The orifice equation shows that, for each section, the flow across the compensator Q_C is determined only by A_C (metering area of the control spool 5):

$$Q_C = c_d A_C \sqrt{\frac{2\left(p_P - p_C\right)}{\rho}} \qquad 7.1$$

Modern hydraulic system layouts have been developed to reduce the energy losses across the control spools as well as those across the compensators. An example is proposed by the displacement controlled actuation principle. It is not a goal of the present dissertation the discussion of such aspects, therefore the reader is directed to the book by Nervegna N. (2003) for additional details about the load-sensing and flow-sharing operations and to the publication by Rahmfeld, R. and Ivantysynova M. (2001) for more details about displacement control actuation.

The PRC system is typically connected only to the transmission lines entering the boom actuator, as it is represented by the box in Fig. 68. An emergency drain is often present in the circuit, but it does not affect the dynamics of the system and therefore it will not be considered in this dissertation. The relief valve 13 prevents excessive pressure in the accumulator 10. The dynamic orifice 12 reduces the risk of instabilities which may occur in the stabilizing valve 9 spool dynamics. The stabilizing valve has four positions which, from left to right, will be indicated as: 9A, 9B, 9C and 9D. The enabling valve 11 is typically deactivated to perform the load handling when the vehicle is moving slowly or standing still. When the enabling valve 11 is off, the stabilizing valve is in a position determined by the accumulator pressure. In case of low accumulator pressure, the stabilizing valve is in position 9B, allowing flow from the raise chamber of the boom cylinder through the integrated check-valve, to pressurize the accumulator. For a larger accumulator pressure, the stabilizing spool moves to position 9C: this corresponds to the complete pressurization of the accumulator and its isolation from the boom actuator. Finally, if the accumulator pressure is excessive, the stabilizing valve moves to position 9D and discharges some flow to the tank.

The enabling valve is typically activated when the vehicle speed overcomes a specific set-point or when the operator commands a specific signal. In fact, the enabling valve is activated when it is required to suppress the vibrations originated by the travel on uneven road. When the enabling valve is on, both piloting areas of the stabilizing valves are in communication with the accumulator pressure: the difference in such areas allows the motion of the stabilizing valve towards position 9A. In this configuration the cylinder pressure oscillations are attenuated by the increased volume of fluid (given by the accumulator) and the dissipation of the energy content of the oscillation through the metering areas of the stabilizing valve.

8.2 Instrumented Experimental Wheel Loader

The picture of the experimental wheel loader is shown in Fig. 69 (Case Construction® model 621F, CNH America LLC ©, 2012). The reference wheel loader was introduced in Sect. 1.3.2. In particular, in Fig. 3 and Fig. 4 the technical drawings of the wheel loader were presented along with

dimensions and the parts nomenclature used in this dissertation. Additionally, machine specifications were presented in Table 1. Typically these machines are used to load piles of dirt from specific point of the construction or mining site into the dump body of a truck. The schematic of the control and acquisition system is shown in Fig. 71 and the specifications of the components are reported in Table 7. The pressure sensor is installed in correspondence of the p_{WR} workport (see Fig. 68). The accelerometers and string potentiometer are installed as indicated in Fig. 72. The two accelerometers are used to measure the cab and boom accelerations ($\ddot{z}_{cab}$ and $\ddot{z}_{boom}$ respectively). The string potentiometer is used to measure the boom cylinder extension from which it is possible to derive the boom position relative to the tractor (angle β_{rel}). The control unit was connected via Ethernet port to a computer and programmed using National Instrument Labview® software. Additionally, the control unit was connected to a control box equipped with an analog lever and switches to be used during the experimental testing to start/stop the acquisitions as well as performing auxiliary functions. The low-power control unit output is directed to the proportional valve driver which amplifies it and generates the control current for the proportional directional valve. An emergency stop installed into the vehicle can be pressed to disconnect the power supply to the valve driver so that the unexpected motions of the boom can be blocked.

Fig. 69: External picture of the instrumented experimental wheel loader used within this research.

Fig. 70: Internal picture of the instrumented experimental wheel loader used within this research.

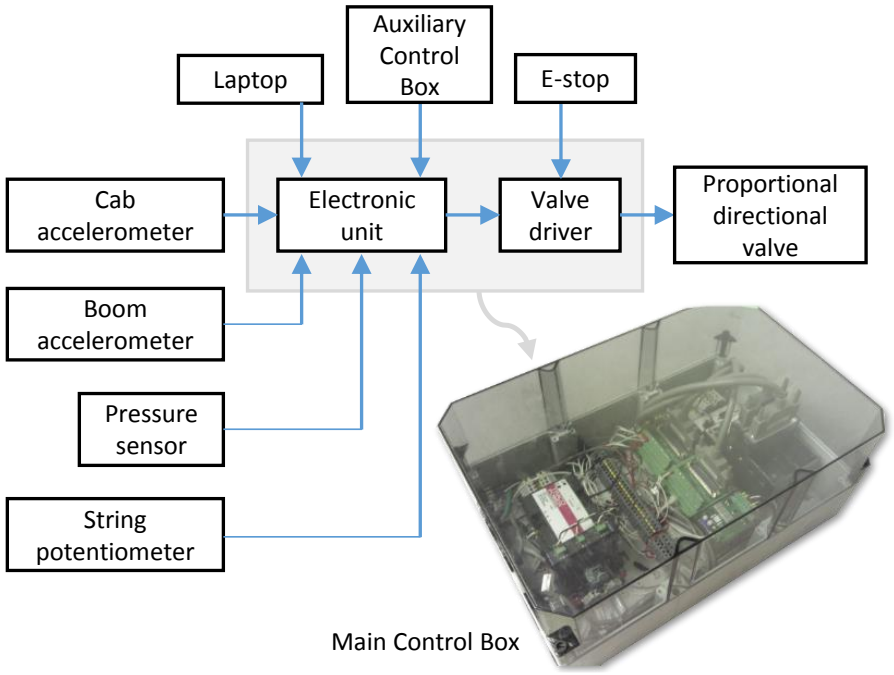

Fig. 71: Block diagram representing the control and data acquisition hardware system for the wheel loader (the picture represents the electronic unit and valve driver box).

Table 7: Specifications of the sensors and the electronic unit used for the acquisition and control of the wheel loader.

Component	Description	Code	Specifications
Electronic unit	Programmable real-time input/output unit	National Instruments® NI CRIO-9076 Integrated Controller and Chassis System	• 400 MHz PowerPC controller, LX 45 Gate FPGA
	Analog input voltage module	National Instruments® NI 9205 (32 channels)	• Measurement range: ±10 V • Bandwidth: 250 kS/s • Resolution: 16-Bit
	Analog output voltage module	National Instruments® NI 9264 (16 channels)	• Measurement range:±10 V • Bandwidth: 25 kS/s • Resolution: 16-Bit
Pressure sensor	Piezo-resistive type	Wika S-10	• Measurement range: 0 – 500 bar
Accelerometers	MEMS accelerometer	SparkFun® IMU Analog Combo Board - SEN-09268 (includes Analog Devices® triple axis ADXL335 accelerometer)	• Measurement range: ±3 g • Bandwidth: 50 Hz
String potentiometer	Draw wire sensor	Micro-epsilon P60	• Measurement range: 0 – 2 m
Proportional valve driver	Analog proportional amplifier with digital microcontroller design	Lynch LE PDX	• Output current: 0 – 3 A • PWM and dither frequency: 40 – 450 Hz • Linearity: 1%

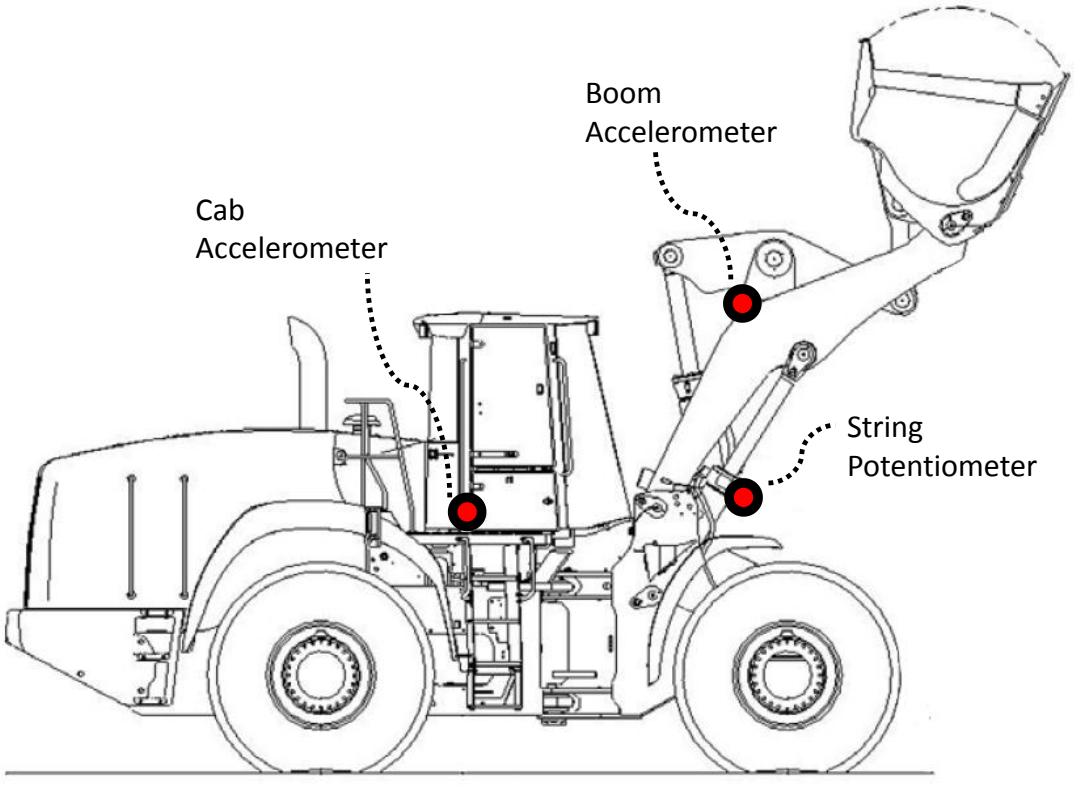

Fig. 72: Location of the motion sensors: cab accelerometer (acceleration of the cab); boom accelerometer (acceleration of the boom); and string potentiometer (extension of the boom cylinder representative of the implement position relative to the tractor).

CHAPTER 9. CASE STUDY 2: WHEEL LOADER: MODELING

The schematic of the wheel loader model used for the analysis of this case study is shown in Fig. 73. The model is composed by a planar mechanical model (Sect. 9.1) and a hydraulic model (Sect. 9.2). All the models are based on the lumped parameters approach.

The wheel loader hydraulic circuit model developed by the sponsor did not include a PRC model which was instead created within this research. Due to confidentiality agreement, only basic information about the planar mechanical and hydraulic circuit models will be provided, whereas more details regarding the PRC model will be presented.

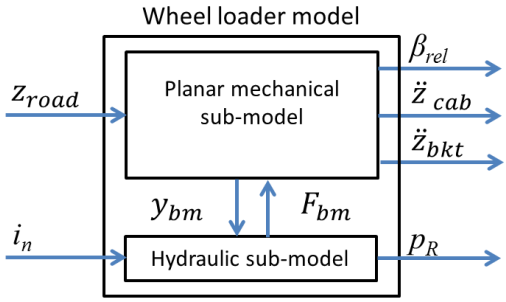

Fig. 73: Wheel loader model schematics, including the two models: planar mechanical and hydraulic.

9.1 Planar-Mechanics

The planar mechanic sub-model evaluates the dynamics of the rigid bodies constituting the machine. The model inputs are: i_n, electric current to the directional valve which controls the boom; z_{road}, road profile. The road profile z_{road} consists in the measurement of the actual irregularities of the ground with respect to the vehicle velocity, and it was provided as look up table from the sponsor. The model outputs are: β_{rel}, inclination of the boom with respect to the tractor pitch angle α_{trc} (see Fig. 75); p_R, pressure in the raise chamber of the boom; $\ddot{z}_{cab}$, vertical acceleration of the cab; $\ddot{z}_{bkt}$, vertical acceleration of the bucket (see Fig. 74).

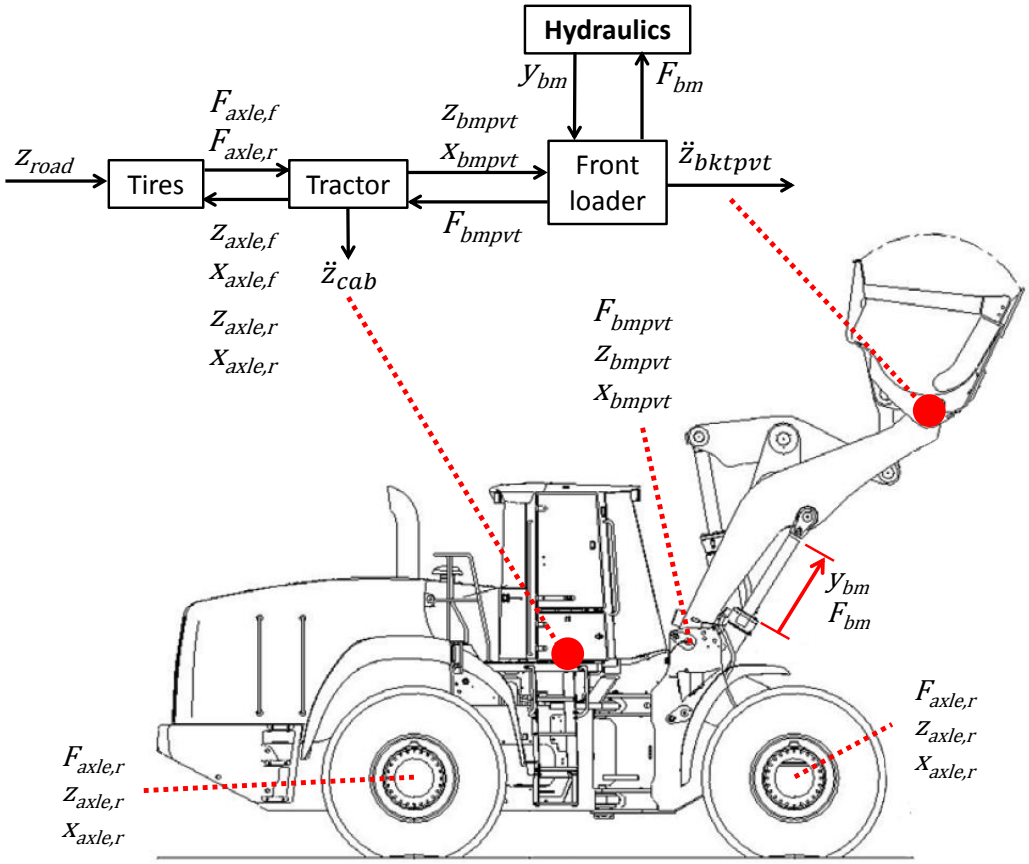

Fig. 74: Schematic of the planar mechanical dynamics wheel loader model.

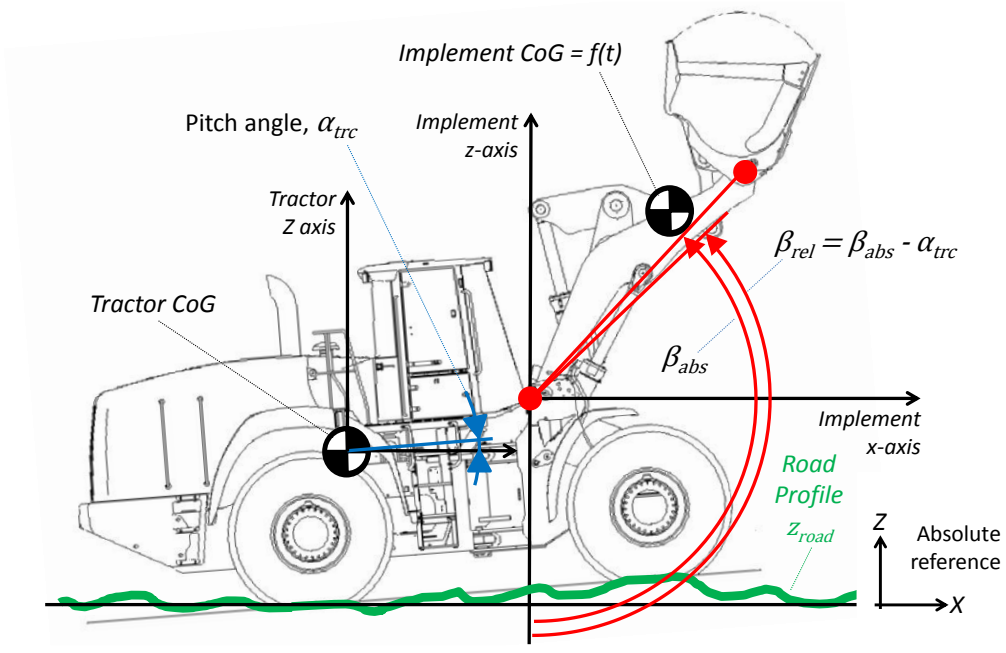

Fig. 75: Schematic representing the reference systems of the wheel loader model.

As already stated in Sect. 1.3.2, the undesired vibrations in case of wheel loaders are mainly those occurring during the drive on uneven road: $\ddot{z}_{cab}$ will be used to quantify these perceived by the driver; $\ddot{z}_{bkt}$ will be used to quantify those responsible for the loss of transported material.
The interaction between the planar mechanical model and the hydraulic one is realized through two variables: y_{bm}, stroke of the boom actuator; F_{bm}, force of the boom actuator.
The planar mechanical model implements the motion equations of all rigid bodies. The tractor and each tire are considered as single rigid bodies. The tractor can rotate with respect to its center of gravity, defining the pitch angle α_{trc}. The implement is composed by several rigid bodies: its center of gravity location changes according to their relative position and the mass of the load.

9.2 Hydraulic Model

The hydraulic model includes the components in Fig. 68. Like the wheel loader kinematics model, the hydraulic circuit was modeled using standard lumped parameters approach. The model includes dynamics which were empirically identified by means of experimental testing of the real components (this includes the case of the directional valve).
The wheel loader hydraulic circuit model developed by the sponsor did not include a PRC model which was created within this research. Due to confidentiality agreement, only basic information about the hydraulic circuit model will be provided, whereas more details regarding the PRC model will be presented below.
This goal of the PRC is to permit the comparison between the current configuration of the commercial machine and the proposed ARC alternatives. The modeling of the PRC system is divided into several sub-models described below.

Pressure Relief Valve (13)

The flow rate across the pressure relief valve is evaluated according to the following piecewise equation:

$$\begin{cases} Q_{PRC,PRV} = 0 \quad if \quad p_{in} \le p_{crack} \\ Q_{PRC,PRV} = K_{pQ}\left(p_{in} - p_{out}\right) \quad if \quad p_{in} > p_{crack} \end{cases} \tag{8.1}$$

Where: p_{in} is the inlet pressure; p_{out} is the outlet pressure; p_{crack} is the cracking pressure (pressure setting for valve opening); and K_{pQ} is the pressure-flow coefficient obtained by linearizing the orifice equation for the nominal operating condition

$$K_{pQ} = \left.\frac{\partial Q}{\partial\left(\Delta p\right)}\right|_0 \tag{8.2}$$

Enabling Valve (11)

The enabling valve is modeled according the following piecewise equation:

$$\begin{cases} p_{PRC,Enabl} = p_T \quad if \quad Off \\ p_{PRC,Enabl} = p_{Acc,Oil} \quad if \quad On \end{cases} \tag{8.3}$$

Where: $p_{PRC,Enabl}$ represents the pressure at the port connected to 12; p_T represents the tank pressure; $p_{Acc,Oil}$ represents the pressure of the oil into the accumulators (10). The conditions on and off represent the commands of the enabling valve.

Stabilizing Valve Spool (9)

The stabilizing valve modeling follows the schematic represented Fig. 76.

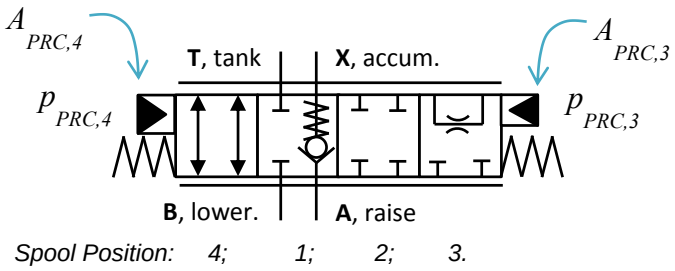

Fig. 76: Schematic of the stabilizing valve spool.

The pressure differential between the side which activates the position 3 and the one which activates the port 4 (weighted on the basis of the ratio of the areas) is expressed by:

$$\Delta p_{PRC,Spool} = p_{PRC,3} - \frac{A_{PRC,4}}{A_{PRC,3}} p_{PRC,4} \tag{8.4}$$

The value of $\Delta p_{PRC,Spool}$ will be referred to as weighted pressure differential of the PRC spool. It is representative of the position of the spool. According to the position of the spool, it is possible to represent the resulting value of the normalized flow areas, as it is shown in Fig. 76.

Being the position 1 the normal position, $\Delta p_{PRC,1} = 0$. The value of $\Delta p_{PRC,2}$ was indicated by the research sponsor. The stabilizing valve datasheet expresses the relationship $\Delta p_{PRC,3} = \Delta p_{PRC,2} + 30bar$. The value of $\Delta p_{PRC,4}$ was not provided, therefore it was determined by an optimization process (minimization of the vibrations on the cab and on the boom, see Sect. 9.2.1).

In the stabilizing valve spool, the flow from the generic port i to the generic port j can be expressed as:

$$Q_{ij} = c_d A_{PRC,norm,ij} A_{PRC,\max,ij} \sqrt{\frac{2\left(p_i - p_j\right)}{\rho}} \tag{8.5}$$

It is therefore necessary to have an accurate estimate of the maximum value of the flow areas, which was obtained by interpolation of the experimental curve printed in the stabilizing valve datasheet.

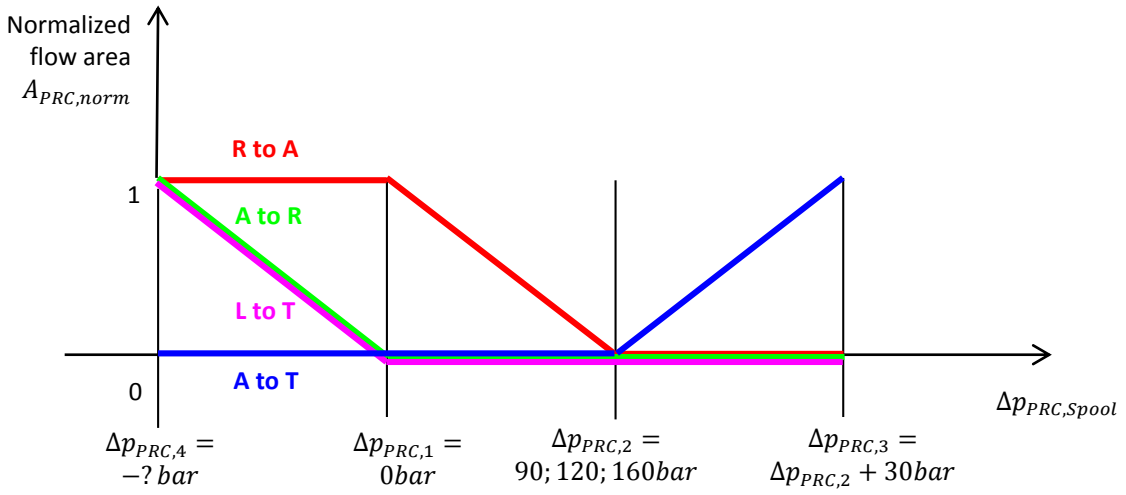

Fig. 77: Representation of the normalized areas in the PRC spool as a function of the weighted pressure differential of the PRC spool.

Dynamic Orifices (12)

The dynamic orifices were approximated according the general expression of a first order linear system:

$$p_{PRC,4} = \frac{1}{s\tau_{PRC} + 1}\, p_{PRC,Enabl} \qquad 8.6$$

Where: $p_{PRC,4}$ is the pressure which activates the position 4 of the stabilizing valve spool; τ_{PRC} is the time constant of the orifices dynamics. Since information about τ_{PRC} were not available, it was determined by an optimization process (minimization of the vibrations on the cab and on the boom, see Sect. 9.2.1).

Accumulator (10)

The accumulator is modeled according to the schematic in Fig. 78.

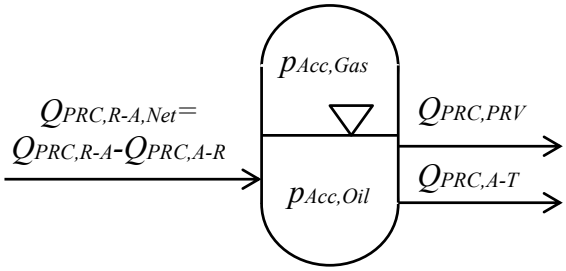

Fig. 78: Schematic of the accumulator of the PRC system.

The net flow of fluid entering the accumulator is equal to

$$Q_{Acc,Net} = Q_{PRC,R-A,Net} - Q_{PRC,PRV} - Q_{PRC,A-T} \qquad 8.7$$

Three different operations of the accumulator are identified by the pressure of the oil inside the accumulator, as it is represented in Table 8.

Table 8: Operations of the accumulator model.

Operation	Equations
Fully charged: $p_{Acc,Oil} \geq p_{Acc,Max}$	$$p_{Acc,Max} = \left(p_{Acc,precharge} + p_{atm}\right)\left(\frac{V_{Acc,Available}}{V_{Acc,Gas,\,fullycharged}}\right)^{\gamma} \quad (8.8)$$ It was assumed: $V_{gas,fullycharged}$=1000. $$\begin{cases} p_{Acc,Gas} = p_{Acc,Max} \\ V_{Acc,Gas} = \frac{V_{Acc,Available}}{1000} \\ p_{Acc,Oil} = \int\left(\frac{\beta}{V_{Acc,Available}} Q_{Acc,Net}\right)dt \end{cases} \quad (8.9)$$
Fully discharged: $p_{Acc,Oil} < p_{Acc,Precharge}$	$$\begin{cases} p_{Acc,Gas} = p_{precharge} \\ V_{Acc,Gas} = V_{Acc,Available} \\ p_{Acc,Oil} = \int\left(\frac{\beta}{V_{Acc,Deadvol}} Q_{Acc,Net}\right)dt \end{cases} \quad (8.10)$$ Where the dead volume is assumed to be: $V_{Acc,Deadvol} = \frac{V_{Acc,Available}}{1000}$
Standard operation: $p_{Acc,Precharge} < p_{Acc,Oil} < p_{Acc,Max}$	$$\begin{cases} p_{Acc,Gas} = p_{Acc,Oil} \\ V_{Acc,Gas} = V_{Acc,Available}\left(\frac{p_{Acc,precharge}}{p_{Acc,Gas}}\right)^{1/\gamma} \\ p_{Acc,Oil} = \gamma\int\left(\frac{p_{Acc,Oil} - p_{atm}}{V_{Acc,Gas}} Q_{Acc,Net}\right)dt \end{cases} \quad (8.11)$$

9.2.1 Optimization of the Undetermined Parameters

All parameters in the equations provided by the research sponsors, except two which were undetermined: τ_{PRC} (time constant used to model the orifice dynamics) and $\Delta p_{PRC,4}$ (weighted pressure differential of the stabilizing valve spool required to reach position 4). Since the ultimate goal of the PRC simulation is the comparison of its performance with those of the proposed alternative vibration damping methods, it is necessary to use the best PRC configuration. For this reason, the undetermined parameters were obtained by optimizing (minimizing) the cost functions

of the cab and boom vibrations. Consequently, this leads to a cautious comparison of ARC and the best PRC possible. The results of the batch simulation can be represented as a series of surfaces where width and depth are τ_{PRC} and $\Delta p_{PRC,4}$, while the height is the percentage vibration damping improvement evaluated as ratio between the cost function of the system with no ride control and the cost function of the system with PRC.

Table 9: Cost functions of the vibrations for variations of the parameters are τ_{PRC} and $\Delta p_{PRC,4}$ (in case of vehicle driving on flat road at 35 km/h).

Percentage improvement of the boom-time cost function.	Percentage improvement of the cab-time cost function.
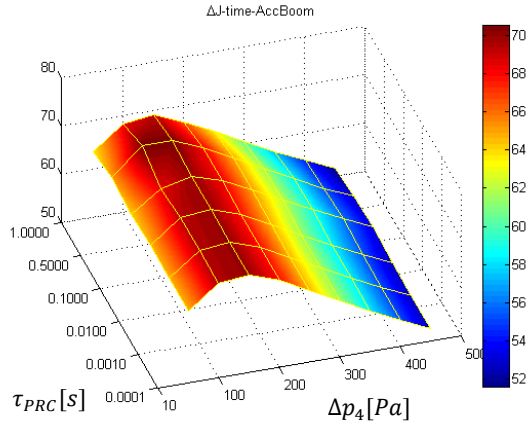	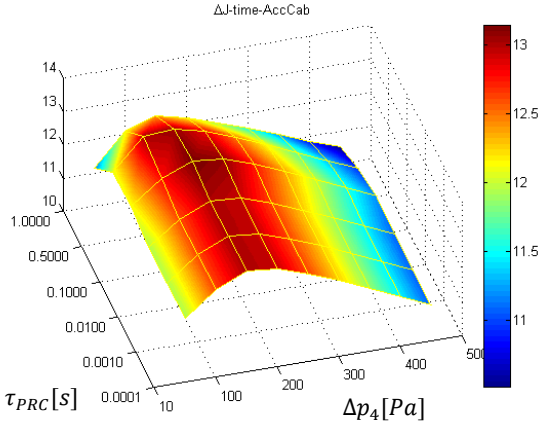
Percentage improvement of the boom-FFT cost function.	**Percentage improvement of the cab-FFT cost function.**
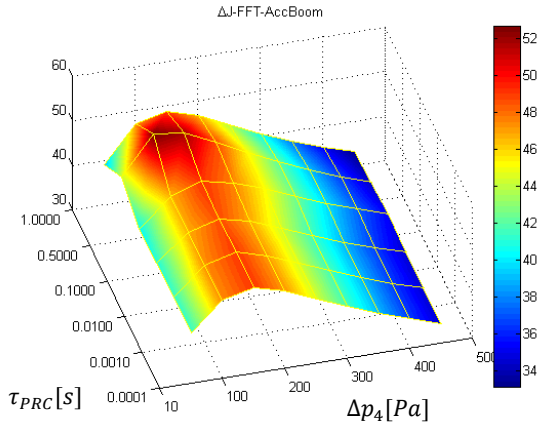	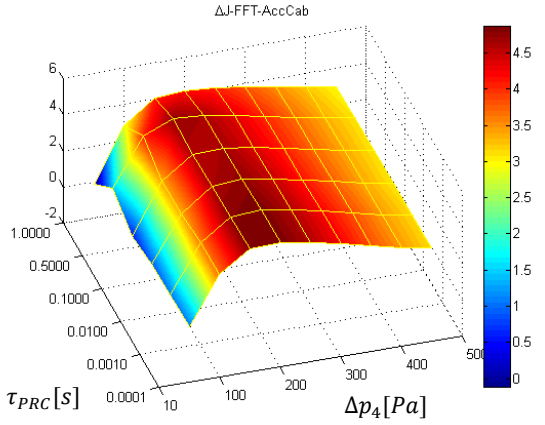

Examples of optimization results are provided in Table 9 in case the vehicle is driving on flat road at 35km/h. the four different surfaces in Table 9 are representative of different methods to commutate the vibration of the machine: boom vibrations with respect to time; cab vibrations with respect to time; boom vibrations with respect to FFT; cab vibrations with respect to FFT. The peak of every surface in Table 9 represents the optimal set of parameters for that specific operating condition and cost function computation method.

9.2.2 Approximate Directional Valve Dynamics

In Sect. 4.2.1, the formulation of the proposed control method was based on the assumption that it is possible to determine an approximate relationship for the directional valve dynamics which is determined at most by the following variables: p_{WR}, p_{WL}, and i_n, (measured); M_L, (estimated from the previous). As observed in the description of the wheel loader hydraulic circuit (Sect. 8.1), the hydraulic power supply is load insensitive and at first approximation the flow can be considered exclusively function of the metering area, which, can be approximated as a linear function of the current i_n.

9.3 Pressure Feedback vs. Acceleration Feedback: Analytical Modeling

The dynamics of the wheel loader can be simplified as it was shown in Fig. 79.

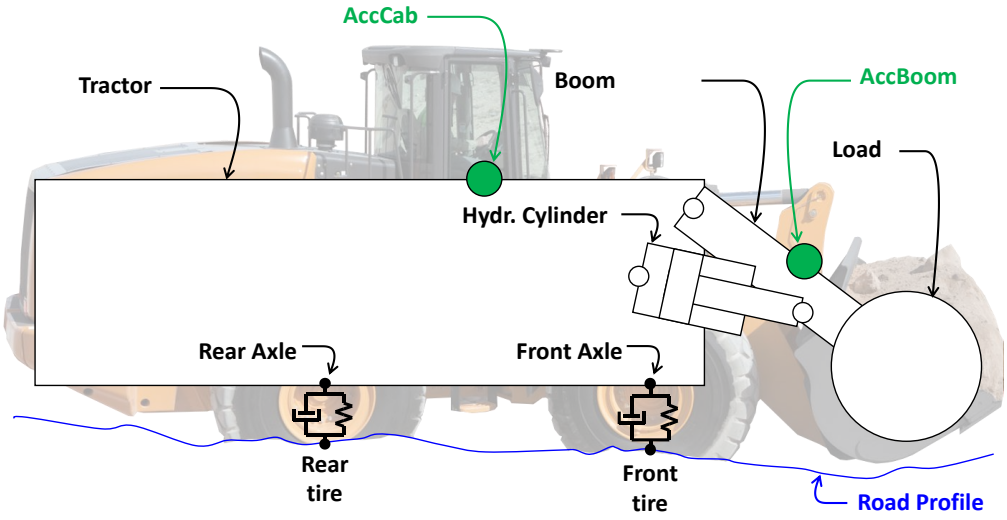

Fig. 79: Schematics of the heel loader rigid bodies considered in the planar mechanical sub-model.

The machine can be seen as constituted by two rigid bodies represented by the tractor and the implement (including load and boom). Tractor and implement are connected through two elements: a pin and the hydraulic cylinder. The tires can be modeled in first approximation as lumped parameter parallel spring-damper systems. Under the hypothesis the tires adhere to the ground, the bottom of the spring-damper system is constraint to follow the road profile itself. In particular, the irregularities of the ground generate variable forces on the machine axles which act as disturbance to the overall system.

The overall system can be further simplified by replacing the hydraulic actuator with the analog mechanical spring-damper model according to the method outlined in Chap. 3. Ultimately, the overall system can be simplified into the mechanical model represented in Fig. 12. For this system,

because of the presence of the disturbance, the measurement of the actuator pressure would not be sufficient to know the position of the two masses (as it was anticipated in Sect. 4.2).

The pressure feedback could therefore be used to dissipate the energy of the disturbance transmitted from the tractor to the implement. By dissipating this energy, both boom and cab vibrations can be reduced at the same time. This mechanism is analogous to the operation of the PRC, however, theoretically better results can be achieved since the active ride control parameters can be adapted to the operating condition of the machine in an easier and more flexible fashion.

Differently, the acceleration feedback, implemented by locating accelerometers on the boom and on the cab, would give a direct measurement of the undesired accelerations. In case of vibration damping of the cab, those will be directly measured by the acceleration feedback controller which can therefore operate the proportional directional valve accordingly. In this case, the operation of the accelerometer feedback would therefore differ from the PRC and pressure feedback cases which are instead targeted to limit the implement vibrations. For these reasons, in case of cab vibrations, it is expected the acceleration feedback will return better performances with respect to the PRC and pressure feedback controller, as it will be investigated in Sect. 10.4.

CHAPTER 10. CASE STUDY 2: WHEEL LOADER: RESULTS

The goals of the case study 2 (wheel loader) were described in Sect. 1.3.2. This chapter will show the main aspects of the vibration damping of wheel loaders by applying the proposed control method. The non-model-based parameters tuning method will be applied to reduce the vibrations perceived by the driver (cab vibrations) and those responsible for the loss of transported material (bucket vibration). Then, simulation results will show the predicted improvement with respect to the PRC in terms of vibration damping. Finally, experiment results show the wheel loader instrumented within this research is operable and an actual reduction of the vibration can be achieved.

10.1 Adaptive Controller Implementation

The general block diagram of the proposed method presented in Fig. 27 is still valid for case study 2. In this case, the position of the boom during the travel is typically at a constant angle (about 70deg), therefore less scheduling variables are required and the general expression of the adaptive controller (Eq. 4.16) can be simplified and rewritten as follows

$$\begin{cases} P^*\left(i_n, M_L\right) = \left[P_R^*\left(M_L\right), P_L^*\left(M_L\right)\right] \\ D^*\left(i_n, M_L\right) = \left[D_R^*\left(M_L\right), D_L^*\left(M_L\right)\right] \end{cases} \quad 9.1$$

The proportional term P^*, according to the sign of i_n, assumes the value P_R^* (raise, $i_n \geq 0$) or the value P_L^* (raise, $i_n < 0$). The raise and lowering proportional terms (P_R^*, P_L^*) are expressed as a function of the load mass M_L.

Another simplification of the schematic represented in Fig. 27 is represented by the possibility of using just one pressure sensor, removing the one used to measure p_L. In fact, as it is shown in the wheel loader hydraulic circuit presented in Fig. 68, the force $p_L A_L$ is always significantly smaller than the force $p_R A_R$.

The mass M_L is identified by the mass estimator, whose expression rather than being indicated by the equation the block H_9 (Sect. 4.2.7), is in this case represented by the simpler expression

$$M_L = f_{M_L}(p_{WR}, \beta_{rel}) \quad 9.2$$

When the boom is in steady-state condition (namely when $i_n = 0$), equation 9.2 can be determined analytically or experimentally since the reference wheel loader already implements an angular sensor to measure β_{rel}. In fact, this angular sensor is often present on wheel loaders to prevent

hazardous operations of the machine (for example, when β_{rel} is too low the PRC is disabled so that an eventual sudden boom motion during its activation cannot occur). In this work, the angle β_{rel} was used as feedback signal for what will be indicated in this dissertation as the *boom angle compensator*. The purpose of the boom angle compensator is to prevent excessive drift of this body during the operation of the active ride control. Ultimately, the structure of the controller is represented in Fig. 80.

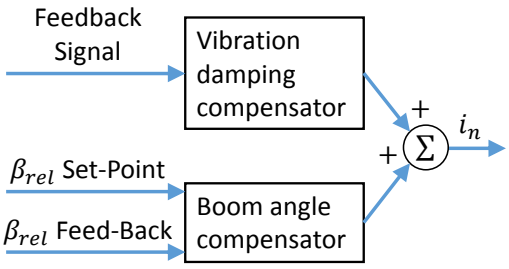

Fig. 80: General structure of the controller for the wheel loader.

The boom angle compensator is combined with the *vibration damping compensator* whose goal is to reduce the vibrations according to the structure in Eq. 9.1. Several sensors configurations can be considered for the current case study. In particular, Fig. 81 summarizes the sensors considered in the current research: angular sensor (β_{rel}); pressure sensor (p_W); cab accelerometer ($\ddot{z}_{cab}$); boom accelerometer ($\ddot{z}_{bkt}$).

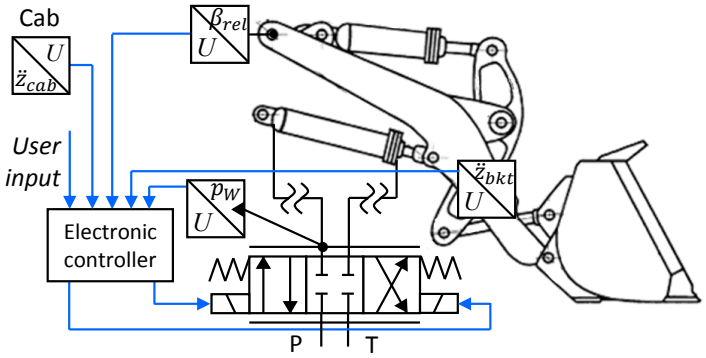

Fig. 81: Wheel loader implement and sensors.

The results of two inputs of the vibration damping compensator are considered: pressure measurement (Sect. 10.2) or the cab acceleration measurement (Sect. 10.4).

10.2 Non-Model-Based Controller Parameters Tuning

The general concept behind the non-model-based controller parameters tuning was introduced in Sect. 4.5. In this section, the general concept will be applied to case study 2.

First of all it is necessary to define the target output, namely the output from the machine dynamics which will be used to evaluate the cost function. The cost function is a number which quantifies the

extent of the vibrations which have to be damped. In case of wheel loader two different quantities are used to evaluate as many cost functions. The acceleration of the cab $\ddot{z}_{cab}$ was chosen as target output to evaluate the cost function J_{cab} which is representative of the vibrations perceived by the operator while driving on uneven road (operator comfort mode). The acceleration of the bucket $\ddot{z}_{bkt}$ was chosen as target output to evaluate the cost function J_{bkt} which is representative of the vibrations on the bucket which cause the loss of transported material during the driving on uneven road (load transport mode).

Many combinations of cost functions formulations have been tested, however it has been observed that among those properly defined, and the results are consistent. In this section, just one alternative will be presented, namely the one which is most intuitive and turned out to be also effective in all tested conditions. For both J_{cab} and J_{bkt}, a similar formulation was used:

$$\begin{cases} J_{cab}(k) = \int_{t_1}^{t_2} \left|\ddot{z}_{cab}(k,t)\right| dt \\ J_{bkt}(k) = \int_{t_1}^{t_2} \left|\ddot{z}_{bkt}(k,t)\right| dt \end{cases} \qquad 9.3$$

where: t_1 is start time of the test; t_2 is the final time of the test. The cost function can be graphically represented as the area between the absolute value of the acceleration and the time axis: Fig. 82 reports an example relative to J_{bkt} (differently, J_{cab} is not reported because it is analogous).

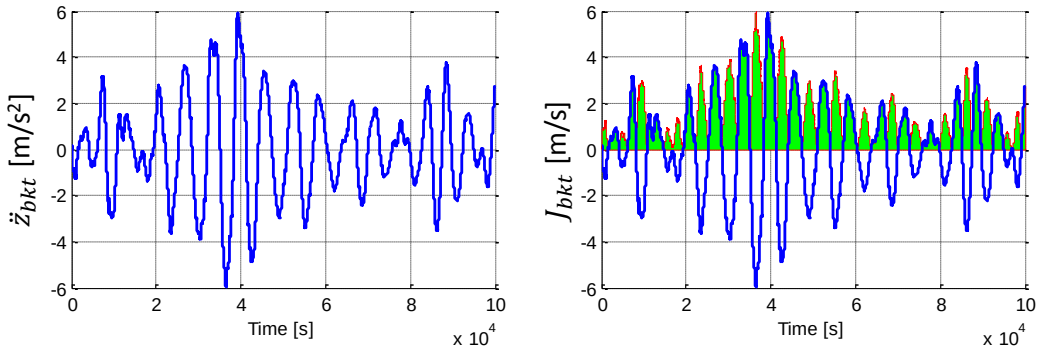

Fig. 82: Example of bucket vertical accelerations over time (left); resulting cost function over time (right).

The resulting cost functions J_{cab} and J_{bkt} are scalar numbers representative of the oscillation amount for the specific k: combination of control parameters set (P^*, I^*, D^*), and load mass M_L. In the case of the wheel loader, during the vehicle travel, the operator command C_n is constantly equal to zero. Once the cost functions J_{cab} and J_{bkt} are determined, it is possible to run the iterative algorithm described in Sect. 4.5: an example of the resulting convergence of the parameters is shown in Fig. 83.

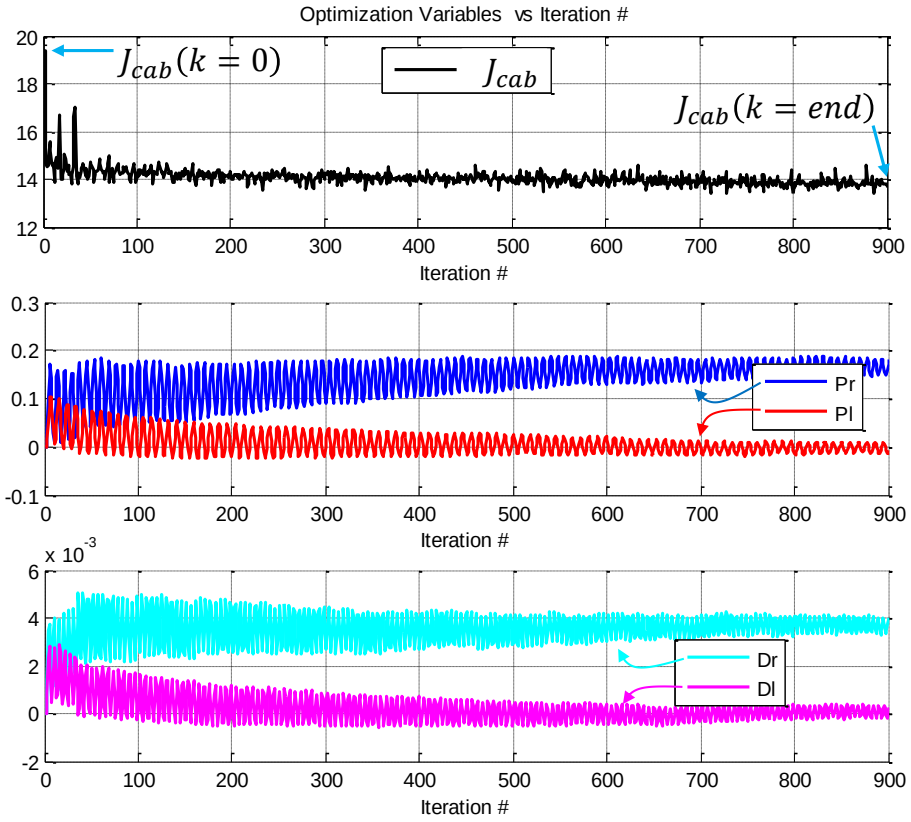

Fig. 83: Example of convergence of the non-model-based controller parameters tuning algorithm for the wheel loader.

For each set of control parameters (P^*, I^*, D^*) obtained thorugh this method, it is possible to test their effectiveness in the relative operating condition defined by the load mass M_L (and W): this test will be performed through simulation results in the next section.

10.3 Pressure Feedback Simulation Results

This section presents the simulation results for case study 2. Several conditions were simulated, for different combinations of vehicle speed, load mass, and road unevenness. For sake of brevity, in this section only one condition is presented: wheel loader drives at 35km/h on uneven ground; the mass load is half of the capacity of the vehicle; the boom is kept in carrying position (β_{rel}=70deg). The research sponsor provided a specific road profile input file which was obtained by experimental measurements. This particular condition was chosen since it is particularly relevant for wheel loader uses. In fact, this condition frequently occurs in constructions sites and also is characterized by large extent of cab vibrations.

10.3.1 Vibration Damping Performance

The case in which the wheel loader does not present any kind of ride control is indicated in Fig. 84 and Fig. 85 by “w/o RC”. This condition is compared with the curves obtained by simulating the PRC in in Fig. 84, and those obtained by simulating the proposed method in Fig. 85.

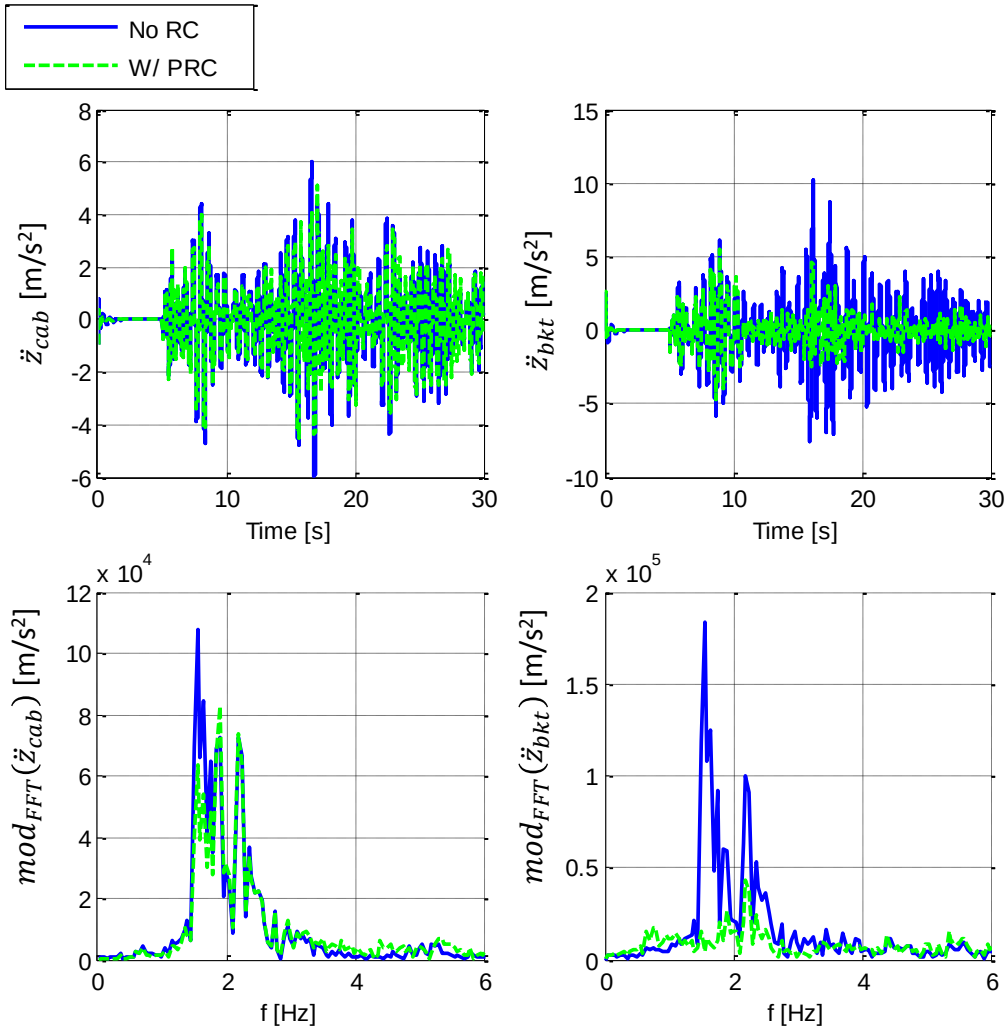

Fig. 84: Simulation results: comparison between the wheel loader with no vibration damping system and the one using PRC.

In particular, Fig. 84 and Fig. 85 show the plot of the vertical acceleration of the cab and bucket: time domain ($\ddot{z}_{cab}$, $\ddot{z}_{bkt}$); frequency domain, expressed as modulus of the FFT ($mod_{FFT}(\ddot{z}_{cab})$, $mod_{FFT}(\ddot{z}_{bkt})$). It is possible to observe both PRC and the proposed method performs better than the case “w/o RC” in all plots.

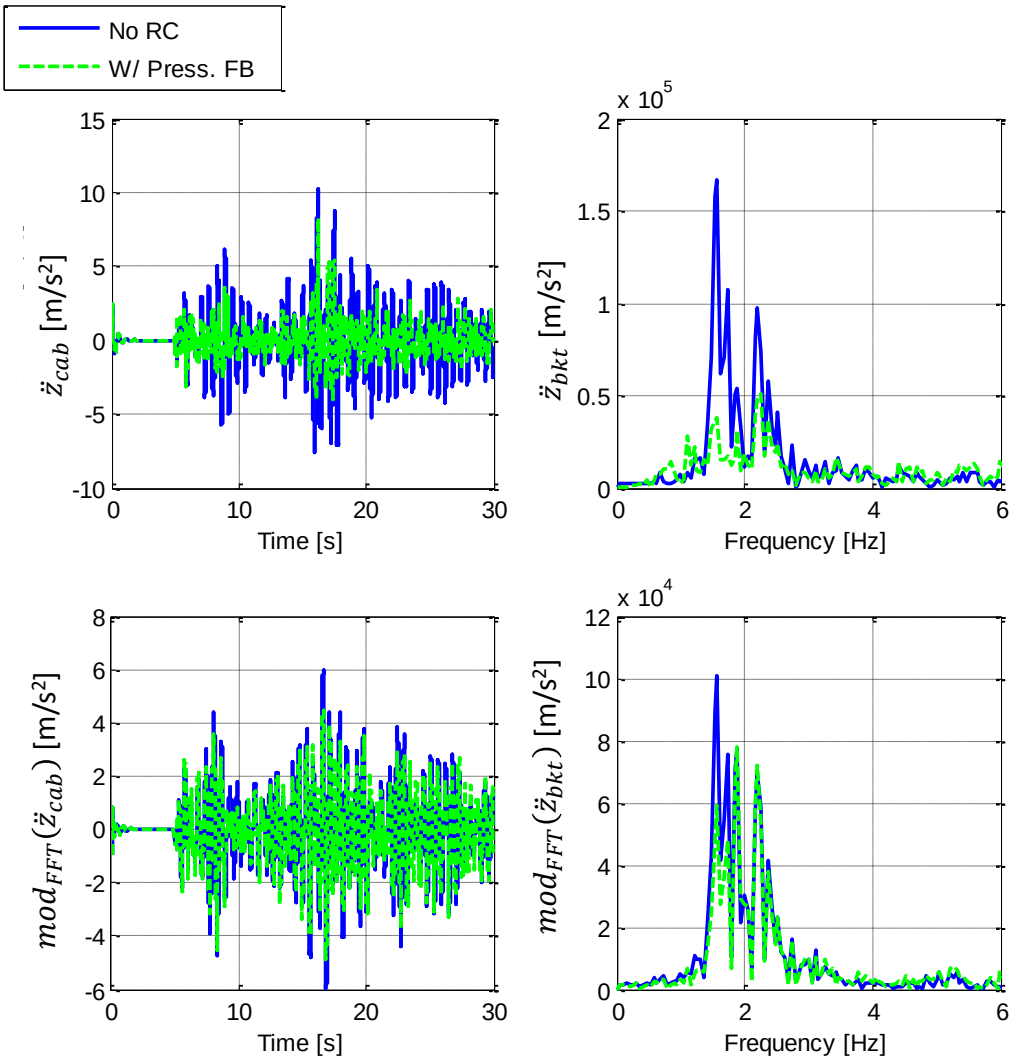

Fig. 85: Simulation results: comparison between the wheel loader with no vibration damping system and the one using the proposed control method (with pressure feedback).

A comparison between the PRC and the proposed method is possible by using Fig. 84 and Fig. 85 to evaluate the reduction of the cost function quantifying the vibrations with respect to the "w/o RC" case. The cost functions for the time domain plots is evaluated according to Eq. 9.3. Differently, a new formulation is defined to evaluate the cost function in frequency domain for the cab and bucket:

$$\begin{cases} J_{cabFFT} = \int_{f_1}^{f_2} \mathrm{mod}_{FFT}\left(\ddot{z}_{cab}\right) dt \\ J_{bktFFT} = \int_{f_1}^{f_2} \mathrm{mod}_{FFT}\left(\ddot{z}_{bkt}\right) dt \end{cases} \qquad 9.4$$

Where f_1 is the lowest vibrational frequency (in this case it was considered equal to 0Hz) and f_2 is the highest vibrational frequency (in this case it was considered equal to 8Hz, since the FFT modulus becomes very low, as observed by the simulations).

It is the possible to collect the percentage improvements in terms of cost functions of the PRC and the proposed method with respect to the "w/o RC" case in the histogram plot in Fig. 86.

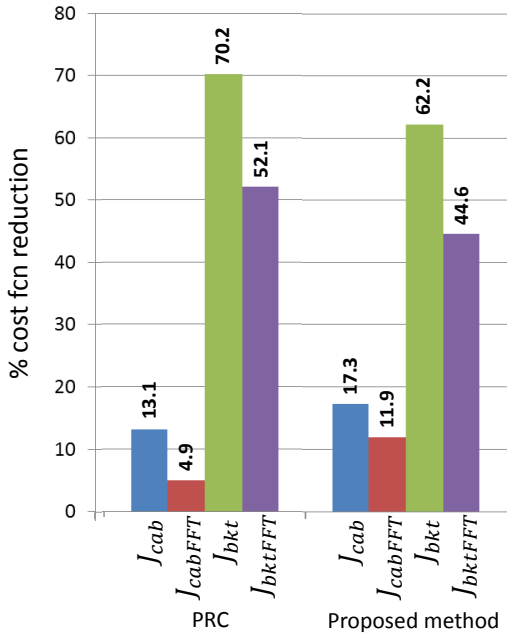

Fig. 86: Histogram showing a comparison between the percentages of attenuation obtained by the PRC and by the proposed method for different vibration cost functions.

It is possible to observe that, as expected, the information provided by the time domain and the frequency domain cost functions are consistent each other. Additionally, it is possible to observe the PRC seems to perform better in case of bucket oscillations, however, the proposed method performs better in the most important condition, namely the cab vibrations damping.

10.3.2 Effect of Proportional Valve Dynamics

The results presented in the previous section (Sect. 10.3.1) were obtained by considering the dynamics of the proportional directional valve of the wheel loader in production. This section summarizes a study aimed to understand how the vibration damping performance of the active ride control based on pressure feedback are affected by the proportional directional valve dynamics.

In particular, the value of the vibration reduction normalized with respect to the value resulting from nominal proportional directional valve dynamics. The case of cab vibration evaluated in terms of time based cost function is represented in Fig. 87, whereas the case of boom vibration evaluated in terms of time based cost function is represented in Fig. 88. In these figures, the nominal valve dynamics is expressed by a unitary normalized natural frequency and unitary nominal damping

ratio. Both plots show significant improvement of the vibration damping method can be result from a fast valve dynamics with an adequate damping.

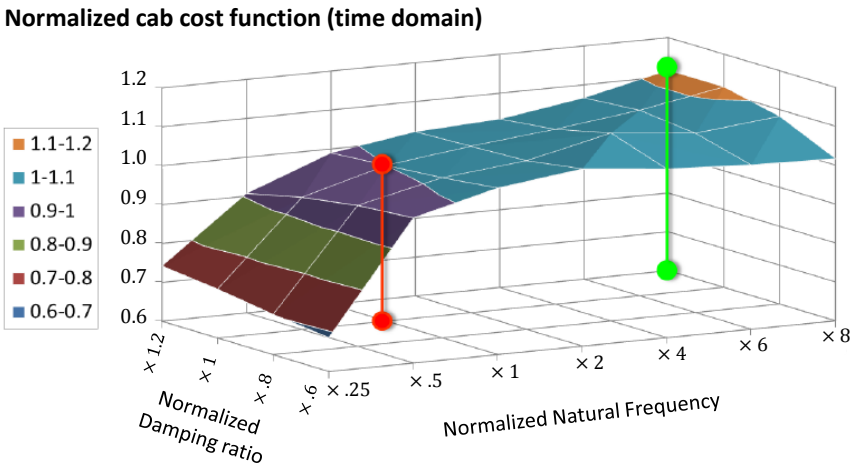

Fig. 87: Reduction of the cab cost function evaluate with respect to time (normalized with respect to nominal proportional directional valve dynamics).

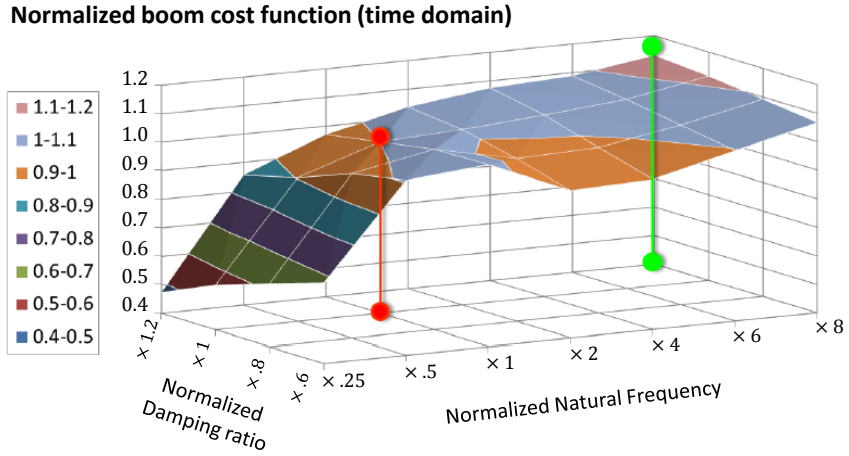

Fig. 88: Reduction of the boom cost function evaluate with respect to time (normalized with respect to nominal proportional directional valve dynamics).

10.3.3 Energy Consumption

The second aspect regards a particular modification of the PRC damping method. In Sect. 10.2 it was shown the proposed method presents an advantage over the PRC in terms of cab vibration damping. In terms of energy efficiency, however, the proposed method is not as good as the PRC is, and this section will present an analysis of the energy consumption and proposes an energy efficient combination of the PRC and proposed method to control the PRC stabilizing valve spool.

The PRC system includes a stabilizing valve which dissipates almost exclusively the energy introduced by the uneven ground, while the energy from the hydraulic power supply is almost

unaltered. In fact, the only dissipation of the power supply in the PRC system is the one required to re-position of the boom at the desired angle. This issue occurs whenever the PRC is enabled and the accumulator pressure differs from the raise cylinder chamber pressure. No quantification of this energy loss has been performed. Differently, the analysis of the energy losses in case of the proposed method is presented in Fig. 89 for the reference cycle from previous section.

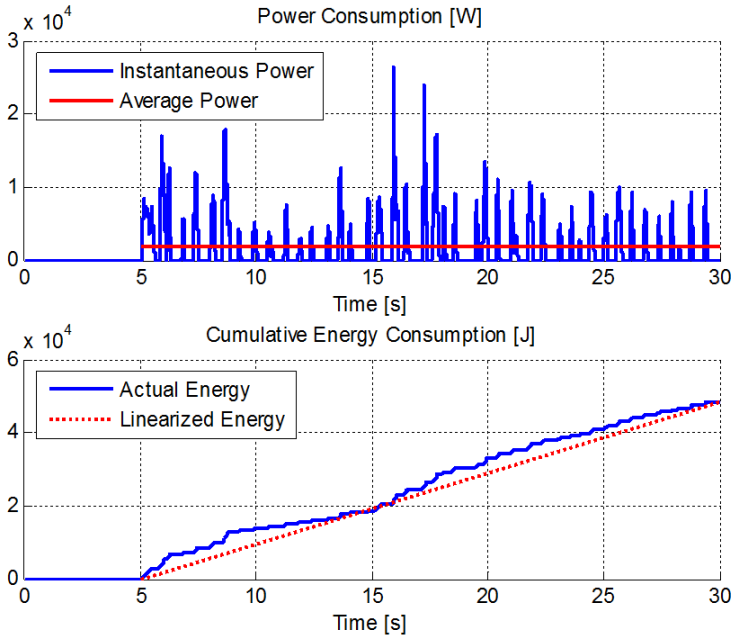

Fig. 89: Estimated power consumption of the proposed control method during the travel of the wheel loader on uneven ground.

Fig. 89 shows the power consumption and the energy consumption for a 25 seconds long drive cycle. It has observed an average power consumption of 1.9kW, which is approximately equal to the 0.79% of the maximum engine power. Considering this value is only relative to the range of time in which the proposed method is activated, this energy consumption becomes not so relevant. However, a solution to combine the benefits of the proposed method (effectiveness of the cab vibration damping; adaptability to varying operating conditions; simplification of the hydraulic circuit) to the energy efficiency of the PRC, a modification of the PRC system is proposed. In particular, with reference to Fig. 68, the enabling valve (indicated by 11 in Fig. 68) can be changed into a proportional valve. The proposed control method will then be applied to such valve rather than the directional valve which is indicated by 5. The analysis of this method represents a potential future work.

10.4 Pressure Feedback vs. Acceleration Feedback: Simulations and Experiments

Results regarding the use of pressure feedback to implement the vibration damping of the wheel loader were presented in Sect. 10.2. Differently, this section presents results deriving from the use

of acceleration feedback, with the goal to compare the two alternative methods. In particular, the results presented in this section are relative to the reduction of the vibration of the cab by using an accelerometer located inside the cab itself.

Fig. 90 shows the plot of the vertical acceleration of the cab and bucket: time domain ($\ddot{z}_{cab}$, $\ddot{z}_{bkt}$); frequency domain, expressed as modulus of the FFT ($mod_{FFT}(\ddot{z}_{cab})$, $mod_{FFT}(\ddot{z}_{bkt})$).

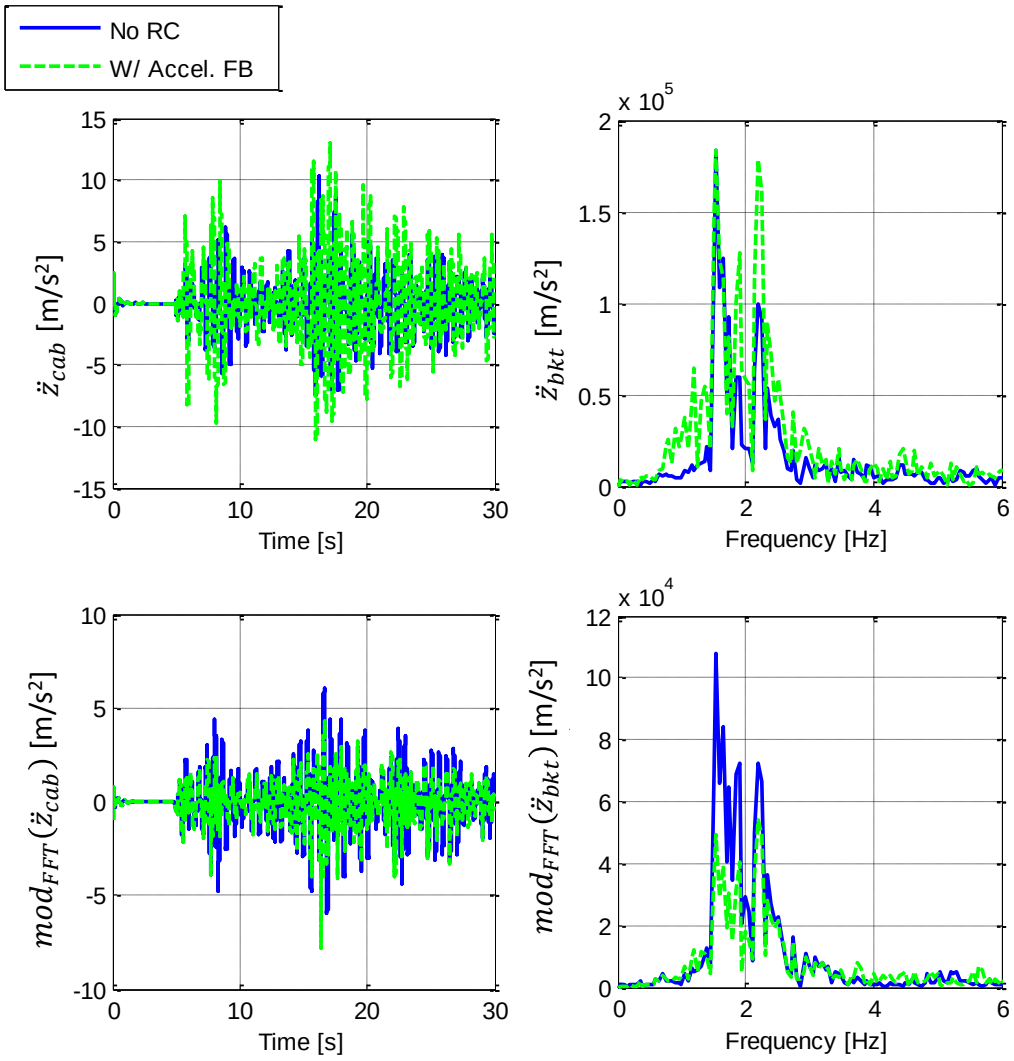

Fig. 90: Simulation results: comparison between the wheel loader with no vibration damping system and the one using the proposed control method (with acceleration feedback).

These plots were obtained by optimizing the controller parameters to minimize the accelerations of the cab. It is possible to observe the cab vibrations are actually attenuated, however, unlike the case with pressure feedback, boom vibrations are increased. By recalling the cost function to quantify the wheel loader vibrations (Eq. 9.4), it is possible to observe the acceleration feedback is suitable to reduce 38.6% cab vibrations with respect to the case with no ride control. This proves

that, as it was anticipated in Sect. 9.3, the acceleration feedback is more effective in reducing cab vibrations than PRC and ARC based on pressure feedback. In fact, in Fig. 86 it was shown PRC and ARC based on pressure feedback were suitable to respectively obtain 13% and 17.3% vibration reduction with respect the case with no ride control. However, it is also possible to observe boom vibrations were amplified in this configuration. In case boom vibrations become excessive, a trade-off with cab vibration reduction can be achieved by using a weighted cost function used for the non-model-based controller parameters tuning.

The conclusion of the project is represented by the proof of concept achieved by means of the experimental wheel loader described in Sect. 8.2. In particular, a series of tests were performed at the research sponsor facilities to show the proposed method can effectively reduce the vibrations of the machine. The experimental tests were performed at the research sponsor facility by driving the wheel loader on the test track inclusive of bump represented in Fig. 91.

Fig. 91: Picture of the experimental wheel loader driving on the bump test track located at the research sponsor facility.

Experimental results are presented in Fig. 92 where it is possible to observe the cab acceleration curves obtained in the flowing cases: no ride control (label “No RC”); passive ride control (label “PRC”); and active ride control with acceleration feedback (label “Accel. FB”). The proposed method reduces the vibrations by 11% and this demonstrates the effectiveness of the proposed vibration damping control as well its practical feasibility. Although the PRC in this test condition presents better performance (vibration reduced by 24%), the proposed method can still presents advantages in terms of cost and hydraulic system simplification. Additionally, in this test condition the proposed method performances were penalized by the fact the non-optimal controller parameters were used. In particular, at this stage of the research the research sponsor could not provide neither a numerical model for the 621F wheel loader nor information suitable to simulate the travel of the wheel loader on a bump. Consequently the controller tuning was based on the

optimization of the available numerical model of the wheel loader 1021F traveling on uneven ground rather than a single bump. Although better results could have been obtained with simulations which better represent the test conditions, experiments were still sufficient to achieve the goals represented by the proof of concept and practical feasibility of the proposed control method.

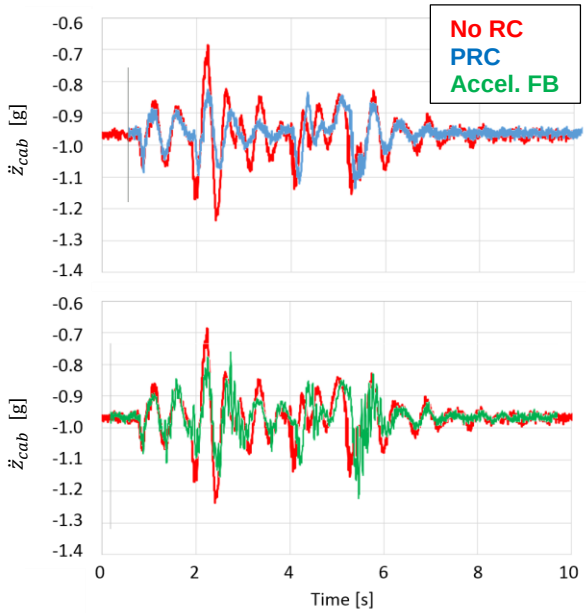

Fig. 92: Wheel loader experimental results: no ride control (No RC); passive ride control (PRC); active ride control based on acceleration feedback (Accel. FB).

CHAPTER 11. SUMMARY AND CONCLUSIONS

The present work proposes an innovative control method to damp vibrations in mobile hydraulic machines. In particular, the features of the proposed method make it suitable to be applied to all hydraulic machines which are controlled through proportional electro-hydraulic valves. The range of applications for the proposed method includes: constructions (e.g. wheel loaders, excavators, backhoes); load handling (e.g. cranes, reach-stackers, aerie lifts); agricultural (e.g. harvesters); forestry; aerospace. In order for the proposed method to be effective, the control valve bandwidth must be significantly higher than the frequency of the undesired dynamics. This condition, which is typically true for the above mentioned applications, is further investigated in the research.

The proposed method does not require the modification of the standard valve controlled machine layout since it only needs for the addition of feedback sensors. The feedback signals are used by the control unit to modify the electric currents to the proportional directional valves and cancel the undesired dynamics of the machine by controlling the actuator motion. The research mostly focuses on the use of pressure feedback. In fact, although the use of position, velocity, or acceleration sensors on the vibrating bodies of the machine would provide a more straightforward measurement of the vibration, they are extremely rare on mobile hydraulic machines where mechanical and environmental stress harm their integrity. A comparison between pressure feedback and acceleration feedback alternatives of the proposed method is investigated with the aim to outline the conditions making one alternative preferable over the other one (for those applications were both alternatives are technically viable in terms of sensors and wiring reliability).

The present work has three goals:

General goal for all machines

A. Improvement of the machine dynamics by reducing mechanical vibrations on mechanical arms, load, as well as operator seat;

Goals relative to specific applications:

B. Reduction of the energy dissipations introduced by current vibration damping methods;
C. Reduction of system slowdowns introduced by current vibration damping methods.

The present work discusses all mentioned goals by presenting two different case studies:

1. Case study 1 - Hydraulic Crane: the goal A and B are pursued.
2. Case study 2 - Wheel Loader: the goal A and C are pursued.

By analyzing two different machines, this work aims to illustrate the capability of the proposed control method to be applied to all valve controlled hydraulic machines. Additionally, for both case studies, the comparison between pressure feedback and acceleration feedback is investigated.

The main contributions of this research to advance the state of the art in the fluid power field included:

- Formulation of a general vibration damping method based on pressure feedback which can be *applied to all valve controlled hydraulic machines*.
- *Proof of observability*: capability to describe the vibrating part vibrations from the measured pressure feedback signals.
- Formulation of a *non-model-based controller tuning algorithm* in which the control parameters are obtained by the optimization of the experimental machine response.
- Formulation of an *adaptation algorithm* in which the optimized parameters are indexed with respect to the operating points.

The capability of the proposed control method to be applied to all valve controlled hydraulic machines was tested on two substantially different applications: hydraulic crane (case study 1), and wheel loader (case study 2).

Case study 1 is finalized to the reduction of the vibration of the mechanical arms of a hydraulic crane. In case study 1 a commercial crane implementing traditional fixed parameters hydro-mechanical vibration damping methods was tested with and without the proposed pressure feedback vibration damping method. The tests were performed on a purposely realized crane lumped parameters nonlinear model and on the instrumented crane which was installed at Maha Fluid Power Research Center (Purdue University) to serve as experimental setup for this research. Both simulations and experiments showed the proposed control method is suitable to reduce the vibrations in all tested conditions with and without load. In particular, it was observed up to 30% vibration reduction with respect to the state of the art vibration damping method for the crane. This study demonstrated that for the case study of the crane installed on a rigid support there is not a clear advantage in using accelerometers on the mechanical arms to provide a feedback signal compared to the use of pressure sensor. The stability analysis of the proposed method was also presented with reference to the simulation model of case study 1. In particular, by analyzing the root locus of the standard crane and the one using the proposed method, it was possible not only proof the stability, but also observe the capability to alter the poles location in a favorable way.

Case study 2 is finalized to the reduction of the cab and bucket vibrations occurring on a wheel loader driving on uneven ground. The passive ride control system was modeled so that it was possible to compare its effectiveness with respect to the proposed method (both in case of pressure feedback and acceleration feedback). A simulation study shows faster valve bandwidth would increase the effectiveness of the proposed method up to 20%. Differently, slower valve bandwidth would exponentially reduce the effectiveness of the proposed method to the point it becomes inapplicable. The comparison between passive ride control, and the proposed control method (both pressure feedback and acceleration feedback based) were performed considering standard valve bandwidth. Simulation results showed the three alternatives are comparable in terms of bucket vibration reduction (up to 70%). Differently, in case of cab vibrations, pressure feedback and acceleration feedback methods are respectively up to 15% and 30% more effective than the passive ride control. Better results of the acceleration feedback method in this specific application are due to the presence of disturbance and flexible support (tires) of the wheel loader cabin. In addition, the proposed control method presents benefits in terms of hydraulic system simplification. Finally, an instrumented wheel loader was used to provide a proof of concept and practical feasibility.

Although research in electro-hydraulic vibration damping methods for mobile hydraulic machines has started decades ago, in most of the cases commercial machines still adopt dated hydro-mechanical methods, and the recourse to more sophisticated electro-hydraulic solutions is still limited. Solving most of the reliability and complexity issues related to the electro-hydraulic based control which prevented their diffusion in commercial machines, the proposed method is candidate to represent an important innovation in the field of fluid power. Beside the general advantage of improved vibration damping effectiveness, the proposed method presents additional benefits respect to the current hydro-mechanical method which could be replaced, in terms of costs and energy consumption. In particular, case study 1 showed potential for improvement in terms of energy efficiency, while case study 2 showed potential for increase the machine speed of response. In both cases, potential for simplification of the hydraulic circuit was observed.

BIBLIOGRAPHY

BIBLIOGRAPHY

Akers, A., Gassman M., and Smith R., 2006, *Hydraulic Power System Analysis*. Taylor & Francis, New York.

Anderson B. R., 2009, *Energy Efficient Load Holding Valve*, Proceedings of the 11th Scandinavian International Conference on Fluid Power (SICFP'09), Linköping, Sweden.

Ariyur K. B., and Krstić M., 2003, *Real-Time Optimization by Extremum Seeking Control*, John Wiley & Sons.

Åström K. J., and Wittenmark B., 2008, *Adaptive Control* - 2nd Edition, Dover Publications.

Atlas Maschinen Gmnh®, 1996, *Atlas 125.2 Technical Data*.

Book W. J., and Lee S. H., 1989, *Vibration Control of a Large Flexible Manipulator by a Small Robotic Arm*, American Control Conference.

Bu F., Yao B., 2001, *Nonlinear model based coordinated adaptive robust control of electro-hydraulic robotic arms via overparametrizing method*, Proceedings 2001 ICRA. IEEE International Conference on Robotics and Automation.

Campanella G., and Vacca A., 2010, *Modeling and Optimization of the Control Strategy for the Hydraulic System of an Articulated Boom Lift*, SAE 2010 Commercial Vehicle Engineering Congress, Rosemont, Illinois, USA

Cao J., Zhu X., Tao G., and Yao B., 2007, *Adaptive Robust Tracking Control of Pressure Trajectory Based on Kalman Filter*. Chinese Journal of Mechanical Engineering.

Chiang M. H., and Huang C.C., 2004, *Experimental implementation of complex path tracking control for large robotic hydraulic excavators*, International Journal of Advanced Manufacturing Technology v. 23: 126–132.

CNH America LLC ©, 2012, *Case Construction® 621F Technical Data*.

CNH America LLC ©, 2012, *Case Construction® 1021F Technical Data*.

Conrad F., 1993, *Transputer Control of Hydraulic Actuators and Robots*, IEEE Transactions on Industrial Electronics, Vol. 43 Issue 1 pp 38 – 47.

Cristofori D., and Vacca A., 2010, *Analysis of the Dynamics of a Proportional Valve Operated by an Electronic Controller*, 6th FPNI – PhD Symposium, June 15-19 2010, West Lafayette (IN), USA.

Cristofori D., and Vacca A., 2011, *The Modeling of Electro-Hydraulic Proportional Valves*, ASME Journal of Dynamic Systems, Measurement and Control, Vol.134, Issue 2, 021008 (13 pages).

Cristofori D., and Vacca A., 2011, *Electro-Hydraulic Proportional Valve Modeling Comprehending Magnetic Hysteresis*, IFPE2011, 52nd National Conference on Fluid Power, March 22-26 2011, Las Vegas, Nevada, USA.

Cristofori D., and Vacca A., 2012, *Adaptive Vibration Damping Method for Hydraulic Machines: the Case of a Hydraulic Crane*, 7th FPNI PhD Symposium on Fluid Power, 27-30 June 2012, Reggio Emilia, Italy.

Cristofori D., and Vacca A., 2012, *A Novel Pressure-Feedback Based Adaptive Control Method to Damp Instabilities in Hydraulic Machines*, Presented at: 2012 SAE Commercial Vehicles Engineering Congress, Oct. 2-3, 2012, Rosemont IL, USA. Selected for publication in: SAE Int. J. Commer. Veh. 5(2):2012.

Cundiff J. S., 2002, *Fluid Power Circuits and Controls: Fundamentals and Applications*, 2nd edition, CRC Press.

DeBoer C. C., and Yao B., 2001, *Velocity Control of Hydraulic Cylinders with only Pressure Feedback*, Proceedings of ASME International Mechanical Engineering Congress and Exposition, IMECE2001.

Edge K. A., 1996, *The Control of Fluid Power Systems – Responding to the Challenges*, Proc Instn Mech Engrs Vol 211 Part 1, IMechE 1997.

Edge K. A., 2003, *On the Control of Electrohydraulic Systems – Some Recent Research Contributions*. 8th Scandinavian International Conference on Fluid Power, Tampere, Finland 2003. (Invited Keynote Paper)

Fialho I., and Balas G. J., 2002, *Road Adaptive Active Suspension Design using Linear Parameter-Varying Gain-Scheduling*, IEEE transactions on Control Systems Technology, Vol. 10, No. 1.

Franklin G. F., Powell, J. D., and Emami-Naeini A., 2009, *Feedback Control of Dynamic Systems*, 6th edition, Prentice Hall.

Garcia C., 2008, *Comparison of Friction Models Applied to a Control Valve*, Control Engineering Practice 16 (2008) 1231 – 1243.

Garimella P., and Yao B., 2002, *Nonlinear Adaptive Robust Observer for Velocity Estimation of Hydraulic Cylinders Using Pressure Measurement Only*. Proceedings of ASME International Mechanical Engineering Congress and Exposition, IMECE2002.

Guglielmino E., and Edge K. A., 2001, *Modelling of an Electrohydraulically Activated Friction Damper in a Vehicle Application*, IMECE2001.

Ivantysyn J., and Ivantysynova M., 2001, *Hydrostatic pumps and motors: principles, design, performance, modelling, analysis, control and testing*, ABI Oversears Limited.

Hong K. S., et al., 2002, *Modified Skyhook Control of Semi-Active Suspensions: A New Model, Gain Scheduling, and Hardware-in-the-Loop Tuning*, ASME, Journal of Dynamic Systems, Measurement, and Control.

Handroos H., Halme J., and Vilenius M., 1993, *Steady State and Dynamic Properties of Counterbalance Valves*, Proceedings of the 3rd Scandinavian International Conference on Fluid Power (SICFP'93), Linköping, Sweden.

International Organization for Standardization, 2004, ISO 2631-5:2004: *Mechanical Vibration and Shock*, Evaluation of Human Exposure to Whole-Body Vibration, International Organization for Standardization, Geneva, Switzerland.

Killingsworth N. J., and Krstić M., 2006, *PID Tuning Using Extremum Seeking, IEEE Control Systems Magazine*, February 2006.

Krstić M., and Wang H. H., 1997, *Stability of Extremum Seekin Feedback for General Nonlinear Dynamic Systems*. Automatica 36 (2000) 595-601.

Krus P., and Palmberg J. O., 1988, *On Load Sensing Fluid Power Systems*, Linköping Studies in Science and Technology, PhD Dissertation No. 198

Krus P., and Gunnarsson S., 1993, *Adaptive Control of a Hydraulic Crane Using On-Line Identification*, The Third Scandinavian International Conference on Fluid Power, Linköping, Sweden.

La Hera P., Mettin U., Manchester I. R., and Shiriaev A., 2008, *Identification and Control of a Hydraulic Forestry Crane*, Proceedings of the 17th IFAC World Congress.

Liu Z., and Luo C., 2006, *Road Adaptive Active Suspension Control Design*, IMACS Multiconference on Computational Engineering is Systems Applications (CESA), October 4-6-, 2006, Beijing, China.

LMS.Imagine.Lab AMESim®, 2010, *Hydraulic Library Rev.10*, Manual.

Lumkes J., and Andruch J., 2011. *Hydraulic Circuit for Reconfigurable and Efficient Fluid Power Systems*, Proceedings of the 12th Scandinavian International Conference on Fluid Power, SICFP (1096):16pg.

Metz D. L., 1993, *Dynamics of Four-Wheel-Steer Off-Highway Vehicles, SAE International Congress and Exposition*, Detroit, MI, March 1-5, 1993.

Milanes V., Gonzalez C., Naranjo J. E., Onieva E., and De Pedro T., 2002, *Electro-Hydraulic Braking System for Autonomous Vehicles*, International Journal of Automotive Technology.

Nervegna N., 2003, *Oleodinamica e Pneumatica*, Politeko, Turin, Italy.

Nevala K. and Jarviluoma M., 1997, *An Active Vibration Damping System of a Driver's Seat for Off-road Vehicles*, Proceedings of the Fourth Annual conference on Mechatronics and Machine vision in Practice, Toowoomba, Queensland, Australia.

Paavilainen H., Savolainen J., and Kullaa J., 2007, *Vibration Damping of the Crane*, Proceedings of the 10th Scandinavian International Conference on Fluid Power (SICFP'07), Tampere, Finland.

Palmer M. K., et al., 1998, *Ride Control System*, US Patent #5733095.

Parker-Hannifin®, 2006, *P70 Mobile Directional Control Valve*, Catalogue: HY17-8546-UK_P70

Peterson K. S., and Stephanopoulu A. G., 2004, *Extremum Seeking Control for Soft Landing of an Electromechanical Valve Atuator*, Automatica 40 (2004) 1063-1069.

Plummer A. R., 2007, *Control Techniques for Structural Testing: a Review*. Proceedings of the Institution of Mechanical Engineers, Part I: Journal of Systems and Control Engineering, 221 (2), pp. 139-169

Rahmfeld R., and Ivantysynova M., 2001, *Displacement controlled linear actuator with differential cylinder - a way to save primary energy in mobile machines*, ICFP 2001: Fifth International Conference on Fluid Power Transmission and Control; Hangzhou; China; 3-5 Apr. 2001. pp. 296-301.

Rahmfeld R., and Ivantysynova, M., 2004. *An overview about active oscillation damping of mobile machine structure*. International Journal of Fluid Power, Vol. 5 (2004), No. 2, pp. 5-24.

Rahmfeld R., Ivantysynova M., and Eggers, B., 2004, *Active Vibration Damping for Off-Road Vehicles Using Valveless Linear Actuators*. Proceedings of the SAE Commercial Vehicle Engineering Congress & Exhibition, Chicago, IL, USA.

Ritelli G. F., and Vacca A., 2013, *Energetic and Dynamic Impact of Counterbalance Valves in Fluid Power Machines,* Journal of Energy Conversion and Management*.*

Ritelli, G.F., and Vacca A., 2013, *Energy Saving Potentials of a Novel Electro-Hydraulic Method to Reduce Oscillations in Fluid Power Machines: The Case of a Hydraulic Crane,* SAE Int. J. Commer. Veh. 6(2):2013, doi: 10.4271/2013-01-2345.

Sinha, A. K., 2010, *Vibration of Mechanical Systems*, Cambridge University Press, 1st edition.

Sun Hydraulics Co., 2012, *LoadMatch® Counterbalance Valves*, Technical documentation.

Virvalo, T. 2002, Hydraulic Motion Control – Robustness against Inertia Load Changes, Proceedings of Japan Fluid Power Symposium JFPS 2002.

Williamson C., Lee S., and Ivantysynova M., 2009, *Active Vibration Damping for an Off-Road Vehicle with Displacement Controlled Actuators*, International Journal of Fluid Power 10 No. 3 pp. 5-16.

Yanada H., and Shmahara M., 1997, *Sliding Mode Control of an Electrohydraulic Servo Motor Using a Gain Scheduling Type Observer and Controller*, Proc Instn Mech Engrs Vol 211, Part 1. IMechE 1997.

VITA

VITA

Davide Cristofori

Education

Ph.D., December 2013, Department of Agricultural and Biological Engineering, Fluid Power Specialization, Purdue University, West Lafayette, Indiana (USA).
Thesis: Advanced Control Strategies for Mobile Hydraulic Application.
Major Professor: Dr. Andrea Vacca.

M.S., March 2009, Mechanical Engineering, University of Parma, Parma (Italy).
Thesis: Numerical and Experimental Analysis of Electrohydraulic Proportional Valves.
Major Professor: Dr. Andrea Vacca.

B.S., December 2006, Mechanical Engineering, University of Parma, Parma (Italy).

Current Employment

CNH Industrial (Plant location: San Mauro Torinese, Turin, Italy).
Excavator Hydraulic Engineer.

Publications

Journal Papers

- Cristofori D., Vacca A., Ariyur K. B., 2012, *A Novel Pressure-Feedback Based Adaptive Control Method to Damp Instabilities in Hydraulic Machines,* Presented at: 2012 SAE Commecial Vehicles Engineering Congress, Oct. 2-3, 2012, Rosemont IL, USA. Selected for publication in: SAE Int. J. Commer. Veh. 5(2):2012, doi:10.4271/2012-01-2035.

- Cristofori D., Vacca A., 2011, *The Modeling of Electro-Hydraulic Proportional Valves*, ASME Journal of Dynamic Systems, Measurement and Control, Vol.134, Issue 2, 021008 (13 pages)

Conference Papers

- Cristofori D., Vacca A., 2012, *Adaptive Vibration Damping Method for Hydraulic Machines: the Case of a Hydraulic Crane*, 7th FPNI PhD Symposium on Fluid Power, June 27-30 2012, Reggio Emilia, Italy
- Cristofori D., Vacca A., 2011, *Electro-Hydraulic Proportional Valve Modeling Comprehending Magnetic Hysteresis*, IFPE2011, 52nd National Conference on Fluid Power, March 22-26 2011, Las Vegas, Nevada, USA
- Cristofori D., Vacca A., 2010, *Analysis of the Dynamics of a Proportional Valve Operated by an Electronic Controller*, 6th FPNI PhD Symposium on Fluid Power, June 15-19 2010, West Lafayette (IN), USA

Awards/Honors

- Best poster award, 2013 CCEFP Annual Meeting, Sarasota, Florida (3rd place out of 33 presenters).
- Paper presented at SAE COMVEC2012 International Conference in Rosemont (IL) was selected for publication on SAE International Journal of Commercial Vehicles.
- CCEFP travel grant, year 2012.
- Top downloaded paper of the ASME Journal of Dynamic Systems, Measurement, and Control in March 2012 and June 2012 (2nd top downloaded in January 2012 and February 2012).
- Purdue Research Foundation Fellowship, 2011 (Purdue University, West Lafayette, Indiana).
- Purdue SURF Graduate Mentor of the summer 2010 (mentee student awarded as best presenter during the 2010 Purdue SURF Symposium).
- Casappa S.p.A. award as one of the three best MS Thesis in Fluid Power in the academic year 2008/2009 at University of Parma.